

NATIONAL AERONAUTICS AND SPACE ADMINISTRATION

Space Programs Summary No. 37-38, Volume III

for the period January 1, 1966 to February 28, 1966

The Deep Space Network

FACILITY FORM 902

N66 26288	
(ACCESSION NUMBER)	(THRU)
116	1
(PAGES)	(CODE)
CP-75155	07
(NASA CR OR TMX OR AD NUMBER)	(CATEGORY)

GPO PRICE \$ _____

CFSTI PRICE(S) \$ _____

Hard copy (HC) 4.00

Microfiche (MF) .75

ff 653 July 65

jpl

JET PROPULSION LABORATORY
CALIFORNIA INSTITUTE OF TECHNOLOGY
PASADENA, CALIFORNIA

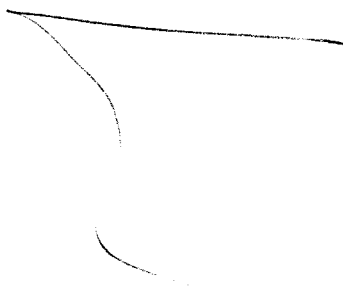
March 31, 1966

NATIONAL AERONAUTICS AND SPACE ADMINISTRATION

Space Programs Summary No. 37-38, Volume III

for the period January 1, 1966 to February 28, 1966

The Deep Space Network



JET PROPULSION LABORATORY
CALIFORNIA INSTITUTE OF TECHNOLOGY
PASADENA, CALIFORNIA

March 31, 1966

Preface

The *Space Programs Summary* is a six-volume, bimonthly publication that documents the current project activities and supporting research and advanced development efforts conducted or managed by JPL for the NASA space exploration programs. The titles of all volumes of the *Space Programs Summary* are:

- Vol. I. The Lunar Program (Confidential)
- Vol. II. The Planetary-Interplanetary Program (Confidential)
- Vol. III. The Deep Space Network (Unclassified)
- Vol. IV. Supporting Research and Advanced Development (Unclassified)
- Vol. V. Supporting Research and Advanced Development (Confidential)
- Vol. VI. Space Exploration Programs and Space Sciences (Unclassified)

The *Space Programs Summary*, Vol. VI consists of an unclassified digest of appropriate material from Vols. I, II, and III; an original presentation of technical supporting activities, including engineering development of environmental-test facilities, and quality assurance and reliability; and a reprint of the space science instrumentation studies of Vols. I and II.



W. H. Pickering, Director
Jet Propulsion Laboratory

Space Programs Summary No. 37-38, Volume III

Copyright © 1966, Jet Propulsion Laboratory, California Institute of Technology
Prepared under Contract No. NAS 7-100, National Aeronautics & Space Administration

Contents

I. Introduction	1
II. DSN Systems Design	3
A. DSN Monitoring System, <i>M. I. Yeater</i>	3
B. Functional System Design Within the DSN Ground Communications System, <i>J. F. Walker</i>	6
C. Simulation Data Conversion Center, <i>J. W. Gustafson</i>	7
III. DSN Inherent Accuracy Project	8
A. Introduction, <i>T. W. Hamilton</i>	8
B. Tracking Data Inherent Accuracy Analysis: DSIF Two-Way Doppler Inherent Accuracy Limitations, <i>D. W. Trask and T. W. Hamilton</i>	8
C. Tracking Data Inherent Accuracy Analysis: Quality of Two-Way Doppler Tracking Data Obtained During the <i>Mariner IV</i> Mission, <i>D. W. Trask</i>	13
D. Orbit Accuracy as a Function of Doppler Sample Rate for Several Data Taking and Processing Modes, <i>D. W. Curkendall</i>	20
E. Theoretical Basis for the Double-Precision Orbit Determination Program (DPODP), <i>T. D. Moyer</i>	24
References	27
IV. Communications Research and Development	29
A. Digital Communication Tracking: A Phase-Locked Receiver Analysis Program, <i>R. C. Tausworthe</i>	29
B. Efficient Data Systems: Error Probability Estimation With Loss-of-Lock Indication, <i>E. C. Posner, J. Ashlock, and S. Lurie</i>	34
C. Efficient Data Systems: Punctured Cyclic Coder-Decoder, <i>W. A. Lushbaugh</i>	35
D. Frequency Generation and Control: Wide-Band Distribution Amplifier, <i>G. D. Thompson</i>	36
E. Frequency Generation and Control: S- and X-Band Central Frequency Synthesizer, <i>G. U. Barbani</i>	39
F. Experimental Closed Cycle Refrigerators (CCR) for Masers, <i>E. R. Wiebe and W. H. Higa</i>	41
G. Continuous Wave (CW) Signal Power Calibration With Thermal Noise Standards, <i>C. T. Stelzried and M. S. Reid</i>	41
H. Simultaneous Lobing Radiometric Tracking System, <i>B. Seidel</i>	48
I. Microwave Maser Development, <i>R. C. Clauss and W. H. Higa</i>	51
J. Venus Station Operations, <i>E. B. Jackson and A. I. Price</i>	53
References	54

Contents (Cont'd)

V. Communications Development Engineering	56
A. Venus Station 1-Mw High Voltage Power Supply, <i>R. E. Arnold</i>	56
B. Waveguide Transfer Switch, <i>R. C. Chernoff</i>	61
C. 455-kc Doppler System, <i>R. B. Crow</i>	62
D. Venus Station <i>Mariner IV</i> Post-Encounter Receiver, X-Band Lunar Radar Receiver, and S-Band Planetary Radar Receiver, <i>C. F. Foster</i>	66
E. DSN/MSFN 20-kw Transmitters, <i>R. L. Leu</i>	72
VI. Tracking Stations Engineering and Operations	73
A. Station Control and Monitor Console Subsystem, <i>G. Jenkins</i>	73
B. Antenna Pointing Subsystem, <i>W. C. Frey</i>	74
C. Telemetry and Command Processors, Phase II, <i>A. Burke</i>	76
D. Antenna Engineering, <i>F. W. Stoller</i>	77
E. Demonstration Doppler Monitor Program, <i>F. B. Leppla</i>	83
F. Goldstone Operations, <i>J. Orbison</i>	84
VII. Flight Project Activities	87
A. <i>Pioneer VI</i> Trajectory Characteristics, <i>R. A. Wallace</i>	87
B. <i>Pioneer VI</i> Orbit Determination Results, <i>J. E. Ball</i>	87
C. <i>Pioneer VI</i> High Frequency Doppler Noise, <i>W. D. Chaney</i>	90
D. <i>Lunar Orbiter</i> Project: Introduction and Early Flight Path Analysis, <i>J. P. Brenkle</i>	92
E. Sensitivities of a <i>Lunar Orbiter</i> to the Lunar Gravity Harmonics, <i>A. Liu</i>	95
F. <i>Apollo</i> Project Activities, <i>D. W. Curkendall</i>	100
G. Goldstone Tracking and Testing Operations, <i>J. Orbison</i>	101
References	102

I. Introduction

The Deep Space Network (DSN), established by the NASA Office of Tracking and Data Acquisition, is under the system management and technical direction of JPL. The DSN is responsible for two-way communications with unmanned spacecraft travelling from approximately 10,000 miles from Earth to interplanetary distances. Tracking and data-handling equipment to support these missions is provided. Present facilities permit simultaneous control of a newly launched spacecraft and a second one already in flight. In preparation for the increased number of U.S. activities in space, a capability is being developed for simultaneous control of either two newly launched spacecraft plus two in flight, or four spacecraft in flight. Advanced communications techniques are being implemented to provide the possibility of obtaining data from, and tracking spacecraft to, planets as far out in space as Jupiter.

The DSN is distinct from other NASA networks such as the Scientific Satellite Tracking and Data Acquisition Network (STADAN), which tracks Earth-orbiting scien-

tific and communication satellites, and the Manned Space Flight Network (MSFN), which tracks the manned spacecraft of the *Gemini* and *Apollo* programs.

The DSN supports, or has supported, the following NASA space exploration projects: (1) *Ranger*, *Surveyor*, *Mariner*, and *Voyager* Projects of JPL; (2) *Lunar Orbiter* Project of the Langley Research Center; (3) *Pioneer* Project of the Ames Research Center, and (4) *Apollo* Project of the Manned Spacecraft Center (as backup to the Manned Space Flight Network). The main elements of the network are: the Deep Space Instrumentation Facility (DSIF), with space communications and tracking stations located around the world; the Ground Communications System (GCS), which provides communications between all elements of the DSN; and the JPL Space Flight Operations Facility (SFOF), the command and control center.

The DSIF tracking stations are situated such that three stations may be selected approximately 120 deg apart in longitude in order that a spacecraft in or near the ecliptic

plane is always within the field of view of at least one of the selected ground antennas. The DSIF stations are:

<i>Station No.</i>	<i>Name</i>	<i>Location</i>
11	Goldstone, Pioneer	Barstow, California
12	Goldstone, Echo	Barstow, California
13	Goldstone, Venus (research and development)	Barstow, California
14	Goldstone, Mars (under construction)	Barstow, California
41	Woomera	Island Lagoon, Australia
42	Tidbinbilla	Canberra, Australia
51	Johannesburg	Johannesburg, South Africa
61	Robledo	Madrid, Spain
62	Cebreros (under construction)	Madrid, Spain
71	Spacecraft Monitoring	Cape Kennedy, Florida
72	Spacecraft Guidance and Command (under construction)	Ascension Island

JPL operates the U.S. stations, and will operate the Ascension Island Station. The overseas stations are normally staffed and operated by government agencies of the respective countries, with the assistance of U.S. support personnel.

The Spacecraft Monitoring Station supports spacecraft final checkout prior to launch, verifies compatibility between the DSN and the flight spacecraft, measures spacecraft frequencies during countdown, and provides telemetry reception from lift-off to local horizon. The other DSIF stations obtain angular position, velocity (doppler), and distance (range) data for the spacecraft, and provide command control to (up-link), and data reception from (down-link), the spacecraft. Large antennas, low noise phase-lock receiving systems, and high-power transmitters are utilized. The 85-ft diameter antennas have gains of 53 db at 2300 Mc, with a system temperature of 55°K, making possible the receipt of significant data rates at distances as far as the planet Mars. To improve the data rate and distance capability, a 210-ft diameter antenna is under construction at the Goldstone Mars Station, and two additional antennas of this size are planned for installation at overseas stations.

In their present configuration, all stations with the exception of Johannesburg, are full S-band stations. The Johannesburg receiver has the capability for L- to S-band conversion. The Spacecraft Guidance and Command Sta-

tion will be basically full S-band when it becomes operational.

It is the policy of the DSN to continuously conduct research and development of new components and systems and to engineer them into the network to maintain a state-of-the-art capability. Therefore, the Goldstone stations are also used for extensive investigation of space tracking and telecommunications techniques, establishment of DSIF/spacecraft compatibility, and development of new DSIF hardware and software. New DSIF-system equipment is installed and tested at the Goldstone facilities before being accepted for system-wide integration into the DSIF. After acceptance for general use, it is classed as Goldstone Duplicate Standard (GSDS) equipment, thus standardizing the design and operation of identical items throughout the system.

The GCS consists of voice, teletype, and high-speed data circuits provided by the NASA World-Wide Communications Network between each overseas station, the Spacecraft Monitoring Station, and the SFOF. Voice, teletype, high-speed data, and video circuits between the SFOF and the Goldstone stations are provided by a DSN microwave link. The NASA Communications Network is a global network consisting of more than 100,000 route mi and 450,000 circuit mi, interconnecting 89 stations of which 34 are overseas in 18 foreign countries. It is entirely operationally oriented and comprises those circuits, terminals, and switching equipments interconnecting tracking and data acquisition stations with, for example, mission control, project control, and computing centers. Circuits used exclusively for administrative purposes are not included.

During the support of a spacecraft, the entire DSN operation is controlled by the SFOF. All spacecraft command, data processing, and data analysis can be accomplished within this facility. The SFOF, located in a three-story building at JPL, utilizes operations control consoles, status and operations displays, computers, and data-processing equipment for the analysis of spacecraft performance and space science experiments, and communication facilities to control space flight operations. This control is accomplished by generating trajectories and orbits, and command and control data, from tracking and telemetry data received from the DSIF in near-real time. The SFOF also reduces the telemetry, tracking, command, and station performance data recorded by the DSIF into engineering and scientific information for analysis and use by scientific experimenters and spacecraft engineers.

II. DSN Systems Design

A. DSN Monitoring System

M. L. Yeater

The previous article on the Deep Space Network Monitoring System (DSN MS) stated the purpose and objectives for the Phase I monitoring system (SPS 37-36, Vol. III). A general description of the DSN Monitor Area which is a subsystem of the DSN MS was given. This and subsequent SPS articles will detail the Phase I design and operation of the DSN MS.

1. DSN MS/ ϕ 1 Functional Description

The Phase I DSN MS will be comprised of four subsystems (Fig. 1), namely:

- (1) Deep Space Instrumentation Facility Monitoring Subsystem (DSIF MS/ ϕ 1)
- (2) Ground Communications System Monitoring Subsystem (GCS MS/ ϕ 1)
- (3) Space Flight Operations Facility Monitoring Subsystem (SFOF MS/ ϕ 1)
- (4) Deep Space Network Monitor Area Subsystem (DSN MAS/ ϕ 1)

The DSIF MS/ ϕ 1, the GCS MS/ ϕ 1, and the SFOF MS/ ϕ 1 will each provide an independent detailed real-time/near real-time monitoring and recording capability. In addition, sets of monitor data will be provided by each of the three subsystems to the DSN MAS for overall DSN system performance evaluation. These sets of monitor data provided by the three subsystems will be representative measurements along the DSN serial data stream from the DSIF sites through the GCS and the SFOF. The flow of the monitor data between the four subsystems of the DSN MS/ ϕ 1 is illustrated in Fig. 1.

2. DSIF MS/ ϕ 1

The Digital Instrumentation Subsystem (DIS), the Station Monitor and Control Console Subsystem (SMC) and the associated DSIF MS/ ϕ 1 Program (Fig. 1) are the principal elements in the DSIF MS/ ϕ 1. The DIS will scan performance and configuration outputs from the DSIF ground equipment such as the Microwave, Receiver, and Transmitter Subsystems for processing and recording on magnetic tape. In addition, the DIS will receive data or functional operating information from the Tracking Data Handling Subsystem (TDH), the SMC, and the Antenna Pointing Subsystem (APS). This information typically consists of tracking, doppler, angle, and

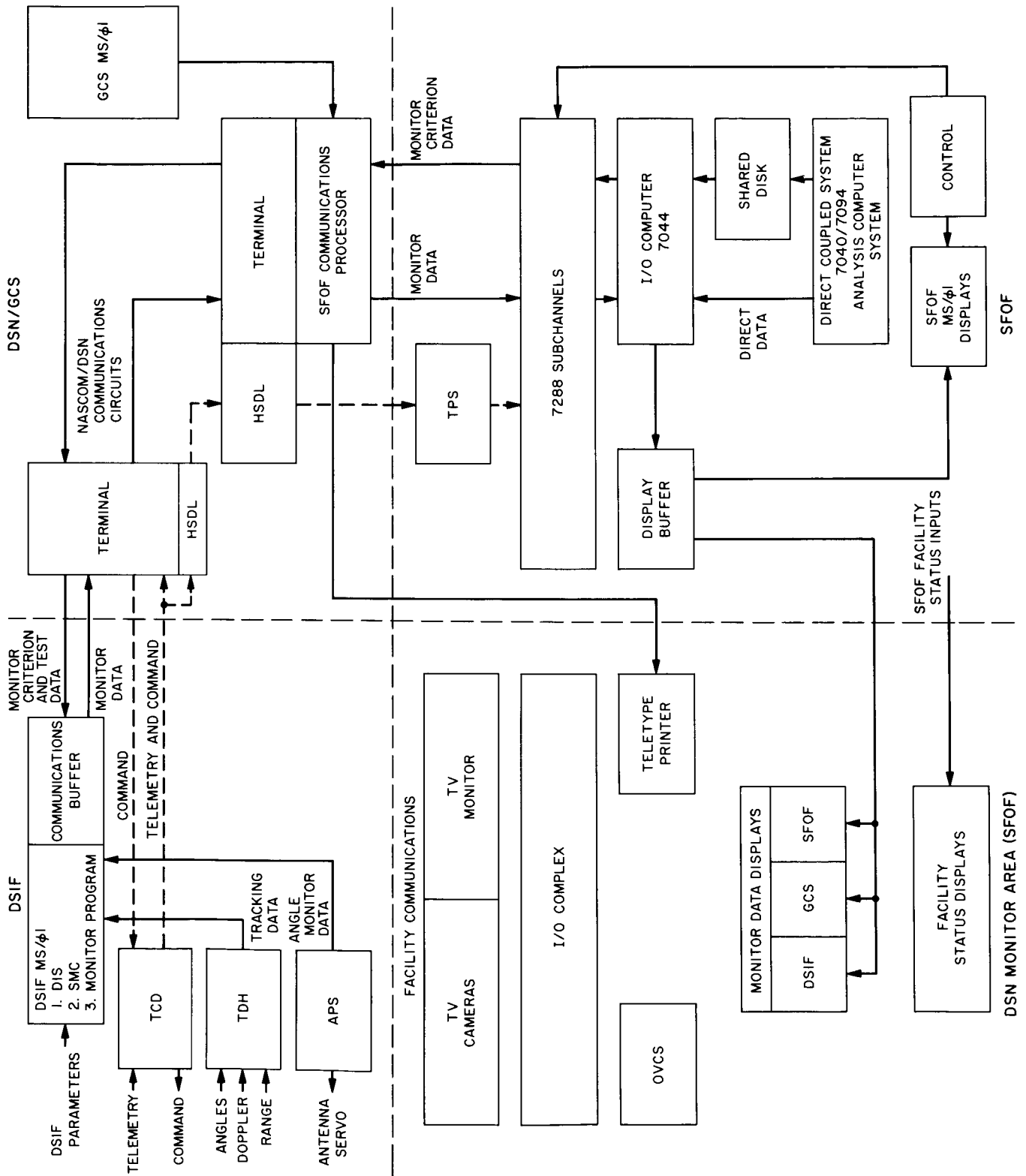


Fig. 1. Deep Space Network Monitoring System, Phase I

range data, and results of certain operation and diagnostic programs.

The monitoring data examined by the DIS will be evaluated in relation to Monitor Criterion Data primarily consisting of specified station configurations, nominal station performance, predicts, and specifications with tolerances applicable to the performance values.

DSIF Monitor Criterion Data as a function of time (mission phase) will be provided to the individual DSIF Monitoring Systems. Performance data, out-of-tolerance alarms, and failure alarms, including configuration go/no-go type decisions as determined by comparison of Monitor Criterion Data with the observed monitoring data, will be distributed to the SMC and to the SFOF for the DSN MAS/ ϕ 1 displays. The DIS output to the SMC will provide real-time performance data to the DSIF Station Manager to aid in instituting corrective action in the event of failure or non-nominal performance. Subsets of the monitor data will be periodically output by the DIS to the GCS for transmission to the SFOF for display within the DSN MAS/ ϕ 1.

3. GCS MS/ ϕ 1

The elements of the GCS MS/ ϕ 1 are the NASCOM/DSN communications circuits, including the High-Speed Data Line (HSDL) circuits, and the SFOF Communications Processor (Fig. 1). Monitoring of the GCS for the DSN MS/ ϕ 1 will be based mainly on (a) the detection of circuit activity, and (b) limited performance measurements, based on parity and/or format checking of portions of the mission-dependent data by the SFOF Communications Processor (CP). The capability to monitor block error rate of data conveyed by the NASCOM furnished HSDL will be accomplished at data block level by use of separate error detection encoders/error detection decoders, should a project utilize NASCOM HSD formats. The block error detection outputs of the decoders will be processed by the SFOF CP to provide outputs to the GCS MS/ ϕ 1 and DSN MAS/ ϕ 1.

4. SFOF MS/ ϕ 1

The SFOF MS/ ϕ 1 basically will be a reworking and expansion of the Data Processing Control Console (DPCC) already in existence, with extensions in capability as required for meeting the requirements of the DSN MAS/ ϕ 1. The SFOF MS/ ϕ 1 (Fig. 1) will monitor the operational status of all major hardware elements in the SFOF Data Processing System (DPS), as well as

the status of the programs operating in the I/O computer, and the flow of data through the various elements of the DPS. Functions such as DPS configuration, program mode, data loss during processing, and program failure to execute will be indicated.

The information provided by the SFOF MS/ ϕ 1 will be used (a) to warn operational personnel of actual or impending failures, (b) to aid in failure isolation, (c) to facilitate rapid recovery from failures, (d) to aid in evaluating the validity of DPS outputs, and (e) to aid in control of the DPS under standard and non-standard conditions.

The major hardware component of the SFOF MS/ ϕ 1 is the set of monitor displays which will be located in the Data Processing Control Area (DPCA). There will be three types of displays, each named for the category of information presented: Data Status, Processing Status, and Equipment Status.

5. DSN MAS/ ϕ 1

The major elements of the DSN MAS/ ϕ 1 are the Monitor Area located in the SFOF and its associated hardware elements (Fig. 1), a DSN Monitor and Analysis Team, the DSN MAS/ ϕ 1 software which resides in the Display Buffer and the I/O computers, and sets of raw, processed, and recorded data from various elements of the DSN. As such, the DSN MAS/ ϕ 1 brings together in a central location the people, the data, and the facilities to permit monitoring and evaluation of the DSN performance as a system. The functions to be performed by the DSN MAS/ ϕ 1 are:

- (1) DSN performance monitoring and analysis.
- (2) DSN data monitoring and analysis.
- (3) DSN data validation and analysis.

The operational consistency and integrity of the DSN MS/ ϕ 1 as a system will be assured through control of the Monitor Criterion Data by the DSN MAS/ ϕ 1. Initialization procedures for providing approved sets of Monitor Criterion Data to the DSN MS/ ϕ 1 subsystems from the DSN MAS/ ϕ 1 will be provided. The DSN MAS/ ϕ 1 Area Chief will be responsible for maintenance and distribution, and, at systems start time, for advising each computer system which set of uniquely defined initialization parameters will be used. Closed-loop tests will then be conducted, controlled, and approved by the DSN MAS/ ϕ 1 Area Chief prior to the monitoring system run time.

6. DSN MS/ ϕ 1 Status

The set of functional specifications for the DSN MS/ ϕ 1 and its four subsystems have been completed, and implementation plans and scheduling documents are now being written.

B. Functional System Design Within the DSN Ground Communications System

J. F. Walker

The DSN/GCS Development Plan establishes ground rules for the development of the DSN/GCS. A new document, the DSN/GCS Functional Specification, will specify detailed system design requirements to a functional level.

Four logical phases have been proposed for establishing a DSN/GCS functional system design, as follows:

1. Phase I

This phase involves the establishment of a functional specification for the 1 January 1967 DSN/GCS system design. Since much of the system design for this time period is already under way, this specification will reflect current planning as well as existing capabilities. A baseline will be provided upon which to accomplish Phases II, III, and IV.

2. Phase II

A system study will be completed during this phase, which will explore communications requirements and concepts through 1970. The following are some of the major areas which will be considered:

- (1) Future projects, NASCOM, and operational requirements through 1970.
- (2) System philosophies within the SFOF and DSIF to insure overall end-to-end compatibility.
- (3) *Voyager* requirements to provide for a system which can be upgraded in an orderly manner to support this project.

Some of the technical areas whose impact on the future DSN/GCS must be considered are:

- (1) Site communications processors.
- (2) High-speed data block transmissions on a message switching basis.
- (3) Communications satellites.
- (4) State-of-the-art advances in the communications field.

It is anticipated that completion of a system study will involve joint participation between the DSN/GCS Project Engineer and the DSIF and SFOF in the form of working groups.

The end result of the system study will be to provide a system design baseline for Phases III and IV and a mechanism for DSN approval through requirements/objectives documents.

3. Phase III

During this phase, a developmental plan will be established for the DSN/GCS through 1970. This plan will provide for an orderly development process to provide a system embodying those concepts explored in Phase II which have been approved by the DSN. Included will be capability updates and expansion of the DSN/GCS on a step-by-step basis with full back alternatives available at each step.

DSN review and approval of the DSN/GCS Development Plan will provide guidelines for accomplishment of Phase IV.

4. Phase IV

Functional specifications will be established for the DSN/GCS through 1970. These specifications will provide direction for system development. It is anticipated that two specifications will be written:

- (1) Functional Specification, DSN/GCS, 1969.
- (2) Functional Specification, DSN/GCS, 1971.

In addition, normal updates based on new requirements and the results of increased system performance analysis will be provided at 6-month intervals.

C. Simulation Data Conversion Center

J. W. Gustafson

The Simulation Data Conversion Center (SDCC) is designed to provide a centralized facility within the SFOF to accomplish the following functions:

- (1) To provide a control center for the conduct of DSN certification and training tests.
- (2) To provide an interface for the generation and insertion of simulated data into the SFOF for use in hardware and computer program validation, and personnel training.
- (3) To provide a means of generating prerecorded simulated data for use at the remote Deep Space Stations (DSS) during DSN tests.
- (4) To provide a source of real-time simulated data for insertion into the DSS sites via the NASA Ground Communications System (NASCOM) consistent with on-site capabilities for receiving and utilizing such data.

In order to provide support to the flight projects during the development of the facility, the implementation has been organized into two stages or phases. Progress in this development has been reported previously in SPS 37-35, Vol. III, and in SPS 37-37, Vol. III. The purpose of this article is to report the current status in the development and use of the center.

1. Phase I Development

Development of the Phase I configuration is complete, and the facility is in daily use in support of *Surveyor* and

Lunar Orbiter mission tests. To aid in this support, certain modifications and additions have been made:

- (1) The *Surveyor* TV simulator, including camera and lunar panorama, has been moved into the SDCC mission-dependent equipment area from another area of the SFOF. Interface hardware has been designed and installed to permit automated camera control by the PDP-1 computer.
- (2) A high-speed Data Products line printer has been attached to the PDP-1. This supplements the console typewriter, which was much too slow for bulk output during real-time operations.
- (3) A third IBM 729VI digital tape transport has been installed on the PDP-1 computer.

2. Phase II Development

The SDCC Phase II development, designed to provide a two-mission simulation capability and improved real-time control, is proceeding according to plan. Recent hardware acquisitions include a PDP-4 digital computer which will be used for input-output processing and for data quality monitoring. Current activities are centered around the detailed definition of interfaces between the SDCC and the SFOF Communication Processor and Data Processing System. Concurrently, definition of mission independent software is under way, with the goal of providing a software package which will be ready for testing and evaluation in June 1966. This schedule will permit the timely integration of a larger digital computer, which is now under procurement, as a major element in the two-mission system. The Phase II facility is intended to be available for operational use in mid-September. Prior to that time, the Phase I capability will be maintained to provide interim support to the flight projects.

III. DSN Inherent Accuracy Project

A. Introduction

T. W. Hamilton

The DSN Inherent Accuracy Project was formally established by the DSN Executive Committee in July 1965. Its goals are:

- (1) To determine and verify the inherent accuracy of the DSN as a radio navigation instrument for lunar and planetary missions.
- (2) To formulate designs and plans for refining this accuracy to its practical limits.

Meeting of these goals is a cooperative task of the JPL Telecommunications and Systems Divisions. To accomplish these goals, the project holds regular monthly meetings to coordinate and to initiate activities that are relevant. The project leader and his assistant are authorized to task project members to conduct analyses of proposed experiments, prepare reports on current

work, and write descriptions of proposed experiments. Further, the Inherent Accuracy Project is authorized to deal directly with flight projects, utilizing the DSN regarding data gathering procedures which bear on inherent accuracy.

B. Tracking Data Inherent Accuracy Analysis: DSIF Two-Way Doppler Inherent Accuracy Limitations

D. W. Trask and T. W. Hamilton

1. Introduction

Although the DSIF data type that is commonly referred to as two-way doppler has consistently exceeded the quality necessary for the successful fulfillment of the

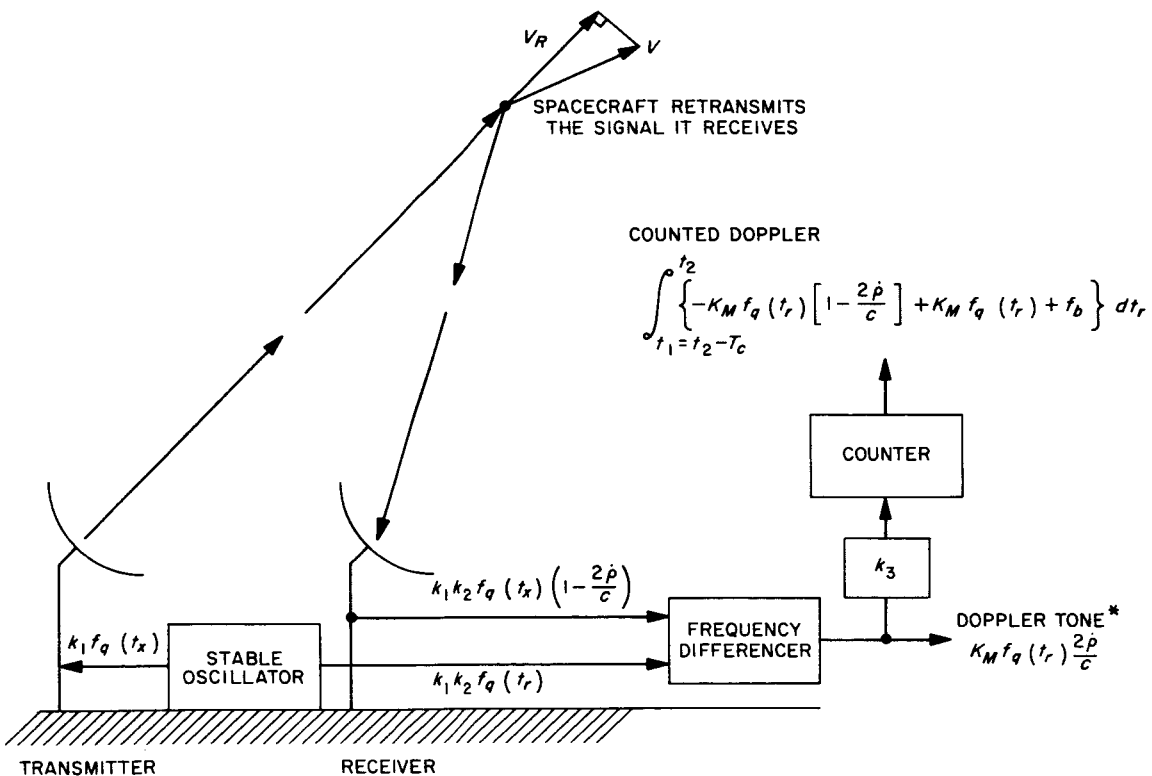
Earth-based radio guidance role to which it has been committed, an effort is continually in progress to improve the quality of this data. This paper surveys two of the factors which can limit the quality of this data, namely doppler counter quantization and transmitter stability. The expected magnitude of the errors contributed by each of the above offenders is presented as a function of time starting with the *Ranger III* lunar mission, in January 1962, and extending towards the advanced planetary missions, circa 1970.

2. Doppler Data Type

The two-way DSIF doppler data configuration is illustrated in Fig. 1. The tracking station transmits a signal to the spacecraft, the signal received at the spacecraft is shifted in frequency by the doppler effect, and then the spacecraft retransmits the received signal. The signal received at the ground receiver has been further doppler-shifted by the radial velocity of the receiver with respect

to the spacecraft. The difference between the received frequency and the current transmitter frequency is called the doppler tone. In practice, the doppler tone is continuously counted, and this continuous count is sampled at fixed time intervals. Relatively high sampling rates of between 1 sec and 1 min are employed for data editing purposes. For the orbit determination process, performed during noncritical portions of a mission or in postflight analyses, the "effective" sample intervals of 10^3 to 10^4 sec may be used. In effect then, the continuously counted doppler is the range difference between the observer and spacecraft which is accumulated over a fixed count interval T_c . The change in range, as observed at the DSIF station, is expressed as follows:

$$c_2(t_2, t_1) \approx \int_{t_1=t_2-T_c}^{t_2} \left\{ K_M \left[-f_q(t_x) \left(1 - \frac{2\dot{\rho}}{c} \right) + f_q(t_r) \right] + f_b \right\} dt_r \quad (1)$$



* THE DOPPLER TONE f_d IS A MEASURE OF THE RADIAL SPEED V_R

$K_M = k_1 k_2 k_3$

INJECTION OF f_b IS NOT ILLUSTRATED

Fig. 1. Simplified doppler system

where

$t_2 - t_1 = T_c$, the count time over which the range difference is accumulated

t_r = the time that the signal left the transmitting antenna

$t_r = t_x + \tau$, where τ is the signal transit time from the transmitter to the spacecraft and back to the receiver

$f_q(t_r)$ = transmitter oscillator frequency at time t_r

f_b = bias frequency

$\dot{\rho}$ = range rate between the spacecraft and the tracking station

c = velocity of light

K_M = constant which represents the multiplication that is performed on the transmitter frequency to bring it up to the effective frequency at the doppler counter.

3. Transmitter Frequency Stability

An error is introduced into f_z which is directly proportional to the net change in the transmitter frequency during the time $[\tau]$ that the signal is in transit from the transmitter to the spacecraft and back to the receiver.

That is, the transmitter is not perfectly stable and

$$f_q(t_r) = f_q(t_x + \tau) \quad (2)$$

is in general different than $f_q(t_x)$. The error in c_2 that is most sensitive to variations in f_q is given by

$$\Delta\rho_{TS} = \frac{c}{2f_q(t_2)} \int_{t_1=t_2-T_c}^{t_2} [f_q(t_r) - f_q(t_x)] dt_r \quad (3)$$

Where $\Delta\rho_{TS}$ is in units of meters. If we define

$$\bar{f}_\tau(b) \equiv \frac{1}{T} \int_{t_1=b-(T/2)}^{t_2=b+(T/2)} f_q(t) dt \quad (4)$$

Then for $\tau \leq T_c$, Eq. (3) can be expressed as

$$\Delta\rho_{TS} = \tau \left(\frac{c}{2f_q} \right) \left[\bar{f}_\tau \left(t_2 - \frac{\tau}{2} \right) - \bar{f}_\tau \left(t_2 - \frac{\tau}{2} - T_c \right) \right] \quad (5)$$

At lunar distance $\tau = 3$ sec, and for $\rho = 1.5$ AU $\tau = 1500$ sec. For purposes of this paper, it is assumed that

$T_c = 10^3$ sec is used at the lunar distance, and $T_c = 10^4$ sec is used at 1.5 AU. Therefore, the $\tau \leq T_c$ condition necessary for Eq. (5) will be realized.

Next, the expected variation in the transmitter frequency is defined, using the expected value operator $E\{\}$, as follows:

$$\Delta\bar{f}_\tau = \left[E \left\{ \left[\bar{f}_\tau \left(t_2 - \frac{\tau}{2} \right) - \bar{f}_\tau \left(t_2 - \frac{\tau}{2} - T_c \right) \right]^2 \right\} \right]^{1/2} \quad (6)$$

To date, the DSIF has utilized voltage controlled oscillators (VCO) under strict temperature control and rubidium standards. Development is in progress towards the introduction of hydrogen masers into the DSIF. For the purposes of Fig. 2, the actually observed variation in transmitter frequency over the T_c, τ region of interest for f_z is approximated by

$$\frac{\Delta\bar{f}_\tau}{f_q} = \frac{k_{osc}}{\tau^{1/2}} \quad (7)$$

for all three of these frequency references. Now for $\tau \leq T_c$

$$\sigma_{\Delta\rho_{TS}} = \frac{1}{2} c k_{osc} \tau^{1/2} \quad (8)$$

White frequency noise is an example of the type of oscillator behavior which would satisfy Eq. (7). In actual

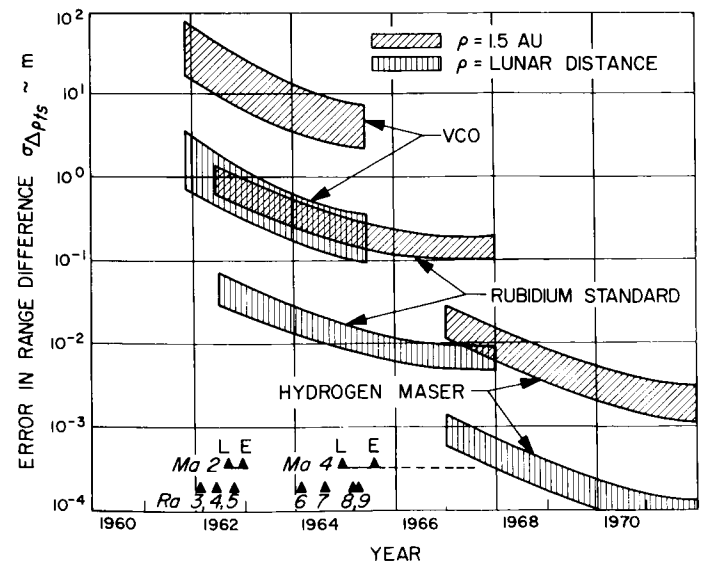


Fig. 2. Transmitter frequency stability

experience, Eq. (7) seems a reasonable approximation, however, the constant k_{osc} tends to be dependent on T_c . That is, k_{osc} tends to decrease with T_c for $T_c < 400$ sec.

The behavior of k_{osc} experienced during past missions with the VCO and the rubidium standard is summarized in Table 1. Notice that, during a mission, the actual performance of the oscillator may vary considerably. During *Mariner IV* it was noticed that when a new rubidium standard was introduced, a "breaking in" period occurred during which its performance improved.

Table 1. Oscillator stability

Frequency reference	Spacecraft	Data source	k_{osc} variation, $\text{sec}^{1/2}$	
			Minimum	Maximum
Temperature controlled VCO	Ra 3	Ref. 1	2.5×10^{-9}	3.0×10^{-9}
	Ma 2	Ref. 2	4.1×10^{-9}	5.3×10^{-9}
	Ra 6	Ref. 3	1.3×10^{-9}	1.9×10^{-9}
	Ra 7	Ref. 4	5.4×10^{-10}	7.7×10^{-10}
Rubidium standard	Ma 2	Unpublished	1.1×10^{-10}	2.7×10^{-10}
	Ma 4	Unpublished	2.5×10^{-11}	4.7×10^{-11}
Hydrogen maser, estimated	1967	—	2×10^{-12}	5×10^{-12}
	1972	—	2×10^{-13}	5×10^{-13}

The error in range attributed to frequency over the period considered is illustrated in Fig. 2. The event markers for the *Ranger III* to *IX* (lunar) missions as well as for the launch and target encounter of the *Mariner II* (Venus) and *Mariner IV* (Mars) missions are superimposed on this figure. As small as this range error appears with the rubidium standard, it still was the largest "visible high frequency" noise on the *Mariner IV* doppler data for $T_c < 600$ sec. For $T_c > 600$ sec and the spacecraft near Mars ($\dot{r} > 16$ km/sec), the software used to process the tracking data became the dominant noise source. This is due to the limited (single) precision of the orbit determination program as explained in a subsequent article (Sect. C).

4. Doppler Counter Quantization Error

Doppler counters read out an integral number of events. For example, in the *L*-band system used for the *Ranger* missions, it recorded the integral number of positive-going zero crossings of the doppler detector output during a preselected time period. This means that the counter reading can differ from the "true count" by up to plus-or-minus 1 cycle. That is, the count period may be started anywhere from just before a zero crossing to just after

a zero crossing. This results in a uniform distribution of counter start errors ranging from 0 to 1 count too long. Similarly the end count will be a uniform distribution ranging from 0 to 1 count too short. The net result is a triangular distribution for round-off errors, with a standard deviation as shown in Eq. (9).

$$\sigma_{\Delta p_{RO}} = \frac{LC}{6^{1/2}} \quad (9)$$

where LC is the value of the least count, in units of distance.

The past and projected history of this error source is illustrated in Figs. 3 and 4. The least count was 0.156 m for the *L*-band system used during the *Ranger* missions which counted every other zero crossing. The *S*-band system first used for the *Mariner* Mars missions had an $LC = 0.065$ m for the every other zero crossing ($\times 1$) system. Shortly after *Mariner IV* launch, a counter was modified at DSIF 11 (Goldstone) to count every zero crossing ($\times 2$, $LC = 0.032$ m), and by April 1965 an experimental $\times 8$ counter ($LC = 0.008$ m) was installed at the station.

Although a $\times 2$ system is the standard mode for the *S*-band stations, work is proceeding towards developing an operational $\times 8$ system as well as an *N*-count resolver which will record the time lapse between the start of the "fixed time" count interval and the first zero crossing during this interval. The LC for a given system will be proportional to the frequency into the "fixed time" counter, that is, it will vary as a function of the spacecraft radial velocity. For the range of lunar and planetary missions which the DSIF is normally required to support, an $LC < 0.0004$ m can be realized with a 100 Mcps

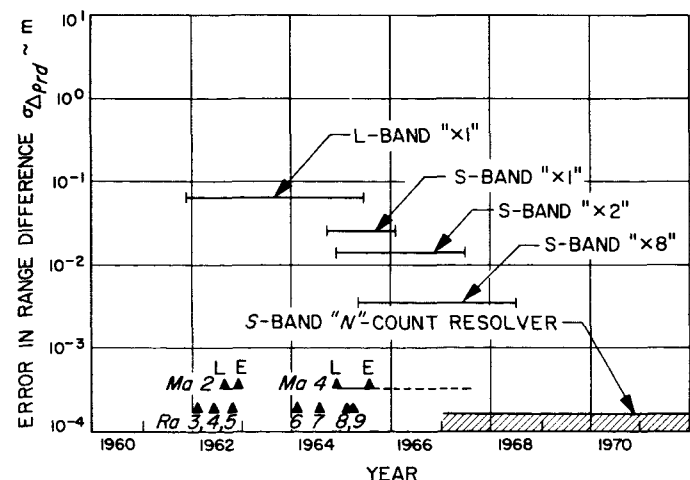
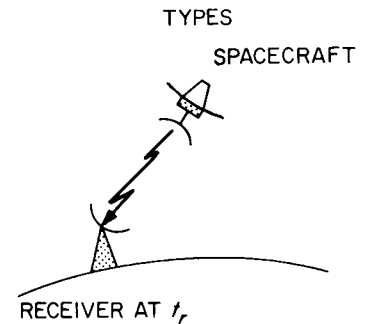
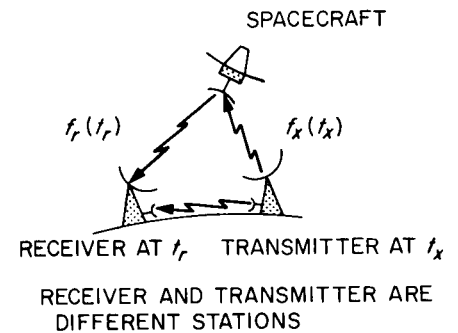


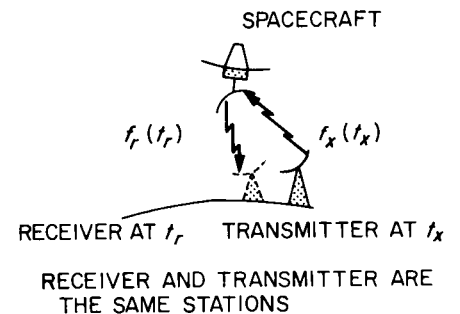
Fig 3. Doppler counter quantization

a. ONE-WAY DOPPLER (f_1):b. COHERENT THREE-WAY DOPPLER (f_{c3}):

$f_r(t_r)$ AND $f_t(t_r)$ ARE COHERENTLY DIFFERENCED AT THE RECEIVING STATION; THIS CONFIGURATION WAS USED DURING THE *Ma II* (VENUS) MISSION BY UTILIZING THE MICROWAVE LINK BETWEEN TWO OF THE GOLDSTONE STATIONS; i.e., DSIF 12 TRANSMITTED, AND DSIF 11 RECEIVED

c. TWO-WAY DOPPLER (f_2):

A SPECIAL CASE OF COHERENT THREE-WAY DOPPLER

d. THREE-WAY DOPPLER (f_3)

NORMALLY THE TRANSMITTING AND RECEIVING STATIONS ARE LOCATED ON DIFFERENT CONTINENTS, AND NO MICROWAVE LINK IS AVAILABLE TO ALLOW THE COHERENT DIFFERENCING OF $f_r(t_r)$ AND $f_t(t_r)$

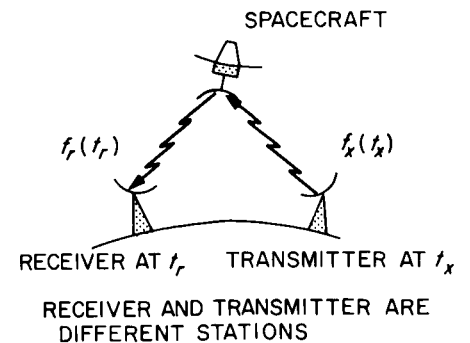


Fig. 4. DSIF doppler data

N-counter. Although Earth-based radio guidance considerations generally do not require this small a quantization error, it can be very useful at *small* sample intervals to monitor spacecraft motion due to the attitude control system (limit cycle motion) or programmed turns which

occur in preparation for a midcourse maneuver. This monitoring would provide an accurate time history of the velocity imparted to a spacecraft during a midcourse maneuver, and it could serve in lieu of, or provide a backup for, the spacecraft telemetry data.

5. Other Error Sources

Future issues of SPS, Vol. III, will contain articles discussing the DSIF tracking data inherent accuracy limitations due to other sources. A partial list includes tropospheric and ionospheric refraction, space plasma, spacecraft motion, DSIF antenna motion, DSIF station locations, time synchronization of the DSIF stations to a time reference, knowledge of universal time and ephemeris time, signal time lags through the spacecraft transponder and the DSIF station, ephemerides, miscellaneous forces on the spacecraft (particle impacts and expulsion, attitude control system, and solar pressure), and other model errors in the "fitters universe" assumed by the Orbit Determination Program.

Although the size of the apparent contribution which each of the above makes to the tracking data is important, this section of the SPS will also be concerned with the item of primary importance, navigational accuracy. Error sources that affect navigational accuracy include the determinations of physical constants such as the masses of the Earth, Moon and target body, the astronomical unit, station locations, and orbital elements of the target body and the Earth-Moon system.

In addition to f_2 , which is the primary DSIF doppler data type, future issues will discuss the one-way (f_1) and three-way doppler (f_3) data as illustrated in Fig. 4 as well as combinations (differenced doppler) of these data types.

C. Tracking Data Inherent Accuracy Analysis: Quality of Two-way Doppler Tracking Data Obtained During the Mariner IV Mission

D. W. Trask

1. Introduction

The noise characteristics observed on the two-way doppler during the *Mariner IV* mission (S-band system)

are reviewed in this report. The doppler noise is presented as a function of the doppler count interval (compared to the *Ranger VII* mission, L-band) and of the spacecraft distance from Earth (compared to the *Mariner II* Venus mission, L-band). The magnitude of the total high-frequency noise for the S-band system is generally $\frac{1}{3}$ that for the L-band system in units of meters per second for a range of comparable conditions. A transmitter frequency stability of 3 to 3.5 parts in 10^{12} was experienced for a signal round-trip time in excess of 400 sec and a 60-sec doppler averaging time. The software used during the orbit determination process is a significant contributor to the "observed" high-frequency doppler noise; and after 1 May 1965, it is a dominant term for doppler averaging times above 600 sec.

2. Variation of Noise with Count Interval

The observed standard deviation on two-way doppler is presented as a function of the count interval over which the doppler has been compressed. Fig. 5 compares *Ranger VII* L-band data with *Mariner IV* S-band data, where both systems counted every other doppler zero crossing (" $\times 1$ " system). Both the *Ranger VII* and the *Mariner IV* data is from the second Goldstone pass after launch. The *Mariner IV* data is of higher quality than the *Ranger VII* data on a cycle per second comparison basis (under a wide range of comparable conditions it is a factor of 3 better for meters-per-second units in that a cycle at L-band is roughly equivalent to 2.4 cycles at S-band). For purposes of comparison, a curve is shown which illustrates the expected standard deviation if the roundoff error at the doppler counter was the only error source present on the data.

The doppler counter quantization error limits the improvement ratio between the L- and S-band systems. If both of these systems had had " $\times 8$ " counters¹ (such as existed at DSIF 11, Goldstone, starting in April 1965), then the S-band system would have (for the conditions of Fig. 5 for a doppler count time, T_c , of 60 sec) $\frac{1}{3}$ the high-frequency noise of the L-band system for two-way doppler (f_2).

A *Mariner IV* pass, 6 days from launch, is compared to one 41 days from launch in Fig. 6 for the case of the every-zero crossing counter. The high-frequency noise

¹The "effective frequency" at the doppler counter for the $\times 8$ system is 8 times the S-band frequency, i.e., 1 count on the doppler counter = 65 mm for the $\times 1$ system, 32 mm for the $\times 2$ system, and 16 mm for the $\times 8$ system.

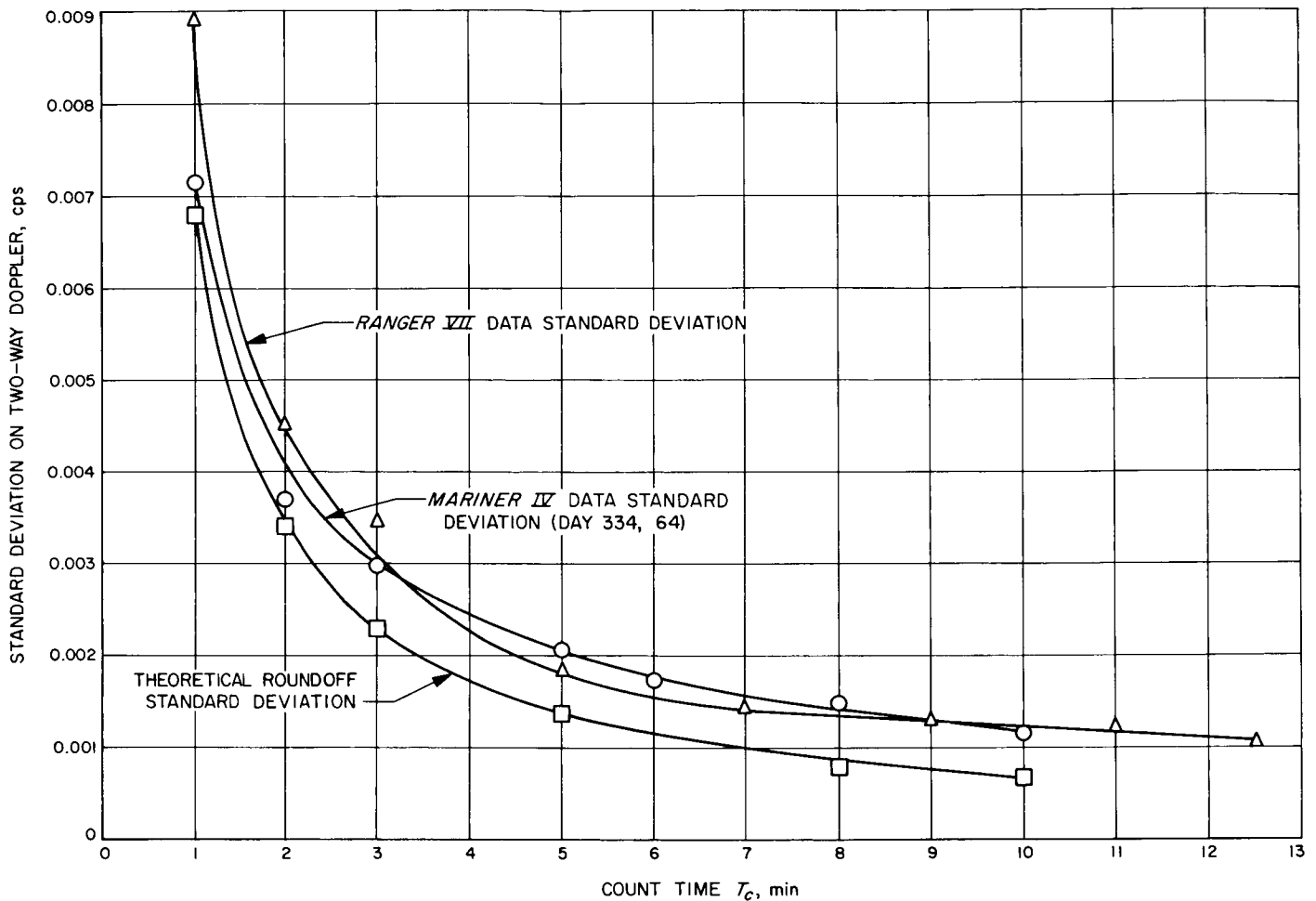


Fig. 5. Data standard deviations for Ranger VII (L-Band) and Mariner IV (S-Band) doppler count based on every other zero crossing, " $\times 1$ "

has shown a marked increase over the 35 days which elapsed between the two passes.

A Mariner IV pass, 129 days from launch utilizing the " $\times 8$ " doppler counter, is shown in Fig. 7. Again, it is seen that the doppler noise has continued to increase over that shown in Figs. 5 and 6.

The standard deviations illustrated in Figs. 5 through 7 were obtained by fitting one pass (approximately 10 hr) of data individually with the Orbit Determination Program (where data taken below a 17 deg elevation angle was rejected). This has the effect of illustrating only the high-frequency component of the doppler noise.

The effects of various error sources tend to be separated when the data noise is presented in the form of Figs. 5 through 7. As $T_c \rightarrow 0$, quantization and phase jitter stand

out; however, as $T_c \rightarrow \infty$, "software noise" (limited precision in computing f_2) becomes dominant.

3. Variation of Noise with Day of Mission

The standard deviation of the high-frequency two-way doppler noise is shown in Fig. 8 versus the calendar day on which the data was taken. (All of the points have been adjusted by removing the theoretical quantization error due to the doppler counter so that the " $\times 1$," " $\times 2$ " and " $\times 8$ " data are presented together in a consistent manner.)* This figure illustrates more clearly the growth of noise with time that occurred with DSIF 11. A distinct jump

*The standard deviation due to roundoff at the doppler counter is $\sigma_{ro} = (LC)/T_c \cdot 6^{1/2}$ cps, where LC is the value of least count of the doppler counter in cycles, and T_c the doppler count time. The flagged symbols in Fig. 8 indicate 1-hr samples of Ma IV f_2 fit with either a 3rd or 4th order polynomial.

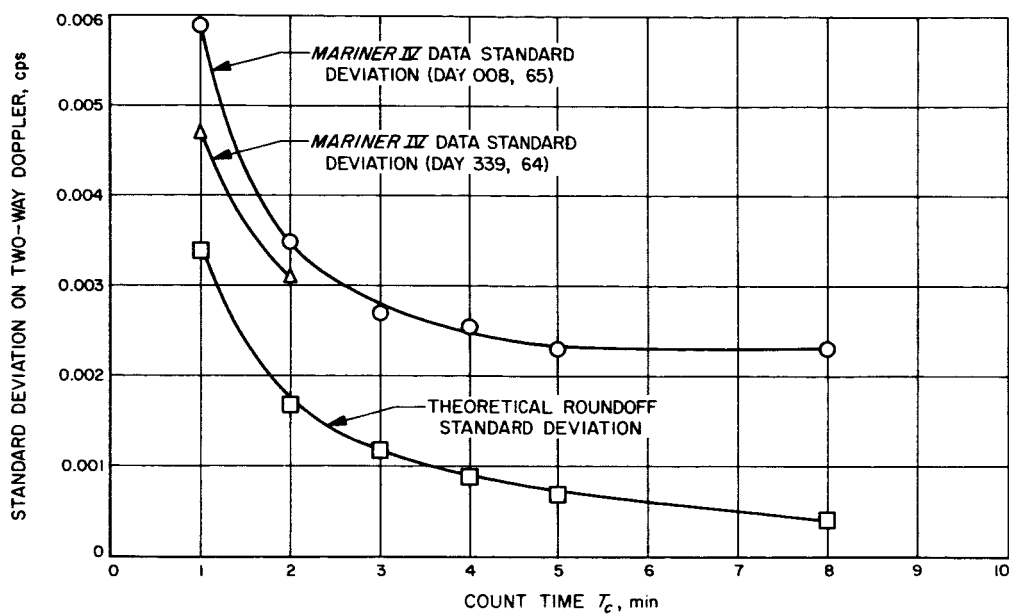


Fig. 6. Data standard deviations for Mariner IV (S-Band) doppler count based on every zero crossing, "x2"

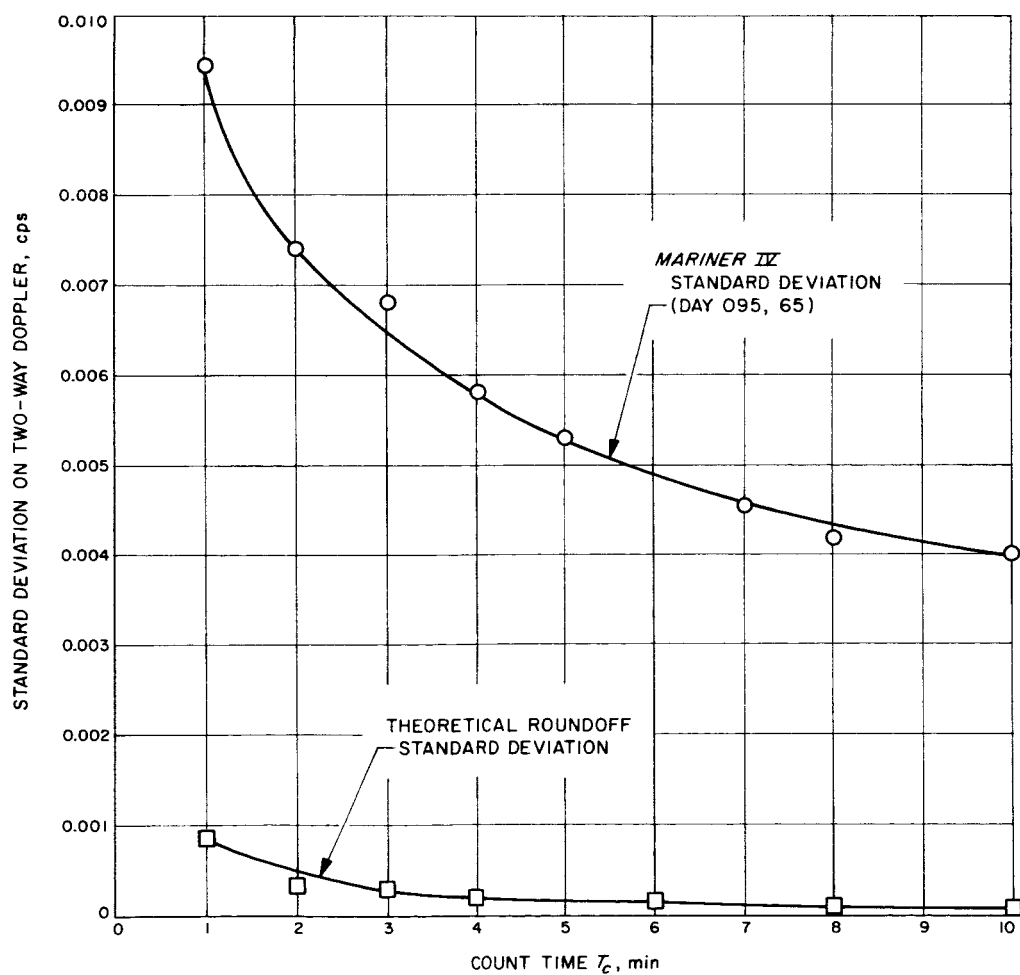


Fig. 7. Data standard deviations for Mariner IV (S-Band) doppler count based on "x8" data

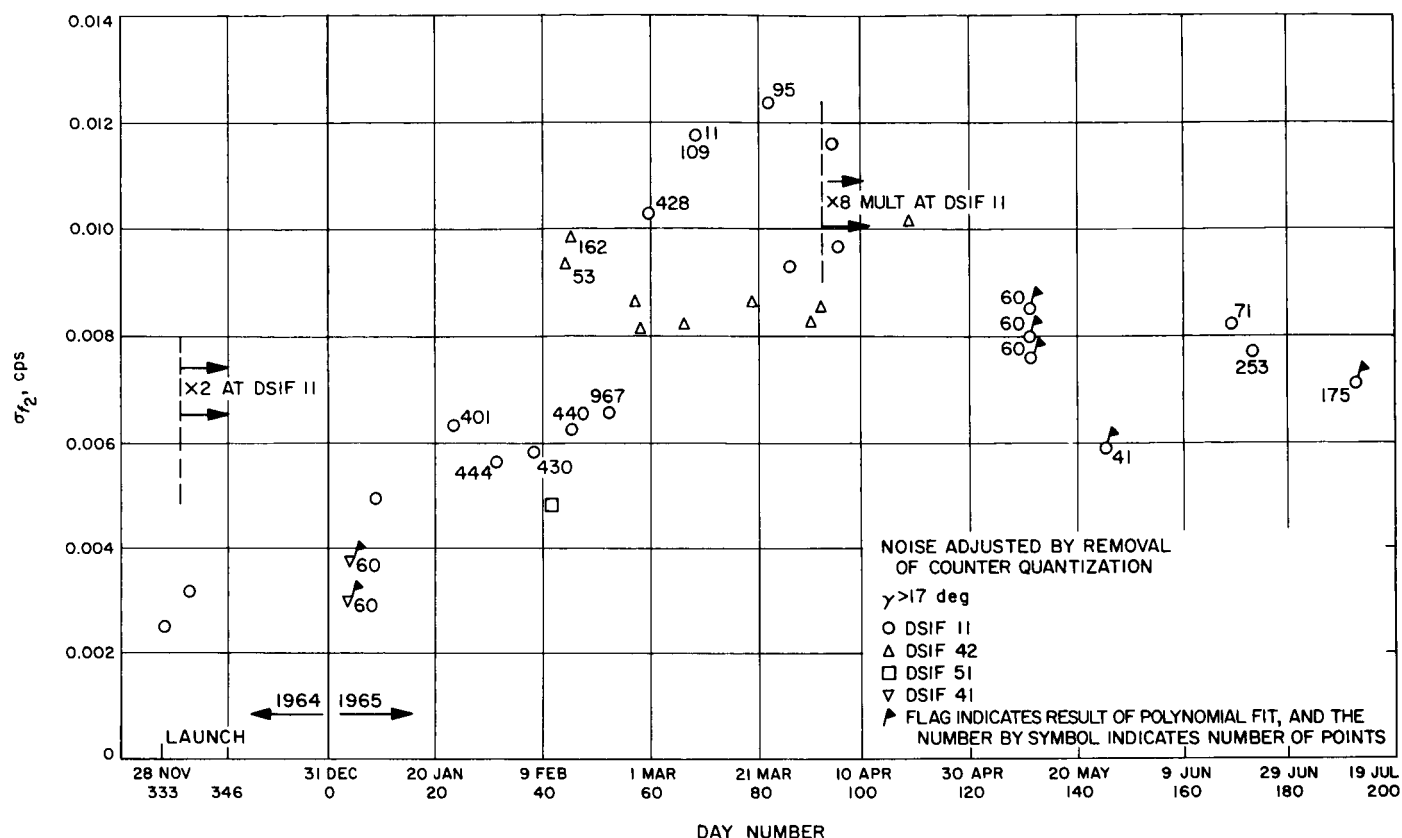


Fig. 8. Two-way doppler noise; $T_c = 60$ sec

in the DSIF 11 noise occurs near the end of February and lasts until the early part of April. Four rubidium frequency standards were being used alternately during this period. The unusually high noise level indicates that a "breaking in" period is experienced during which the performance of the frequency standard improves. The flagged symbols in Fig. 8 are based on data from R. Ball. They indicate that 1-hr samples of $Ma IV f_2$ were fit with either a 3rd or 4th order polynomial in time (as opposed to the ODP).

The trends of the $Ma II$ and of the $Ma IV$ doppler high-frequency (HF) noise are compared as a function of spacecraft geocentric range in Fig. 9. The $Ma II$ data was sampled every 60 sec, but the doppler was accumulated over only 50 sec ($T_s = 60$ sec, $T_c = 50$ sec). The empirical formula which fit the $Ra VII$ data (see Ref. 5) was used to adjust the $Ma II T_c = 50$ sec data to equivalent $T_c = 60$ HF noise. Both the actual and adjusted $Ma II$ data are shown on Fig. 9. The coherent three-way doppler (f_{c3}), with DSIF 12 transmitting and DSIF 11 receiving the signal from the spacecraft plus the DSIF reference frequency via microwave link (Ref. 6), did not show a

significant trend with spacecraft geocentric range, i.e., signal round-trip transit time, τ . This suggests that the HF noise on the microwave link between DSIF 11 and 12 masked the effect due to transmitter instability for the τ experienced during the $Ma II$ mission. After the doppler counter roundoff error has been eliminated, the f_{c3} ($Ma II$) HF noise is 10 times (in m/sec) the noise experienced on f_2 ($Ma IV$) near Earth for $T_c = 60$ sec.

4. Noise Contribution Due to Software

The contribution to the two-way doppler noise on DSIF 11 due to software is illustrated in Fig. 10. This HF computing noise arises in the final steps of computing the range rate at a given time point from the spacecraft ephemeris and tracking station positions. The error due to a truncation which takes place in the computation will have the form of a uniformly distributed bit error in the last position (because it represents a truncation, it will also bias the data). The magnitude of this error will be a function of how many of the available bits are needed to represent the whole number portion of \dot{p} . For the case of single precision, a number is represented by 27 bits.

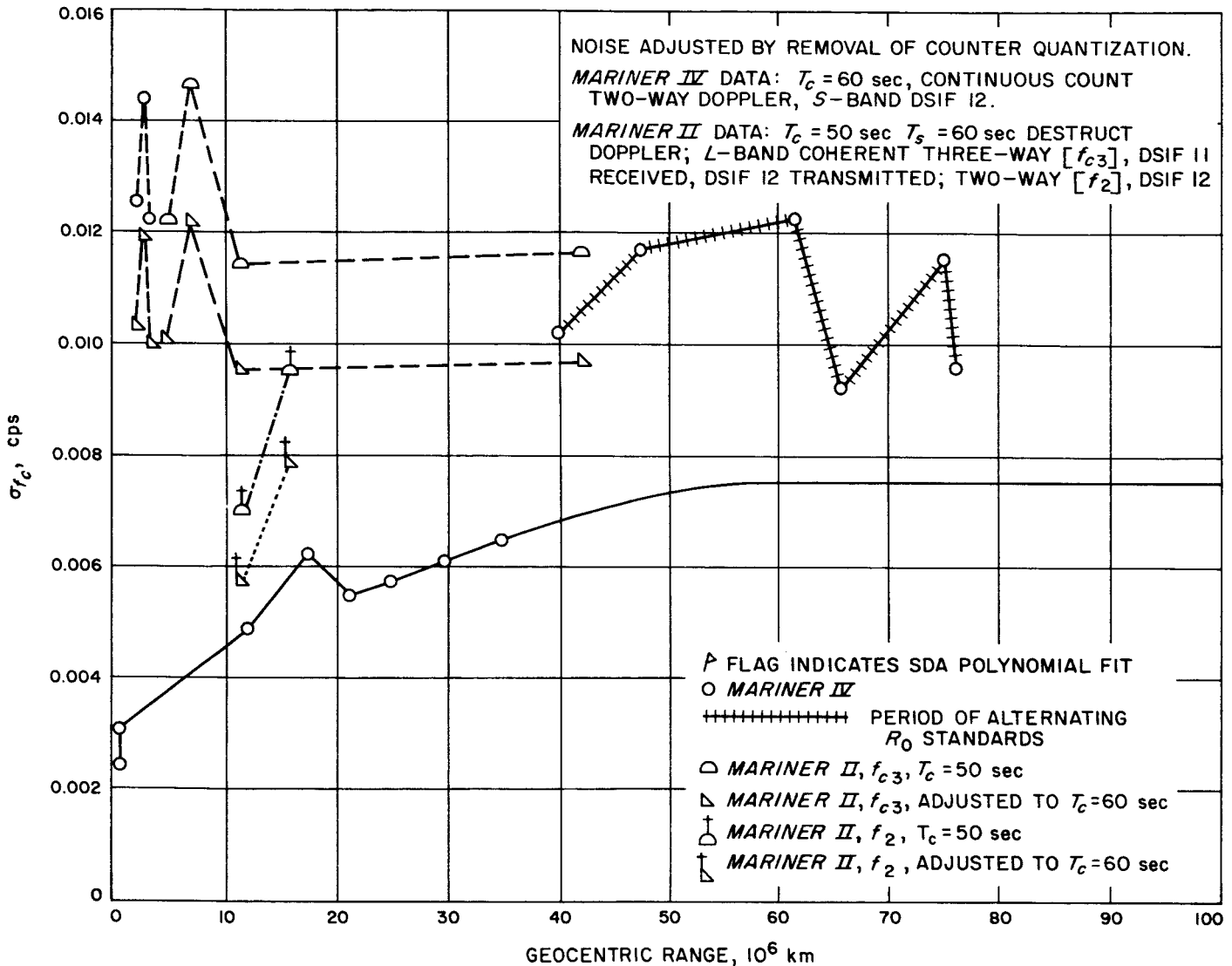


Fig. 9. Doppler noise comparison between Mariner II and Mariner IV

Therefore the formula for the value of the least significant bit (LBV) is

$$LBV = 2^{p-b}$$

where b is the number of available bits = 27 for single precision, and p is defined by $2^p < \dot{\rho} \text{ (km/sec)} \leq 2^{p+1}$ (or $2^p < f_{2,bs} \text{ (cps)} \leq 2^{p+1}$, see below).

The two-way doppler observable ($f_{2,bs}$) after the 1 Mc bias has been subtracted (in the case of S-band) is also involved in the computation of the doppler residual. Therefore, a formula similar to the above exists for $f_{2,bs}$ (cps). Fig 10 shows the time period during which $\dot{\rho}$ and $f_{2,bs}$ change in magnitude through a given exponent of 2.

The dotted curve indicates the least-bit value behavior (considering both $f_{2,bs}$ and $\dot{\rho}$) versus time. The actual size of the error in the ODP will be a function of how many truncations (at the highest "significance level") take place at a given time point during the computation of $f_{2,bs}$. That is, the noise due to software (σ_{sw}) has the form

$$\sigma_{sw} = (LBV) (m/3)^{1/2}$$

where m represents the number of "significant" truncations, and LBV the least-bit value. Notice that the dotted curve also represents the size of the error for $m = 3$.

A simulation was performed with the ODP in an effort to approximate the high-frequency noise contributed by

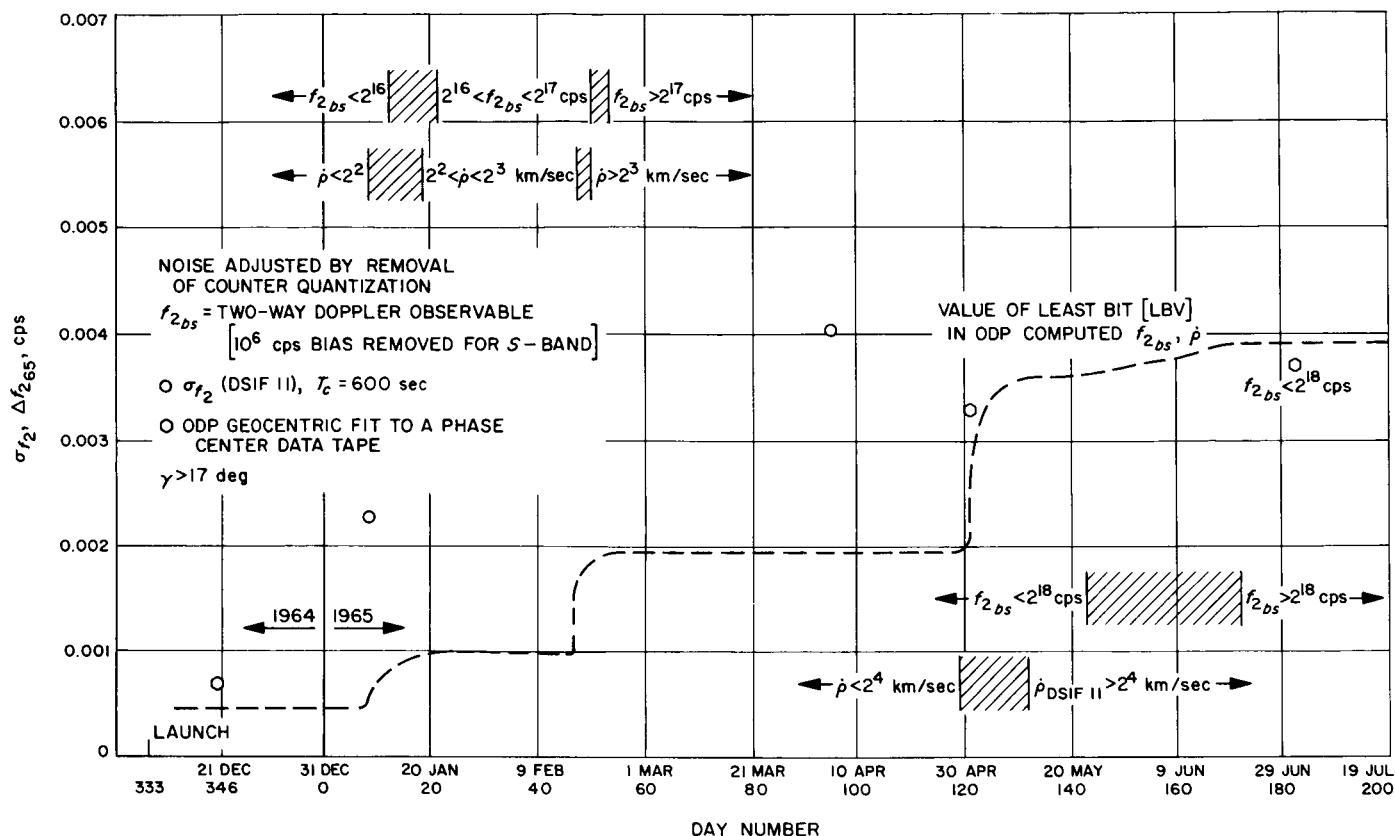


Fig. 10. Software contribution to noise on DSIF f_2 ; Mariner IV

the software. This was done by generating a clean data tape while running the trajectory in the phase center integration mode and then fitting the data while running the trajectory in the geocentric integration mode³. Three days were investigated, 10 December 1964, 1 May 1965, and 1 July 1965. (On 1 July 1965 the doppler simulated was below 2^{18} cps although data actually received that date exceeded 2^{18} cps.) In addition, the $T_c = 600$ sec points, based on Figs. 5 to 7 but adjusted for the quantization error, are shown on Fig. 9. These form an upper bound on the software contribution, i.e., notice in Fig. 5 that $\sigma_{f_2} = 0.0012$ cps at $T_c = 600$ sec for *Ranger VII*. However, both theory and an empirical fit (Ref. 5) to this data shows that the software contribution is negligible.

The f_2 HF noise (without the doppler counter quantization contribution) was computed for selected regions assuming 3, 6 and 9 "highest significance" truncations

($m = 3, 6$ and 9). These results are presented in Table 2 and plotted in Fig. 11. The $m = 0$ curve is based on the data presented in Fig. 8, which has an apparent scatter of ± 0.0005 cps. The doppler HF noise (after the software contribution has been extracted) should continue to increase with spacecraft geocentric range (actually τ) until, depending on the transmitter stability characteristics, it levels off after a sufficiently large τ . It would not be expected to decrease.

The contribution due to the single-precision computation of the doppler observable increased during the *Ma IV* mission, and based on this preliminary analysis (the material presented in Figs. 8, 10 and 11), the value is between 0.0035 and 0.004 cps after 1 May 1965. This compares to the total HF f_2 noise of 0.0096 cps at $T_c = 60$ sec and 0.004 at $T_c = 600$ sec on 5 April 1965 (Fig. 7)⁴, and (minus the effect of the doppler counter quantization) 0.0024 cps near Earth, $T_c = 60$ sec. Unlike the other error

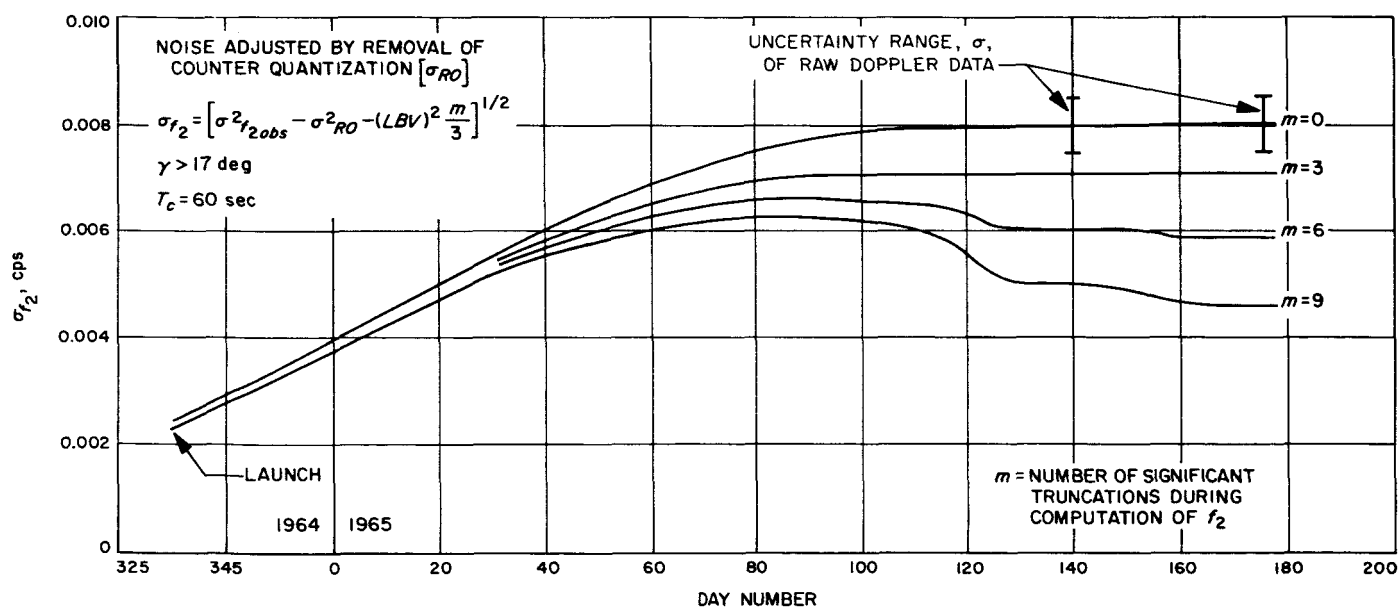
³This is somewhat of a heuristic approach in that some of the computations are common to both integration modes. A complete analysis has not been carried out to determine if these results are optimistic or pessimistic.

⁴These values were found during the high noise period at DSIF 11. The corresponding estimate for the normal system is between 0.007 and 0.008 cps at $T_c = 60$ sec and 0.0022 to 0.0025 cps at $T_c = 600$ sec for $\tau > 600$ sec.

Table 2. Effect of software noise on observed *Mariner IV* f_2 noise

Date (Day No.)	Observed f_2 noise "adjusted" by elimination of doppler counter roundoff, cps	Least bit value (LBV), cps	$\sigma_{\text{Software}}^a$, cps			f_2 Noise "adjusted" by elimination of software "noise" and doppler counter roundoff, cps		
			$m = 3$	$m = 6$	$m = 9$	$m = 3$	$m = 6$	$m = 9$
29 Nov 64 (334)	0.0024	0.00049	0.00049	0.00069	0.00085	0.00236	0.00231	0.00225
4 Dec 64 (339)	0.0035	0.00049	0.00049	0.00069	0.00085	0.00306	0.00302	0.00298
31 Jan 65 (31)	0.00555	0.00098	0.00098	0.00139	0.00170	0.00544	0.00537	0.00528
14 Feb 65 (45)	0.00612	0.00098	0.00098	0.00139	0.00170	0.00604	0.00597	0.00588
21 Feb 65 (52)	0.00645	0.00195	0.00195	0.00276	0.00338	0.00614	0.00583	0.00550
~20 May 65 (140)	0.008	0.0036	0.0036	0.0051	0.0062	0.0072	0.0062	0.0050
~25 June 65 (176)	0.008	0.0039	0.0039	0.0055	0.0068	0.0070	0.0058	0.0043

^a $\sigma_{\text{Software noise}} = (\text{LBV}) (m/3)^{1/2}$

Fig. 11. *Mariner IV*, f_2 computer truncated effects

sources considered, the software truncation effect is independent of T_c (in units of cps or m/sec). Although masked at $T_c = 60$ sec by transmitter instability the software "noise" is a dominant *Ma IV* f_2 HF error source beyond 1 May 1965 for $T_c > 600$ sec.

It should be noticed that the leveling off of the f_2 HF noise (after accounting for 0.0035 cps due to software) between 0.007 and 0.008 cps implies a transmitter stability between 3 to 3.5 parts in 10^{12} for a 60 sec doppler averaging

time. The data from Fig. 8 indicates a better stability below $\tau \approx 400$ sec.

5. Conclusions

The analysis of the *Mariner IV* doppler data has produced the following conclusions:

- (1) The rubidium standards maintained a frequency stability between 3.0 to 3.5 parts in 10^{12} for $T_c = 60$

sec and $400 \text{ sec} < \tau$. (The stability is better below $\tau \approx 400 \text{ sec}$.)

- (2) The limited (single) precision of the ODP contributes between 0.0035 cps and 0.004 cps (per a preliminary analysis) after 1 May 1965. This compares to transmitter instability which accounts for between 0.007 and 0.008 cps (the largest contributor) at $T_c = 60 \text{ sec}$ or between 0.003 and 0.004 cps at $T_c = 600 \text{ sec}$. (The software contribution is independent of T_c .) The total f_2 HF noise minus the effect of the doppler counter quantization was 0.0024 cps near launch.
- (3) The S-band system outperforms the L-band system by a factor of 3 in terms of HF f_2 noise in units of m/sec for a range of comparable conditions. The doppler counter quantization error tended to limit the improvement ratio (1 cps at L-band = 2.4 cps S-band in m/sec). If "×8" counters had been used in the S- and L-band systems, then the S-band systems would outperform the L-band system by a factor of 5 (in m/sec) near Earth at $T_c = 60 \text{ sec}$.
- (4) After eliminating the doppler counter quantization error, the coherent three-way doppler (f_{ca}) of *Ma II* has 10 times the HF noise as the *Ma IV* near Earth f_2 . The microwave link used between DSIF 11 and 12 during *Ma II* is the suspected cause of the added noise.

Acknowledgements. The bulk of the data presented here was gathered by C. Vegas, C. Cary, G. Null, and G. Pease in support of the *Mariner IV* Project and as a result of the analysis of the *Mariner IV* data for the *Apollo* Project.

D. Orbit Accuracy as a Function of Doppler Sample Rate for Several Data Taking and Processing Modes

D. W. Curkendall

1. Summary

In a typical doppler tracking data handling system, the observed doppler shift frequency between the station and the spacecraft is integrated by counting the doppler cycles with an electronic counter. In this note, the

resultant orbit accuracy is determined analytically for a one-dimensional problem (rectilinear motion) assuming that these integrated doppler frequency measurements are corrupted by white phase noise. Several methods of taking and processing the data are treated:

- (1) Destructively-counted doppler.
- (2) Continuously-counted, differenced doppler.
- (3) Continuously-counted, total count doppler.

The concept of minimum variance (MV) versus uniformly weighted (UW) estimation is introduced into the analysis to show the relative power and complexity of using the continuously counted data as either differenced or total count doppler. It is found that by destructively counting the data, much of the inherent accuracy of the doppler system is lost. The analysis also shows that, even though MV estimates yield identical results for either (2) or (3), the UW estimate utilizing the data as total-count doppler can be made considerably more powerful than the corresponding estimate employing differenced data.

2. The Basic Model

Imagine that there is a spacecraft moving with constant but unknown speed, v , relative to a tracking station which is placed at the center of the Earth. This station is receiving a continuous signal whose frequency is directly proportional to v . There exists a device which integrates this frequency, yielding a phase measurement which is corrupted by white noise, i.e.,

$$\Phi_i = \phi(t_i) + \varepsilon(t_i)$$

where

Φ_i = measurement of phase at $t = t_i$,

$\phi(t_i)$ = true phase at t_i ,

$\varepsilon(t_i)$ = noise on the measurement with
 $E[\varepsilon(t_i)\varepsilon(t_j)] = \sigma^2\delta(t_i - t_j)$

$E[\cdot]$ denotes expected value of $[\cdot]$

$\delta(\cdot)$ is the Dirac delta function

What we basically wish to do is to obtain an understanding of our ability to determine from the tracking data the value of the unknown velocity of the spacecraft, v . In each case considered, the total observation time, T , will be held fixed and the resultant orbit accuracy will be expressed as a function of the number of data points, N , taken during T .

3. How Data Is Taken and Processed

a. Continuously counted data. Here, the total interval over which the spacecraft is observed, T , is broken into N measurements of the integral of the frequency. These measurements are spaced at even intervals, $\Delta t = T/N$. If this data is to be used as "differenced" doppler, each observation is formed

$$y_i = \frac{\Phi_i - \Phi_{i-1}}{\Delta t} = (\Phi_i - \Phi_{i-1}) N/T \quad (1)$$

If, however, a total count scheme is used, each measurement is differenced back to the original measurement to obtain the observation

$$y_i = \Phi_i - \Phi_0 \quad (2)$$

b. Destructive count data. In a practical destructive counting mechanization, a gate on the doppler counter is opened at an even time (GMT), and the time it takes for precisely n cycles of doppler to be counted is measured. The system then resets and stays idle until the next even GMT arrives. At this time the sequence is reinitiated. The essential feature of this system is that gaps appear in the counting sequence, destroying the coherence between successive observations. It is sufficient for our purposes here to analyze a similar counting scheme that retains this feature. In this equivalent scheme, phase measurements are taken according to the following schedule:

- (1) At $t = t_{11} = 0$.
- (2) At $t_{12} = \Delta t(1 - \alpha)$, where $0 < \alpha < 1$.
- (3) At $t_{21} = \Delta t$, $t_{22} = \Delta t(2 - \alpha)$, etc.
- (4) Additional measurements are made until the allowed length of time, T , has elapsed, as is shown in Fig. 12.

Each pair of measurements is differenced and divided by $\Delta t(1 - \alpha)$

$$y_i = \frac{\Phi_{i2} - \Phi_{i1}}{\Delta t(1 - \alpha)} \quad (3)$$

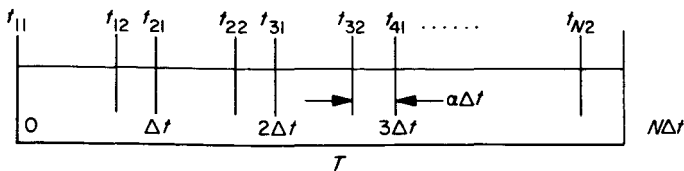


Fig. 12. Measurement scale

4. Results and Discussion

a. Destructively counted data. If the measurements given by Eq. (3) are combined in a single observation vector, then

$$y = \begin{bmatrix} y_1 \\ y_2 \\ \vdots \\ y_N \end{bmatrix} = \frac{1}{\Delta t(1 - \alpha)} \left\{ \begin{bmatrix} \phi_{12} - \phi_{11} \\ \phi_{22} - \phi_{21} \\ \vdots \\ \phi_{N2} - \phi_{N1} \end{bmatrix} + \begin{bmatrix} \epsilon_{12} - \epsilon_{11} \\ \epsilon_{22} - \epsilon_{21} \\ \vdots \\ \epsilon_{N2} - \epsilon_{N1} \end{bmatrix} \right\} \quad (4)$$

or

$$y = Av + \epsilon$$

where A is the $N \times 1$ matrix of $\partial y_i / \partial v$, i.e., in this case

$$A^T = [1, 1, 1, \dots, 1]$$

The covariance matrix of the noise vector is given by

$$\Lambda_\epsilon = E[\epsilon\epsilon^T] = \frac{2\sigma^2}{\Delta t^2(1 - \alpha)^2} I \quad (5)$$

where I is the $N \times N$ identity matrix.

If the data vector is used to determine v , the variance of the error in the MV estimate is given by Ref. 7 as

$$Q(N) = E[(v - v^*)^2] = (A^T \Lambda_\epsilon^{-1} A)^{-1} \quad (6)$$

where v^* is the estimate of the true speed, v . Substituting (5) into (6) and employing

$$\Delta t = T/N$$

we have

$$Q(N) = \frac{2\sigma^2 N}{T^2(1 - \alpha)^2} \quad (7)$$

Eq. (7) is plotted versus N in Fig. 13 which emphasizes the essential feature of this result that the estimate formed has error variance directly proportional to the number of data points taken during the fixed interval, T .

b. Continuously counted, differenced data. If a continuous-count method is employed and the observations are given by Eq. (1), then it can easily be shown that

$$\Lambda_\epsilon = \frac{2\sigma^2}{\Delta t^2} \begin{bmatrix} 1 & -\frac{1}{2} & 0 & 0 & \cdots & 0 \\ & 1 & -\frac{1}{2} & 0 & \cdots & 0 \\ & & 1 & -\frac{1}{2} & \cdots & 0 \\ & & & \ddots & \ddots & \vdots \\ \text{Sym} & & & & & -\frac{1}{2} \\ & & & & & 1 \end{bmatrix} \quad (8)$$

$$= \frac{2\sigma^2}{\Delta t^2} S$$

where S is the $N \times N$ "stripe" matrix as shown. The ij element of S^{-1} can be found in Ref. 8. It is

$$s_{ij}^{-1} = s_{ji}^{-1} = \frac{2i(n+1-j)}{(n+1)} \quad i \leq j \quad (9)$$

Again, employing Eq. (6)

$$Q(N) = \left[\frac{T^2}{2\sigma^2 N^2} \sum_{j=1}^N \sum_{i=1}^N s_{ij}^{-1} \right]^{-1} = \frac{12\sigma^2 N}{T^2 (N+1)(N+2)} \quad (10)$$

Eq. (10) is also plotted in Fig. 13, showing the contrasting result that the error variance is inversely proportional to the number of samples taken.

To obtain this error variance with differenced data involves the inversion of S and other difficult numerical operations in the formation of the MV estimate. It is customary to replace the MV estimate in favor of the simpler uniformly weighted, or UW, estimate. The resultant error variance is shown in Ref. 8 to be

$$Q(N) = (A^T W A)^{-1} A^T W \Lambda_\epsilon W A (A^T W A)^{-1} \quad (11)$$

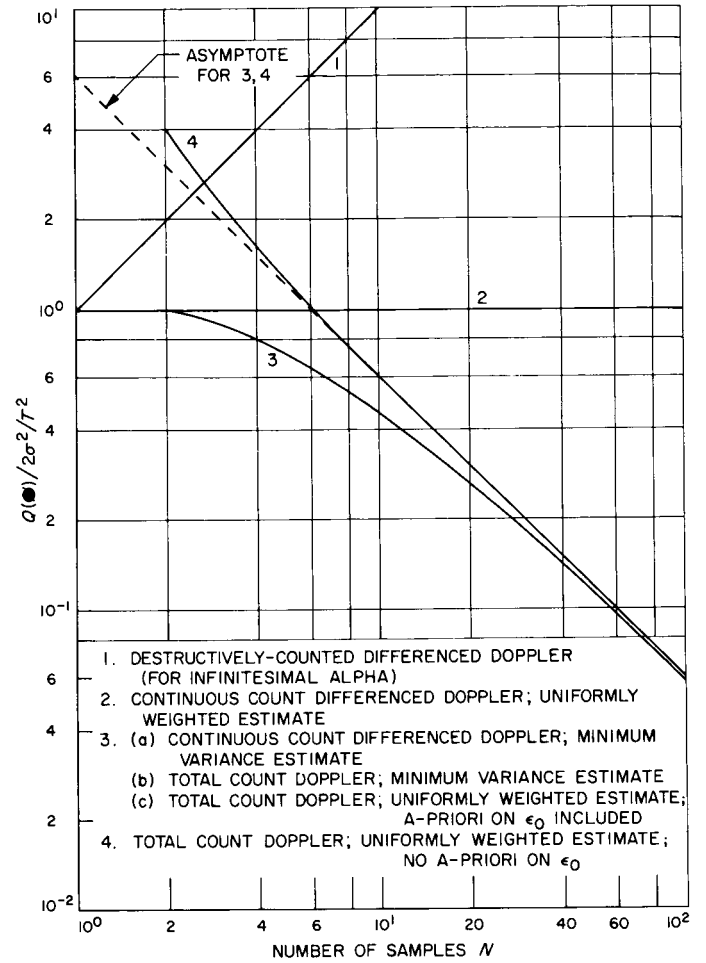


Fig. 13. Estimation accuracy, $Q(N)$, versus number of samples, (N) , for a fixed observation time, T

where $W = k^2 I =$ diagonal weighting matrix employed. Substitution of Eq. (8) into Eq. (11) yields the desired result,

$$Q(N) = \frac{2\sigma^2}{T^2} \quad (12)$$

For comparison, this is also plotted in Fig. 13.

c. Continuously-counted, total count doppler. If each phase measurement is differenced, not with the previous reading, but with the reading at the start of the data interval, the data vector becomes:

$$y = \begin{bmatrix} \phi_1 \\ \phi_2 \\ \vdots \\ \phi_N \end{bmatrix} + \begin{bmatrix} \epsilon_1 - \epsilon_0 \\ \epsilon_2 - \epsilon_0 \\ \vdots \\ \epsilon_N - \epsilon_0 \end{bmatrix} \quad (13)$$

Expressing Eq. (13) in terms of the unknown velocity, we have

$$y = \begin{bmatrix} (T/N) \\ 2(T/N) \\ \vdots \\ N(T/N) \end{bmatrix} v + \begin{bmatrix} \varepsilon_1 - \varepsilon_0 \\ \varepsilon_2 - \varepsilon_0 \\ \vdots \\ \varepsilon_N - \varepsilon_0 \end{bmatrix} \quad (14)$$

The covariance of the noise vector is

$$\Lambda_\varepsilon = \sigma^2 \begin{bmatrix} 2 & 1 & 1 & 1 & \cdots & 1 \\ & 2 & 1 & 1 & \cdots & 1 \\ & & 2 & 1 & \cdots & 1 \\ & \text{Sym} & & \ddots & \ddots & 1 \\ & & & & \ddots & 1 \\ & & & & & 2 \end{bmatrix} \quad (15)$$

This form of Λ_ε is numerically as difficult to handle as the stripe matrix that arose when dealing with the differenced doppler data. If, however, ε_0 is treated as a constant subject to estimation, Eq. (14) becomes

$$y = \begin{bmatrix} (T/N) & 1 \\ 2(T/N) & 1 \\ 3(T/N) & 1 \\ \vdots & \vdots \\ \vdots & \vdots \\ N(T/N) & 1 \end{bmatrix} \begin{bmatrix} v \\ -\varepsilon_0 \end{bmatrix} + \begin{bmatrix} \varepsilon_1 \\ \varepsilon_2 \\ \varepsilon_3 \\ \vdots \\ \vdots \\ \varepsilon_N \end{bmatrix} = A \begin{bmatrix} v \\ -\varepsilon_0 \end{bmatrix} + \varepsilon \quad (16)$$

Formulating the problem in this manner has the beneficial effect of creating a diagonal noise matrix

$$\Lambda_\varepsilon = \sigma^2 I \quad (17)$$

Substituting (17) and the $2 \times N$ A matrix given in Eq. (16) into (6) yields the 2×2 error variance for the estimation of v and ε_0 . We are only fundamentally interested in the scalar $E[(v - v^*)^2]$ and this is given by

$$Q(N) = \frac{12\sigma^2 N}{T^2(N^2 - 1)} \quad (18)$$

Eq. (18) is plotted in Fig. 13 and is seen to asymptotically approach the MV result for differenced doppler data. It is slightly above the preceding result, because in the estimation of ε_0 , no a-priori knowledge of ε_0 was used.

If this is inserted, the UW estimate using total-count data has error variance

$$Q(N) = \frac{12\sigma^2 N}{T^2(N+1)(N+2)} \quad (19)$$

making it identical to the MV estimate using differenced data.

5. Conclusions

It should be emphasized that all of the above is predicated on the assumption of white phase noise. This assumption gives rise to the unrealistic result that it is possible to drive the error variance to zero by simply sampling at a high enough rate. In a real situation, the noise between successive measurements would become correlated as the time between them became short. At this point, the simple equations presented here become invalid, and higher sampling rates bring no substantial improvement in orbit accuracy.

The extent to which these relationships may be generalized to include multi-dimensional estimates influenced by time varying A matrices is imperfectly understood, although one certainly suspects the correspondence is almost one-to-one in most reasonable situations. With these provisos in mind the following statements can be made:

- (1) Because the only properties of white noise that were used were (a) stationarity and (b) no correlation between points, all the relationships derived apply to physically realizable stationary phase noise as long as the count time is much longer than the correlation time.
- (2) Interrupting the doppler wave even for short intervals increases the error variance considerably over any other method treated. The implication is that any form of destructive counting seriously degrades the data quality in the presence of white, or other short correlation time, noise.
- (3) If the data is differenced and a UW estimate is made, the error variance will be independent of the sampling frequency. If a MV estimate is employed, the error variance will decrease with increasing sampling rate until the stipulation in (1) is violated.
- (4) By including the original noise value as a parameter subject to estimation, the UW estimate using total-count data is the MV estimate.

6. Plans for Future Work

The results presented in this note can be extended to the more general case of correlated noise. The specific case of exponentially correlated noise will be treated in a forthcoming note. The destructive count mechanism, even when used to minimize quantization error, is self-defeating and is of little continuing interest. Plans are being made to pursue the basic notions discussed here further. A deeper understanding of the multi-dimensional case is certainly to be desired, and the use of total-count doppler in post-flight (and perhaps real-time) orbit determination is an attractive possibility. As has already been mentioned, the results obtained with the white noise model readily extend to other circumstances, with the constraint that the noise must consist of bounded phase errors. That is, no frequency noise, which is integrated by the doppler counter, producing "random-walk" type (or unbounded) phase errors, can be treated with these techniques. Most of the readily identifiable doppler error sources (such as counter quantization and atmospheric effects) produce the simple phase errors treated here. One source that may not be the frequency standard itself, and a future note will develop the concepts needed to determine the character of frequency standard induced noise.

E. Theoretical Basis for the Double Precision Orbit Determination Program (DPODP)

T. D. Moyer

1. Introduction

A third-generation orbit determination program, called the Double Precision Orbit Determination Program (DPODP), is currently being developed at JPL. This program will be used to determine values of the parameters which specify the spacecraft trajectory for lunar and planetary missions. The program will be used for real-time and post-flight reduction of data. The DPODP differentially corrects a-priori estimates of injection parameters, physical constants, maneuver parameters, and station locations to minimize the sum of weighted

squares of residual errors between observed and computed quantities. The DPODP has more accurate mathematical models, a significant increase in computational accuracy, and more flexibility than the current (second-generation) Single Precision Orbit Determination Program (SPODP).

This article is the first of a series which will present the theoretical basis for the DPODP. The equations of motion, equations for computing the observables, partial derivatives of the observables with respect to the solve for parameters, and the statistical formulas will be described.

2. Differential Correction Process

Given the a-priori estimate of the parameter vector q , the program integrates the probe acceleration using the second-sum numerical integration method to give position and velocity at any desired time. Using the probe ephemeris along with the ephemerides for the other bodies within the solar system, and the parameter vector q , the ODP computes values for each observed quantity (normally doppler, range, or angles) and forms the observed minus computed (O-C) residuals. In addition to integrating the acceleration of the probe to obtain the probe ephemeris, the ODP integrates the partial derivative of the probe acceleration with respect to (wrt) the parameter vector q using the second-sum numerical integration procedure to give the partial derivative of the probe state vector X (position and velocity components) wrt the parameter vector q , $\partial X/\partial q$. Using $\partial X/\partial q$, the ODP computes the partial derivative of each computed observable quantity z wrt q , $\partial z/\partial q$. Given the (O-C) residuals, $\partial z/\partial q$, and the weights applied to each residual along with the a-priori parameter vector and its covariance matrix, the program computes the differential correction Δq to the parameter vector. Starting with $q + \Delta q$, the program computes a new probe ephemeris, residuals, and partial derivatives and obtains a second differential correction Δq . This process is repeated until convergence is obtained and the weighted sum of squares of residual errors between observed and computed quantities is minimized.

3. Subjects for Future Articles

a. Time transformations. The DPODP uses ephemeris time, ET; atomic time, AI; broadcast WWV time, UT1 (to compute the angular position of the Earth); and station time, ST, for each observing station. The transformations between the various time scales are represented

by time polynomials. The coefficients of these polynomials are generated from information supplied by the U.S. Naval Observatory.

b. Probe trajectory. The probe trajectory is obtained by a second-sum numerical integration of the probe acceleration relative to some central body. The center of integration will change with time and normally will be that body within whose sphere of influence the probe lies. It will be the Sun unless the probe is near a planet or the Moon. The acceleration of the probe relative to the center of integration is the Newtonian acceleration due to n non-spherical bodies, plus the acceleration due to solar radiation pressure, motor burns and spring separations, and operation of the attitude control system. Relativistic perturbative accelerations may also be added. When the center of integration is changed, the position and velocity are incremented by the position and velocity of the old center relative to the new center.

c. Corrected ephemerides. Numerically integrated ephemerides for the celestial bodies within the solar system are available for use by the DPODP. They consist of the heliocentric ephemerides of eight planets and the Earth-Moon barycenter and the geocentric lunar ephemeris. For any of these ephemerides, the orbital elements of an osculating conic at some epoch are solve for parameters. The ephemeris correction consists of the difference between the solve for conic and the osculating conic.

d. Heliocentric state vectors of probe and tracking stations. The observable quantities are computed from the heliocentric state vectors (position and velocity components) of the probe and tracking stations involved in the data type, where the vectors are referred to the mean Earth equator and equinox of 1950.0. The heliocentric state vector of the probe is the sum of the state vector relative to the center of integration and the heliocentric state vector of the center of integration, computed using the corrected lunar and planetary ephemerides. The heliocentric state vector of a tracking station is the sum of the body-centered state vector of the station and the heliocentric state vector of the body on which the station is located.

e. Light time solution. The probe and each tracking station involved in an observable quantity are known as direct participants, and each participant has an epoch of participation. If the observable is two-way doppler, a signal is transmitted from a tracking station on Earth toward the probe at the epoch t_1 . The signal is received

by the probe at the epoch t_2 and retransmitted toward the same tracking station on Earth, which receives the signal at the epoch t_3 . The heliocentric state vector of the receiving station is computed at t_3 . Solving the light time problem for the down leg gives the epoch t_2 and the heliocentric state vector of the probe at t_2 . Solving the light time problem for the up leg gives the epoch t_1 and the heliocentric state vector of the transmitting station at t_1 . The motion of light in the heliocentric (strictly barycentric) space-time frame of reference is obtained from general relativity.

f. Computation of observables. The observable quantities are computed from the parameter vector q and the heliocentric state vectors of each direct participant evaluated at their epochs of participation. The normal observable quantities are doppler, range, and angles. The observable equations account for the effects of general relativity. The computational accuracy for doppler observables is 10^{-5} meters per second.

g. Partial derivatives. The partial derivative of the observable z wrt the parameter vector q is formed from several sub-partial derivatives. Among them are (1) the partial derivatives of the observable z wrt the state vectors X (position and velocity components) of each direct participant, (2) the partial derivatives of each X wrt q and the partial derivatives of each epoch of participation wrt q , (3) special partial derivatives of z wrt parameters affecting the transformations between the various time scales, and (4) the partial derivatives of z wrt q holding the state vectors X of each participant constant.

The partial derivative of the heliocentric state vector of the probe wrt the parameter vector q is the sum of two terms corresponding to the state vector of the probe relative to the center of integration and the heliocentric state vector of the center of integration. Similarly, the partial derivative of the heliocentric state vector of each tracking station wrt q is the sum of two terms corresponding to the body-centered state vector of the station and the heliocentric state vector of the body on which the station is located.

The partial derivative of the probe state vector relative to the center of integration wrt the parameter vector q is obtained by numerical integration of the variational equations. The partial derivative of the probe acceleration wrt q is integrated numerically by the second-sum method, to give the partial derivative of the probe state vector relative to center wrt q .

h. Statistical formulas. The parameter estimation formula converts observed minus computed residuals to a differential correction of the solve for parameter vector, using the partial derivatives of the observables wrt the parameter vector and the weights applied to each residual. The weight applied to a given residual is the reciprocal of the effective variance of the observation. The criterion for parameter estimation is that the weighted sum-of-squares of residual errors between observed and computed quantities is minimized, where the a-priori estimates of the parameters are treated as observables, the computed values being the parameter estimates themselves. The method accounts for exact and inexact relations (constraints) between the solve for parameters.

Given the weights applied to each observation, the partial derivatives of each observable wrt the parameter vector q , and the a-priori covariance matrix for the parameter vector, the program computes the covariance matrix for the estimated parameter vector. The option is available to degrade the covariance matrix due to the uncertainty in parameters which affect the observables but which were not solved for.

4. Solve for Parameters

The parameters which the DPODP can solve for are the following:

a. Injection parameters. Rectangular components of injection position and velocity referred to mean Earth equator and equinox of 1950.0.

b. Reference parameters. The following parameters affect the position and velocity of the planets and the Moon:

A_E = astronomical unit, km/au. This factor converts the heliocentric ephemerides of eight planets and the Earth-Moon barycenter from astronomical units to units of kilometers.

R_E = scaling factor for lunar ephemeris, km/length unit. This factor converts the geocentric lunar ephemeris from dimensionless length units to kilometers.

E = osculating orbital elements for the ephemeris of a planet, the Earth-Moon barycenter, or the Moon.

μ_E, μ_M = gravitational constants for the Earth and Moon, km^3/sec^2 .

c. Gravitational constants. μ_i = gravitational constant for body i , such as the Sun, a planet, or the Moon. Note that μ_E and μ_M are also listed under reference parameters.

d. Harmonic coefficients. J_n, C_{nm}, S_{nm} = harmonic coefficients which, along with the gravitational constant μ , describe the gravitational field for a planet or the Moon.

e. Parameters affecting the acceleration of the spacecraft due to solar radiation pressure.

f. Parameters affecting the acceleration of the spacecraft due to operation of the attitude control system.

g. Parameters affecting spacecraft motor burns and spring separations.

h. Parameters affecting the transformation from universal time to ephemeris time.

i. Polynomial coefficients. These are used for transformation from tracking station time to broadcast WWV time (universal time).

j. Station parameters. Radius, latitude, and longitude or equivalent parameters for tracking stations or a landed spacecraft on a planet or the Moon. For a tracking ship, add velocity and azimuth.

k. Speed of light. This is an adopted constant which defines the light second as the basic length unit, normally not included in the solution vector.

l. Spacecraft transmitter frequency for one-way doppler.

m. Constant bias for observed range.

n. Constant biases to observed angles.

References

1. Sjogren, W. L., *The Ranger III Flight Path and Its Determination From Tracking Data*, TR 32-563, Jet Propulsion Laboratory, Pasadena, Calif., 15 September 1965.
2. Chaney, W. D., *Final Mariner II Tracking System Data Analysis Report*, TR 32-727, Jet Propulsion Laboratory, Pasadena, Calif., 1 September 1965.
3. Sjogren, Curkendall, Hamilton, Kirhofer, Liu, Trask, Winneberger, Wollenhaupt, *The Ranger VI Flight Path and Its Determination From Tracking Data*, TR 32-605, Jet Propulsion Laboratory, Pasadena, Calif., 15 December 1964.
4. Wollenhaupt, Trask, Sjogren, Piaggi, Curkendall, Winneberger, Liu, Berman, *The Ranger VII Flight Path and Its Determination From Tracking Data*, TR 32-694, Jet Propulsion Laboratory, Pasadena, Calif., 15 December 1964.
5. Trask, D. W., and Sjogren, W., "Radio Tracking of the Mariner and Ranger Missions and Its Implications," *IEEE Proceedings of 6th Winter Convention on Military Electronics*, Vol. IV, 3 February 1965.
6. Chaney, W. D., *Final Mariner II Tracking System Data Analysis Report*, TR 32-727, Jet Propulsion Laboratory, Pasadena, Calif., 1 September 1965.
7. Solloway, C.B., *Elements of the Theory of Orbit Determination*, EPD 255, Jet Propulsion Laboratory, Pasadena, Calif., December 9, 1964.
8. Marcus, M., "Basic Theorems in Matrix Theory," *NBS Applied Mathematics Series 57*, Government Printing Office, Washington, D.C., January 22, 1960.

IV. Communications Research and Development

A. Digital Communication Tracking: A Phase-Locked Receiver Analysis Program

R. C. Tausworthe

1. Introduction

The circuit responsible for much of the gains achieved in receiver technology today is an electronic servo-mechanism which operates as a coherent detector by correcting the frequency of its local oscillator continuously, according to a measurement of the error between the phase of the incoming signal and that of its local oscillator. The precise relationship between its input and response functions is a nonlinear integro-differential equation from which very little information concerning loop behavior is analytically available, at least in the general case. The case in which additive noise is present has been treated by a variety of approximate methods. The first approach—and still the most widely used—was one which assumed that phase errors were very small, nominally less than approximately 0.1 rad. Naturally, the method begins to fail as larger phase errors are encountered. Other methods extending the region of analysis to moderately larger phase errors have been put forth, but these too are limited. These analyses, regardless of their limitations, have not been of mere academic interest.

They have paved the way for building the most narrow-band, sensitive, flexible receivers in the world.

Most engineers agree that when the loop phase error increases to the point at which a linear analysis fails, the receiver ceases to be useful in gathering reliable data communicated to it. At the other end of the picture, when the input Signal-to-Noise Ratio (SNR) is very large, the linear theory may hold well enough, but unknown noises internal to the loop prevent the analysis from being carried further.

Thus, the engineer faced with verifying that a particular receiver operates correctly over its entire dynamic range finds that the linear theory predicts performance over only a limited range in the middle, and does not tell him if there are anomalies above or below.

The program described in this report is a means for analyzing phase-locked receivers over a very large range of input SNR, all the way up to the point where VCO noise begins to make a difference. It is flexible in that it can be used to analyze loops with or without limiters, with either signal or noise variations, given either measured or design parameter sets. However, the normal mode assumes a standard DSIF receiver. It performs an analysis from threshold to 40 db above, in 2-db steps.

2. Loop Model

The nonlinear theory of loop operation which this program embodies is developed in SPS 37-31, Vol. IV, pp. 292-300 and Refs. 1 and 2; the more interested reader is referred to these for detailed information. Basically, the program solves an equation

$$a^2 = \frac{1}{m} \left(\frac{w_{L(eq)}}{w_{L_0}} \right) \left(\frac{\Gamma}{\gamma^2} \right) \quad (1)$$

in which m is the receiver margin above threshold (threshold defined as 1 rad rms phase jitter in the linear loop model), w_{L_0} is the two-sided *linear theoretic value* of loop bandwidth at threshold, $w_{L(eq)}$ is the actual equivalent loop bandwidth, Γ is a limiter performance factor, and γ^2 is a parameter relating to nonlinear operation of the loop. Both $w_{L(eq)}$ and γ^2 are functions of the parameter a^2 , so Eq. (1) is transcendental. The program uses Newton's method to find a solution a^2 .

Once a^2 is found, it is related to the phase error variance by an approximate formula

$$\sigma^2 = \frac{\pi^2}{3} \left\{ 1 - \exp \left[- \frac{3a^2}{\pi} (1 + 0.13a^2) \right] \right\} \quad (2)$$

Once a^2 is found, the remainder of the loop performance parameters follow by mere substitution (Ref. 1).

3. The Program

The program was Fortran compiled using Scientific Data Systems (SDS) series 900 Fortran II from which a paper tape dump was made, suitable for either the SDS 930 or SDS 920 without further modification. It would be a simple matter to recompile and dump to provide an SDS 910 program. The tape is entered into the machine by a "standard fill."

Upon completion of the fill, control is automatically given to the program, causing the typewriter output

IF NORMAL DSIF RECEIVER, TYPE 'GO'

IF NOT, TYPE 'OTHER'

whereupon the operator would type nominally GO. The computer would then ask for certain measured parameter values to be given via the typewriter. An example is shown in Fig. 1, with operator response in brackets. Supplied with these numbers, computation and output proceeds.

Had the operator desired different data input and output media, different analysis detail, different input parameter set, or a receiver without a limiter, he could have typed OTHER; the computer would have then asked for certain assignments to be made. When the operator specifies NO LIMITER, he must also specify whether it is the signal or noise which is to vary in the analysis.

The output in the OTHER mode is shown in Fig. 2. Again, operator response is given in brackets.

4. Parameters

Values called for by the analysis are:

WL0 = w_{L_0} loop linear theoretic two-sided base bandwidth at threshold (cps)

R0 = loop parameter ratio

$$= r_0 = AK \tau_2^2 / \tau_1 \approx 4\zeta^2$$

T2 = numerator time constant of loop filter (sec)

$$= \tau_2$$

T1 = denominator time constant of loop filter (sec)

$$= \tau_1$$

BH = predetection one-sided bandwidth (cps)

$$= w_H / 2$$

MARGIN = starting value of analysis (db)

$$= m$$

Δ MARGIN = difference in margin between steps (db)

T = noise temperature ($^{\circ}$ K)

KD = phase detector gain (v/rad)

$$= K_d$$

KVCO = VCO gain (rad/sec/v)

$$= K_{vco}$$

F = dc gain of loop filter

$$= F(0)$$

VCO MULT FAC = frequency multiplier in VCO output

$$= M$$

IF NORMAL DSIF RECEIVER, TYPE 'G0'
IF NOT, TYPE 'OTHER'

[G0]

ENTER IN F FORMAT: T2[SEC], T1[SEC], T[DEG K]
KD[V/RAD], KVC0[RAD/SEC/VOLT], F, BH[CPS], VC0 MULT FAC

[.1249, 1250., 50.,
4.66, 8595., .9, 22000., 96.,]

SECOND-ORDER PHASE-LOCKED LOOP PERFORMANCE ANALYSIS

INITIAL PARAMETERS

T, DEG K = 50.00E 00	WL0, CPS= 1.201E 01	THRESH, DBM = -1.738E 02
T2, SEC = 1.248E-01	R0 = 1.999E 00	ZETA0 = 7.070E-01
T1, SEC = 1.250E 03	T2/T1 = Z = 9.991E-05	ALPHA OR A = 4.626E 02
BH, CPS = 2.200E 03	LIMITER = 1.E 00	LIM PERF FAC= 1.159E 00
L00P GAIN= 3.463E 06	VARY BW = 0.E 00	PREDET SNR 0 = 2.728E-03

L00P PERFORMANCE

MARGIN, DB = 4.000E 01	PH ERR, DEG = 1.591E 00	L00P BW, LIN = 1.753E 02
SIG LEV, DBM= -1.338E 02	PH ERR, RAD = 2.776E-02	L00P BW, ACT = 1.752E 02
N0, DBM/CPS = -1.846E 02	ERROR, RAD SQ= 7.709E-04	DAMPING, LIN = 3.271E 00
ALPHA OR A = 9.902E-01	L00P N/S, LIN = 1.459E-03	DAMPING, ACT= 3.270E 00
PREDET SNR = 2.729E 01	L00P N/S, ACT = 1.459E-03	LIM PER FAC = 5.278E-01

MARGIN, DB = 3.800E 01	PH ERR, DEG = 2.025E 00	L00P BW, LIN = 1.742E 02
SIG LEV, DBM= -1.358E 02	PH ERR, RAD = 3.534E-02	L00P BW, ACT = 1.741E 02
N0, DBM/CPS2= -1.846E 02	ERROR, RAD SQ= 1.249E-03	DAMPING, LIN = 3.260E 00
ALPHA OR A = 9.839E-01	L00P N/S, LIN = 2.299E-03	DAMPING, ACT= 3.259E 00
PREDET SNR = 1.722E 01	L00P N/S, ACT = 2.298E-03	LIM PER FAC = 5.430E-01

MARGIN, DB = 3.600E 01	PH ERR, DEG = 2.589E 00	L00P BW, LIN = 1.724E 02
SIC LEV, DBM= -1.378E 02	PH2ERR, RAD = 4.519E-02	L00P BW, ACT = 1.722E 02
N0, DBM/CPS2= -1.846E 02	ERROR, RAD SQ= 2.042E-03	DAMPING, LIN = 3.243E 00
ALPHA OR A = 9.734E-01	L00P N/S, LIN = 3.606E-03	DAMPING, ACT= 3.241E 00
PREDET SNR = 1.086E 01	L00P N/S, ACT = 3.602E-03	LIM PER FAC = 5.656E-01

Fig. 1. Phase-locked receiver analysis program output in GO mode (normal MEASURED parameter set input)

IF NORMAL DSIF RECEIVER, TYPE 'G0'
 IF NOT, TYPE 'OTHER'

[OTHER]

TYPE IN THE INPUT AND OUTPUT MEDIA, LOOP CONFIGURATION,
 AND PARAMETER SET DESIGNATION

INPUT: CARD, TYPE, PAP TAPE
 OUTPUT: PRINTER, PUNCH, TYWRITER, PLOTTER
 CONFIGURATION: NO LIMITER, LIMITER, SIGNAL VAR, NOISE VAR
 PARAMETER SET: DESIGN, MEASURED
 SEPARATE BY C/F

[TYPE
 TYWRITER
 LIMITER
 DESIGN]

ENTER IN F FORMAT: WL[CPS], R, T2/T1, BH[CPS], NOISE TEMP
 MARGIN[DB], ΔMARGIN[DB], NUMBER OF STEPS

[12., 2., .0001, 2200., 50.,
 40., -2., 20.,]

SECOND-ORDER PHASE-LOCKED LOOP PERFORMANCE ANALYSIS

INITIAL PARAMETERS

T, DEG K = 50.00E 00	WL, CPS= 1.200E 01	THRESH, DBM = -1.738E 02
T2, SEC = 1.249E-01	R = 2.000E 00	ZETA = 7.071E-01
T1, SEC = 1.250E 03	T2/T1 = Z = 9.999E-05	ALPHA OR A = 4.625E-02
BH, CPS = 2.200E 03	LIMITER = 1.E 00	LIM PERF FAC= 1.159E 00
LOOP GAIN= 3.459E 06	VARY BW = 1.E 00	PREDET SNR = 2.727E-03

LOOP PERFORMANCE

MARGIN, DB = 4.000E 01	PH ERR, DEG = 1.591E 00	LOOP BW, LIN = 1.753E 02
SIG LEV, DBM= -1.338E 02	PH ERR, RAD = 2.777E-02	LOOP BW, ACT = 1.752E 02
N0, DBM/CPS = -1.846E 02	ERROR, RAD SQ= 7.711E-04	DAMPING, LIN = 3.272E 00
ALPHA OR A = 9.902E-01	LOOP N/S, LIN = 1.460E-03	DAMPING, ACT= 3.271E 00
PREDET SNR = 2.727E 01	LOOP N/S, ACT = 1.459E-03	LIM PER FAC = 5.278E-01

MARGIN, DB = 3.800E 01	PH ERR, DEG = 2.026E 00	LOOP BW, LIN = 1.742E 02
SIG LEV, DBM= -1.358E 02	PH ERR, RAD = 3.535E-02	LOOP BW, ACT = 1.741E 02
N0, DBM/CPS = -1.846E 02	ERROR, RAD SQ= 1.250E-03	DAMPING, LIN = 3.261E 00
ALPHA OR A = 9.839E-01	LOOP N/S, LIN = 2.300E-03	DAMPING, ACT= 3.260E 00
PREDET SNR = 1.721E 01	LOOP N/S, ACT = 2.299E-03	LIM PER FAC = 5.430E-01

Fig. 2. Phase-locked receiver analysis program output in OTHER mode, with DESIGN parameter set input

The output parameters given are:

$$\text{LOOP GAIN} = \begin{cases} K & \text{(simple loop)} \\ K_d K_{vco} MF & \text{(limiter loop)} \end{cases}$$

$$\text{LIMITER} = \begin{cases} 1 & \text{(limiter)} \\ 0 & \text{(no limiter)} \end{cases}$$

$$\text{VARY BW} = \begin{cases} 1 & \text{(signal varied, no limiter)} \\ 0 & \text{(noise varied, no limiter)} \end{cases}$$

THRESH = signal level giving 1 rad rms phase jitter in a linear loop

$$= \frac{1}{2} k T \omega_{L_0} = A_0^2$$

ZETAO = linear theoretic damping factor at threshold

$$= \zeta_0$$

ALPHA = limiter signal voltage suppression factor

$$= \alpha$$

A^2 = input signal power

LIM PERF FAC = factor expressing action of limiter on phase variance

$$= \Gamma$$

PREDET SNRO = predetection SNR at threshold

$$= \omega_{L_0} / \omega_H = \rho_{H_0}$$

NO = two-sided noise spectral density

$$= kT/2$$

5. Cautions

To eliminate as much operator failure as possible, several error checks were put into the program. Some things of note are:

- (1) False input characters recognized:

[TYRITER]

NOT ACCEPTABLE RESPONSE, MESSAGE IGNORED.

- (2) To restart, put machine in IDLE, press START, then STEP-IDLE-RUN. Also can be done by manual branch to Cell 03507.

- (3) Restart can also be achieved by depressing BKPT1 during analysis printout, or during typing input parameters.

- (4) Only the first four letters of assignment words are recognized, although nominally these are given as:

INPUT: CARD, TYPE, PAP TAPE

OUTPUT: PRINTER, PUNCH, TYWRITER, PLOTTER

CONFIGURATION: NO LIMITER, LIMITER, SIGNAL VAR, NOISE VAR

PARAMETER SET: DESIGN, MEASURED

- (5) The parameter set designation must be entered last; the others may be entered in any order, or changed by retyping desired mode any time prior to parameter set.

- (6) The PLOTTER subroutine is not yet installed:

[PLOTTER]

NOT YET INSTALLED

- (7) If temperature is not entered, it is assumed 50°K.

- (8) If VCO multiplication factor not inserted, it is assumed to be 96.

- (9) $BH = b_H = \omega_H/2$ is not required when a limiter is not part of the loop. Any value can be inserted for BH in the NO LIMITER case.

6. Future Changes Foreseen

Except for perhaps a few changes in output format, the program described is applicable to DSIF station operation wherever SDS 900 series units are available. For receiver design purposes, a plotter routine may be desirable, and a provision in the program for this has been made, requiring only a few changes plus recompilation and core dump.

B. Efficient Data Systems: Error Probability Estimation With Loss-of-Lock Indication

E. C. Posner, J. Ashlock¹, and S. Lurie¹

1. Introduction

Some recent results presented in SPS 37-36, Vol. IV, are being applied to the problem of estimating the probability of error and of command rejection in spacecraft command receivers when a loss-of-lock indication is available.

Spacecraft command receivers such as those on *Ranger* and *Mariner* use a binary communication system in which the ultimate decision as to whether a transmitted bit is a "0" or "1" is made by a threshold device such as a Schmitt trigger. The error probabilities in these systems are estimated at JPL using the so-called extreme-value theory (Refs. 3, 4, and 5), which estimates the probability of detector output voltage exceeding the error threshold. This estimation is carried out by selecting the maximum value of, e.g., 100 detector outputs to define a new random variable. In turn, e.g., 30 independent samples of this new random variable are used to estimate the two parameters of Gumbel's double exponential distribution. These two parameters having been estimated, the probability of exceeding the error threshold is then estimated.

The *Mariner*-type system under consideration here has, in addition to a threshold device, a *loss-of-lock indicator*. The idea is that this lock indicator will show whether spacecraft receiver lock is lost. If the lock indicator output rises above a certain threshold, loss-of-lock is assumed to have occurred. The probability of the transmitted bit being correctly detected then drops to such a dangerously low level that an *inhibit* is generated and the entire command is rejected.

While the probability of bit error in a command system such as the one under discussion is certainly a very important parameter, it is also important to know the probability of getting a correct command into the spacecraft. After all, the bit error probability can be made arbitrarily low merely by setting the loss-of-lock threshold low. In that case, bit errors are not made, but most commands are rejected because of loss-of-lock being declared prematurely.

The purpose of this report is to describe work being done to generate a procedure for estimating the bit and command error and erasure probabilities in such a two-channel system. The techniques to be used are those of bivariate extreme-value theory (SPS 37-36, Vol. IV, pp. 317-325).

2. Estimating Error Probabilities

Let us suppose that a complete command is m bits long, where m is approximately 100. Such an m is considered large enough for bivariate extreme-value theory to be applicable. The probability that the entire command is read in correctly can easily be written down as an event, once it is realized that whenever loss-of-lock is declared, an inhibit pulse is produced which inhibits not merely the one bit in question, but in fact the entire command of length m .

Let the output of the bit detector be denoted by the random variable X , and let the output of the lock indicator be denoted by Y . Assume that the notation has been so chosen that the event $X > x_0$ denotes a bit error, whereas the event $Y > y_0$ denotes a loss-of-lock indication.

If $X > x_0$ and $Y > y_0$, a bit error is not made, but the entire command is rejected. Hence, this situation is called a *detected bit error*. The loss-of-lock indicator detects errors, causing events which are called *erasures*. An *undetected bit error* occurs if and only if $X > x_0$ and $Y < y_0$. In a well-designed system, Y will be large when X is, so that erasures are more likely to occur with errors than without them. The event $X < x_0$ and $Y > y_0$ is called a *false erasure*. The event $X < x_0$ and $Y < y_0$ is called a *correctly received bit*, the desired situation.

Thus, to have a *correct command* read into the command receiver command buffer, all m bits must have been correct; furthermore, loss-of-lock must never have been declared. That is, X must have been less than x_0 on all m trials, and Y must have been less than y_0 on all m trials. Conversely, if $X < x_0$ and $Y < y_0$ on all m trials, a correct command is read in. [If a correct command is not read in, either a wrong command is read in (if $X > x_0$ on one of the m trials, but $Y < y_0$ on all of the trials), or else no command is read in (if $Y > y_0$ on one of the m trials).]

The probability that $X < x_0$ and $Y < y_0$ on all m trials is thus needed. Define $X^{(max)}$ as the maximum of m (independent) X 's, and $Y^{(max)}$ as the maximum of m of the Y 's.

¹JPL Section 334

Note that $X^{(maz)}$ and $Y^{(maz)}$ need not occur on the same bit among the m . Now take M , e.g., 30, independent samples of the pair of random variables $X^{(maz)}$ and $Y^{(maz)}$. These M pairs are used to estimate the distribution of $(X^{(maz)}, Y^{(maz)})$, using bivariate extreme-value theory. From knowledge of the joint distribution comes knowledge of $\text{pr}(X^{(maz)} < x_0, Y^{(maz)} < y_0)$, which is the probability of reading in a correct m -bit command.

Techniques suggested in SPS 37-36, Vol. IV, pp. 317-323, are used to find the joint distribution of $(X^{(maz)}, Y^{(maz)})$. The distributions considered have five parameters: four parameters are two sets of the two parameters of the Gumbel distribution of $X^{(maz)}$ and of $Y^{(maz)}$, respectively.

The fifth parameter is a coefficient describing the way $X^{(maz)}$ and $Y^{(maz)}$ are correlated. These five parameters are jointly estimated using large-sample maximum-likelihood theory.

Once the five parameters are estimated, the distribution of $(X^{(maz)}, Y^{(maz)})$ is estimated, and hence the probability of the region $\{X^{(maz)} < x_0, Y^{(maz)} < y_0\}$ can be estimated. This last probability is exactly the probability of reading in a correct m -bit command. The probabilities of the other three regions can be similarly estimated: $\{X^{(maz)} < x_0, Y^{(maz)} > y_0\}$ is the *false command erasure* region, etc.

To estimate the bit error probability p , use the values of the two parameters for the Gumbel distribution of $X^{(maz)}$. These are two of the five parameters estimated previously. The probability $1 - p_{maz}$ that $X^{(maz)} < x_0$ is then estimated; since $(1 - p)^m = 1 - p_{maz}$, p can be estimated. The same applies to the bit erasure probability.

The probability b of a correctly received bit can be estimated as follows: $b^m = \text{pr}(X^{(maz)} < x_0, Y^{(maz)} < y_0)$, and the latter probability has been estimated. The probability of a false bit erasure is merely the difference between the probability that $X < x_0$, which is estimated above, and the probability of a correctly received bit. In a similar fashion, all four regions of bit error-erasure events have their probabilities estimated.

A program has been written for the SDS 930 machine in JPL Section 334 to do the maximum-likelihood estimation. The program is now running on data taken from a *Mariner* command detector. The results to date appear reasonable.

C. Efficient Data Systems: Punctured Cyclic Coder-Decoder

W. A. Lushbaugh

1. Introduction

The punctured cyclic coder-decoder, discussed in previous issues of SPS², is a device for coding and decoding any group code of six or fewer information bits. The device utilizes the parent (63,6) code, which is a maximal shift register sequence with six generating bits. One then punctures or deletes fixed coordinates of the code to obtain the other codes of shorter lengths. Decoding is accomplished by dictionary comparison.

2. Random Error Generation

The random pulse generator (RPG) discussed in SPS 37-29, Vol. III, pp. 92-95, has been adapted for use with the punctured cyclic coder-decoder to create a binary symmetric channel. With the RPG running on the same system clock as the coder, random pulses appear synchronously with the encoder bit clock, and so can be used to cause this bit of the coded word to be in error.

Group codes are guaranteed to correct a certain minimum number of errors, but can correct certain error patterns beyond this minimum. The introduction of a random number of errors per word confuses the issue of how well the code performs with more than the minimum number of errors. For this reason, an *error segregator* was built which determines the number of random errors to be inserted. The segregator counts the number of random errors inserted in a word and only transmits this word to the decoder if the number of errors equals the desired number of errors, which value was selected by a set of switches. In this way, the performance of the code with k random errors, $1 \leq k \leq 31$, can be observed.

3. Experimental Results

Most of the work in this reporting period was concentrated on the (60,6) code. This code has the 7th, 8th, and 13th bits of the (63,6) code punctured and is guaranteed to correct any pattern of 14 or fewer errors. While it was known that this code was not close-packed, the exact distribution of the error rate for more than 14 errors was not known. Table 1 gives the experimental results of the

²SPS 37-23, Vol. IV, pp. 149-151; 37-27, Vol. III, pp. 97-103, and 112-115; 37-20, Vol. IV, pp. 104-105.

Table 1. Experimental results of (60,6) code performance for 15-24 errors

Word sent	Errors/word	No. of samples	Word errors	Error rate
All	15	3,127,000	193	0.000074
All	16	2,880,000	2,374	0.00082
All	17	1,200,000	6,044	0.00504
All	18	300,000	6,475	0.02158
All	19	504,000	36,726	0.07316
All	20	1,450,000	284,630	0.1963
All	21	270,000	113,786	0.4214
All	22	1,007	709	0.7041
All	23	503	457	0.9085
All	24	501	493	0.9926
First	18	1,200,000	4,456	0.0037
Last	18	100,000	4,046	0.0404
All	$p = 1/4$	250,000	12,131	0.0485

code's performance for 15-24 errors and the observed performance of the code on the complete array of errors from a channel with bit error rate of $1/4$.

One other interesting experiment performed was a test of the effect of the decoding algorithm on the word error probability of a fixed word. Since dictionary comparison is used, and the dictionary in the decoder is always in the same sequence, one would expect a difference in the error rate between the first and last word in the dictionary. This is because of the fact that if two words are the same distance apart, the decoder decides on the first one reached as the transmitted word. The difference, as shown in Table 1, was a rather high ratio of about 10 to 1, for 18 randomly distributed errors.

D. Frequency Generation and Control: Wide-Band Distribution Amplifier

G. D. Thompson

1. Introduction

As reported in SPS 37-36, Vol. III, pp. 54-63, the programmed exciter (PE) system requires an output amplifier for distribution of the output signal to other systems.

The PE can be used as a local oscillator centered at any frequency from 10 kHz to 50 MHz. In order to preserve the versatility of the PE, a distribution amplifier with such a bandwidth is required. Commercially available amplifiers did not fulfill the requirements for unity gain, 13-dbm signal level, 10-kHz to 50-MHz bandwidth, and multiple (six) outputs. Therefore, a development program for such a wide-band distribution amplifier (WBDA) was initiated.

2. Circuit Description

The final circuit configuration is shown in Fig. 3. The design was strongly influenced by the requirement that the output must remain between 13 and 16 dbm when the input varies between 3 and 23 dbm. Since the basic amplifier is a linear device, an automatic gain control (AGC) system was required. The 20 db of AGC was obtained by varying the resistance of a thermistor in an attenuator at the input. The output signal is detected; the resulting dc voltage is amplified in the AGC amplifier, and the dc current through the thermistor is varied to change its resistance.

The transistor Q1 follows the attenuator as a stage of isolation. A voltage amplification of ten times is obtained by Q2 feeding the high impedance emitter follower Q3. The use of the Q2-Q3 combination for high level broadband voltage amplification was proposed by Drew, King, and Atwood in Ref. 6.

At the emitter of Q3, the signal level is somewhat larger than is needed so that the remainder of the amplifier is purely distribution. The Q4-Q5 complementary transistor pair is used for the final stages and, as used here, is more efficient than conventional emitter followers. The Q4-Q5 transistor pair operates push-pull in a class A mode and provides an impedance transformation from approximately 600 to 10Ω . This circuit will drive a 50Ω load at 1 v rms over the required bandwidth.

The sole adjustment for the WBDA is a potentiometer in the AGC amplifier which sets the output level. The WBDA is unique in its use of a thermistor in the RF signal path and in its use of the complementary pair output circuits.

3. Performance Characteristics

A prototype of the WBDA has been built and completely tested. The bandpass characteristic appears in Fig. 4. The output is flat within 1 db from 10 kHz to 50 MHz with 3-db points at 460 Hz and 70 MHz. The

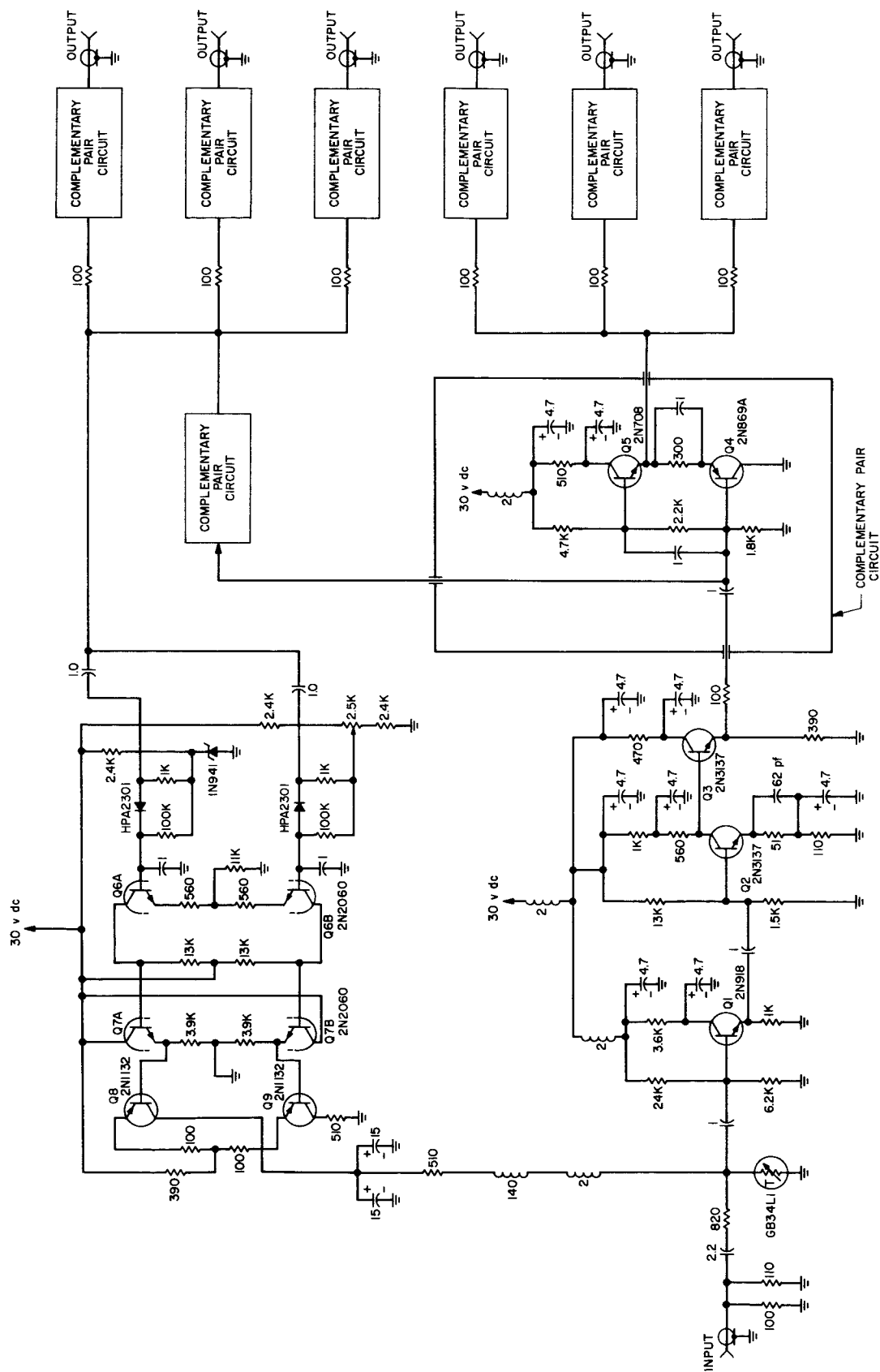


Fig. 3. WDBA schematic

UNLESS OTHERWISE NOTED:
RESISTANCE IN OHMS
CAPACITANCE IN MICROFARADS
INDUCTANCE IN MILLIHENRYS

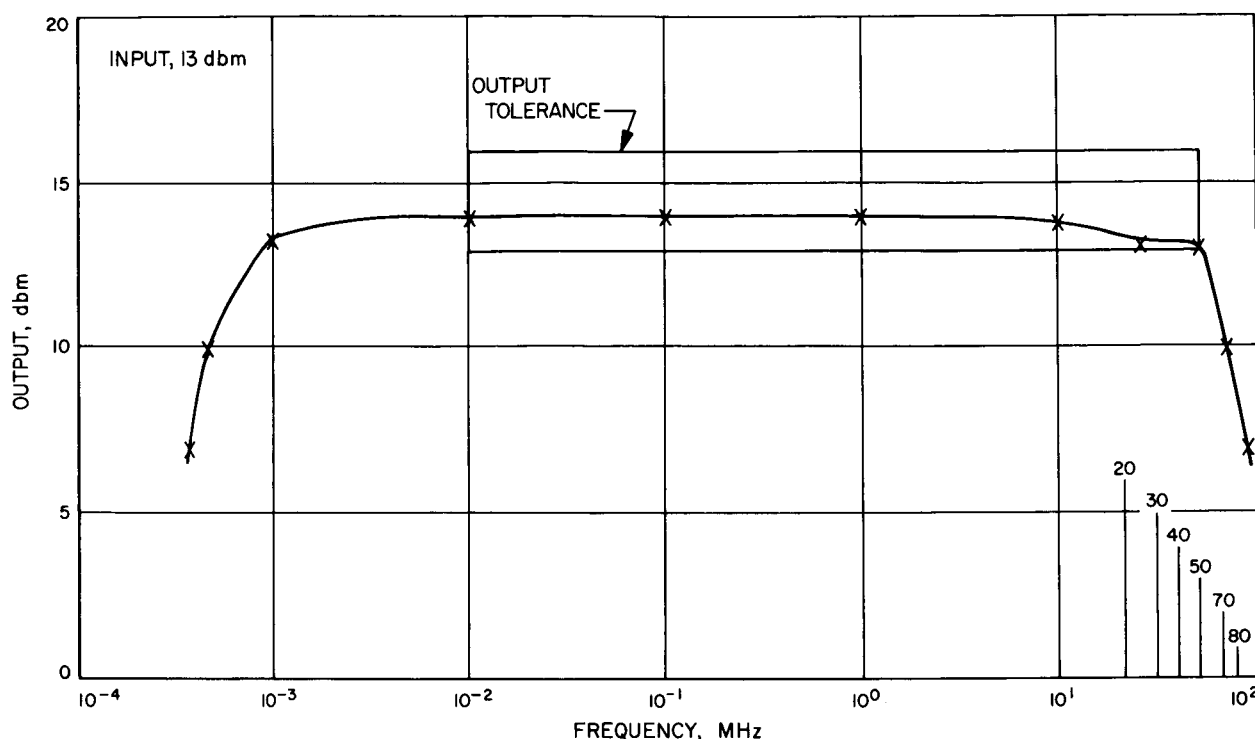


Fig. 4. WBDA frequency response

effectiveness of the AGC at 10 kHz, 10 and 50 MHz can be seen in Fig. 5.

The input voltage standing wave ratio (VSWR) is less than 1.10 for input levels from 7 to 20 dbm over the entire bandwidth. The output noise with no signal applied is 100 μ V for a 1-MHz bandwidth.

As shown in Table 2, the distortion in the output waveform is less than 5% over the entire bandwidth. Isolation between output ports is greater than 30 db up to 40 MHz and greater than 26 db at 50 MHz.

The prototype is housed in a gold-plated aluminum module. Leakage of RF signals from the module is less than 1 μ V from 10 kHz to 50 MHz. The module operates within specification for a 0 to 50°C temperature variation. The WBDA requires 250 ma from a 30-v dc power supply.

Following the prototype, several other WBDA modules were constructed. The circuit design of the WBDA has proved to be reproducible with no especially selected components. The WBDA will be used to distribute the output signal of the PE.

Table 2. WBDA output harmonic distortion

Frequency	Db down from fundamental		Distortion, %
	2nd harmonic	3rd harmonic	
10 kHz	33	51	2.5
150 kHz	33	49	2.5
1 MHz	32	52	2.8
10 MHz	32	36	4.1
25 MHz	31	33	5.0
50 MHz	27	44	5.0

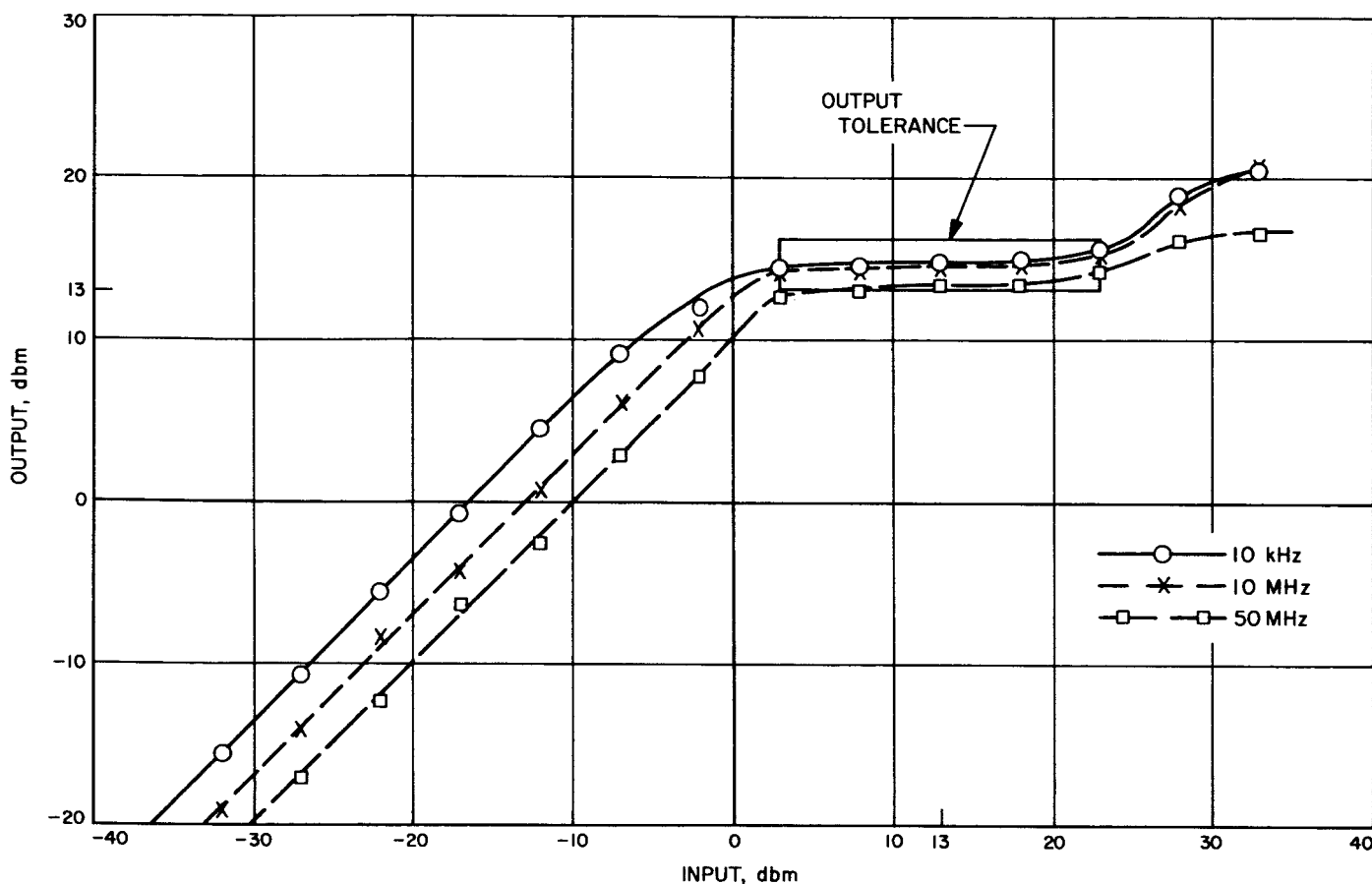


Fig. 5. WBDA limiting characteristics

E. Frequency Generation and Control: S- and X-Band Central Frequency Synthesizer

G. U. Barbani

Two multipliers and two dividers have been bread-boarded and fabricated by a local vendor to complete the frequency transformations required. Also, six high frequency distribution amplifiers have been completed.

Description. Since the $\div 2$, $\div 4$, and $\times 2$ modules were similar in electronic and mechanical design, one R&D chassis was used to check out the design refinements for each. Mechanically, they resemble the $\div 5$ described

in SPS 37-35, Vol. III, p. 68. The $\times 8$ was tested separately since its frequency demanded large scale component changes (a block diagram is shown in SPS 37-36, Vol. III, p. 68).

Multipliers. A $\times 2$ multiplier (200 to 400 kc) was developed to meet the frequency input requirements for the 31.44- and 31.84-Mc phase-lock loops. Fig. 6 shows the conventional means of frequency multiplication and Table 3 gives test data.

The $\times 8$ frequency multiplier raises the 1.0-Mc input signal to 8-Mc dual outputs (Fig. 7 and Table 4).

Dividers. Frequency transformation from 1.0 Mc to 125 kc was accomplished with two individual dividers: the $\div 2$ and $\div 4$ separated by distribution amplifiers. This satisfies one of the frequency requirements for the 35.075-Mc phase-lock loop (SPS 37-36, Vol. III, p. 68). Test data are available in Table 3.

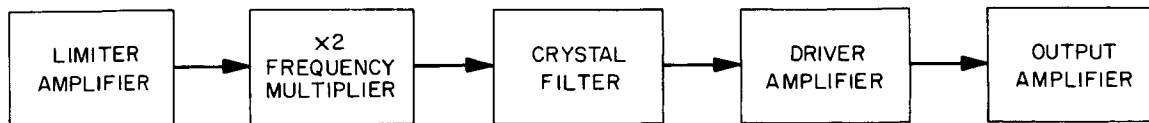
Fig. 6. $\times 2$ frequency multiplier

Table 3. Performance data for multipliers and dividers

Module	Frequencies, Mc	RF leakage (all frequencies), μv	Dynamic range input for constant output, db	Input impedance, VSWR	Harmonic distortion, %	Variation of output for power supply variation of 10%, %	Isolation from input to output, db	Bandwidth at 6 db, cps	Output versus temperature, 0–50°C, mv/°C	Output noise (input terminated), μv	Ripple, db
$\times 2$	0.20–0.40	<0.5	20	≤ 1.10	2.9	10.1	>60	33.1	0.00	75	0.0
$\times 8$	1.0 –8.0	<0.5	15	≤ 1.10	0.03	5.3	120	7210	1.0	70	0.5
$\div 2$	1.0 –0.50	<1.0	23	≤ 1.10	0.07	10.0	120	412	4.0	63	0.5
$\div 4$	0.5 –0.125	1.0	20	≤ 1.10	1.5	11.8	55	830	0.6	30	0.0

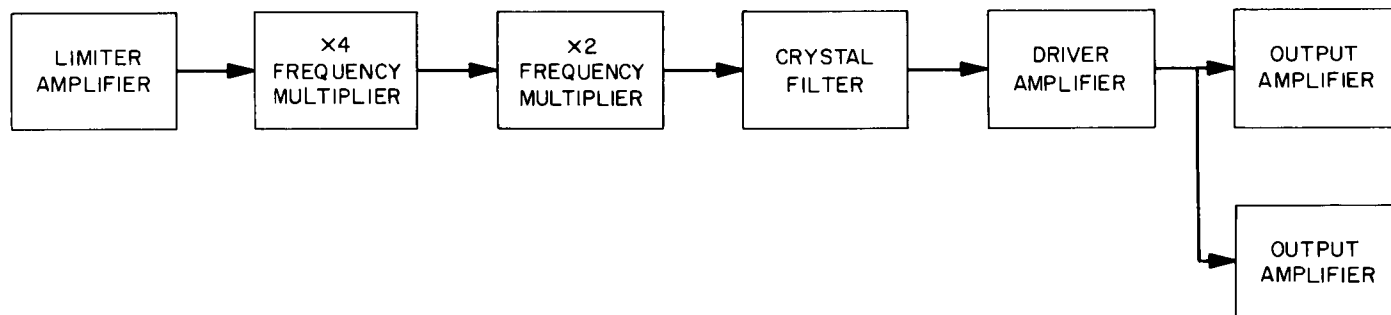
Fig. 7. $\times 8$ frequency multiplier

Table 4. Performance data for distribution amplifiers

Amplifiers, Mc	Isolation		Output noise (input terminated), μv	Dynamic range of input for constant output, db	RF leakage, μv	Power supply variation of 10% versus output, %	Harmonic distortion, %	Spurious signals, μv
	Output to input, db	Output to output, db						
30.0	100	48	1.0	20	<1.0	12.2	0.11	0.0
30.455	70	40	9	20	<1.0	6.7	0.16	0.0
31.44	90	70	<3	20	1.0	7.1	0.14	0.0
31.84 (No. 1)	70	70	<5	15	<1.0	9.6	0.52	0.0
31.84 (No. 2)	72	72	<5	15	<1.0	9.6	0.63	0.0
35.075	90	47	2.5	20	<1.0	11.1	1.2	0.0

Distribution amplifiers. Six high frequency distribution amplifiers were fabricated to complete the amplifier requirements; they are: one each of 30, 30.455, 31.44 and

35.075 Mc, and two 31.84 Mc. All are similar in structure to those reported in SPS 37-35, Vol. III, p. 71. Performance data are given in Table 4.

Conclusion. The central frequency synthesizer now has its full complement of RF modules except for the 1.0-Mc crystal filter which is undergoing evaluation. Module power and coaxial cables are being installed which complete Areas 1, 1A, and 2 (SPS 37-32, Vol. III, p. 44).

F. Experimental Closed-Cycle Refrigerators (CCR) for Masers

E. R. Wiebe and W. H. Higa

Some difficulty is being experienced in finding suitable materials for seals and valves in the gas-balanced refrigerator (SPS 37-31 through 37-36, Vol. III). This difficulty, paradoxically, has become severe ever since the oil-separation technique in the compressor assembly was perfected. Evidently the microscopic amount of oil carried over from imperfect compressor assemblies was enough to keep plastic parts adequately lubricated.

1. Dry Compressors

An Air Products & Chemicals, Inc., compressor (Model 3D2) has been undergoing tests and has accumulated approximately 800 hr of running time. The first 300 hr were due to initial evaluation and were the result of on-off operation. The last 500 hr, however, have been accumulated on a continuous basis with an operating test refrigerator. These initial results are encouraging for this machine which is not oil-lubricated.

Piston rings made of one of the fluorocarbons provide the self-lubricated seal and the crankshaft assembly utilizes grease-packed bearings. Hence, no oil separators are required, although it appears advisable to use some filtration to capture spurious impurities.

A further advantage is that, with some care, the compressor may be mounted directly on the antenna, assuring proper mechanical orientation. This feature is particularly important for an advanced maser system which is operated at temperatures below 4.2°K. The dry compressor could be used as a vacuum booster pump in this application and would be mounted near the CCR for maximum pumping efficiency.

The specifications for the Air Products compressor are similar to those of the A. D. Little, Inc., oil-lubricated

system. The pumping capacity is slightly higher with higher electrical efficiency.

2. Fluorocarbon Seals

Various fluorocarbon materials are being evaluated for use as seals and valves in the gas-balanced CCR. Apparently, the microscopic amount of oil carried over from an oil-lubricated compressor system was adequate to give long-term lubrication to those parts. However, with the perfection of oil-separation techniques, a problem has arisen because these parts must now operate without lubrication. The dry gas was, of course, desirable for the Joule-Thompson circuit.

Teflon and a new material, Rulon, with various dopants, are being tested for low friction and high thermal stability.

G. Continuous Wave (CW) Signal Power Calibration With Thermal Noise Standards

C. T. Stelzried and M. S. Reid³

1. Introduction

An attempt to improve the accuracy of the calibration of the CW received signal power in the DSN is under way. A convenient measure of a spacecraft received power level is the received AGC voltage, which is calibrated for absolute received power, defined at the receiver input, with a calibrated test transmitter. The theory, method of data acquisition, and equipment have been discussed previously (SPS 37-35, Vol. III, p. 58; SPS 37-36, Vol. III, p. 44). Preliminary computed results from the Echo Station have been presented and discussed (SPS 37-37, Vol. III, p. 35). Antenna efficiencies, used in the normalization process, have been measured using radio star tracks over an extended period, typically 3 or 4 wk. A statistical data reduction method for these measurements has been developed which takes into account an atmospheric loss term. Antenna efficiencies of the three stations where the CW power calibrations were undertaken were determined by this method and the results

³On leave of absence from National Institute for Telecommunications Research, Johannesburg, South Africa.

presented and summarized in Tables 1-3, SPS 37-37, Vol. IV, pp. 217-218.

This report describes refinements to the CW power calibration statistical data reduction and presents results from the *Mariner IV* spacecraft for the Pioneer, Echo and Venus Stations. These results are discussed and compared with the theoretical, predicted values. Finally, an equation is derived which relates the best estimate of received spacecraft power with data for approximately 30 days, centered about the Mars encounter.

2. Improvements in Data Reduction Method

Improvements in the data reduction method have been the result of further study of the statistical techniques and the experience of the preliminary computations of the Echo Station results (SPS 37-37, Vol. III, p. 37). These improvements are listed and discussed below.

The AGC curves are computed and plotted with power level considered as the dependent variable (ordinate) and AGC voltage as the independent variable (abscissa). This makes the solution for power level from a given AGC voltage simpler.

The correction factor, essentially a power level adjustment of the nominal AGC curve, is found from the middle of the calibrated AGC curve rather than averaging the difference between the nominal and AGC curves over the whole of the calibration range. The new method is simpler and the differences between correction factors computed by the previous and new methods are negligible.

Normally the first AGC reading, after the precalibration routine and with the antenna on the spacecraft, was used in the determination of received spacecraft power. This ensured that any receiver gain change, after the precalibration would be minimized. A better method is to fit a curve to the spacecraft AGC voltage data. Provisions have been made in the program to do this and to include the resultant probable errors in the over-all error analysis.

The computerized data reduction method has been extended to the calculation, on a daily basis, of system temperature from input data of: (1) ambient load temperature; (2) five Y-factors consisting of ratios of system temperature with the receiver connected to the antenna at zenith, and system temperature with the receiver con-

nected to the ambient load. This calculation was previously carried out manually and the result formed part of the daily input data. By using the temperature and Y-factors as input data, correct probable errors of the Y-factor measurement can be calculated, and these numbers used in the daily determination of the probable error of system temperature measurement.

The error analysis previously discussed (SPS 37-36, Vol. IV, p. 268) has been included in the data reduction method and has been extended to take account of all computed measurement errors derived from the input data. Probable errors associated with the nominal, calibrated, and normalized received power levels are printed out.

3. Results

Figs. 8(a) and (b) show the computer output for DSIF Stations 11 and 12, respectively, for July 14, 1965, the day of the Mars encounter. The day number has been taken from January 1 in order to make the computer program general. The top of each figure shows input data as described in SPS 37-37, Vol. III, p. 35. The Y-factors used in the calculation of system temperature are shown under the subheadings SKY and AMB. In order to make provision for the AGC versus TIME extrapolation back to the time origin, NORMALIZED TIME (that is, referred to the time of calibration) is used. The bottom of each figure is a summary of the computed data. The nominal and calibrated AGC curve constants and the correction factor have been discussed previously (SPS 37-37, Vol. III, p. 37). The computations associated with the subheading RECEIVED SIGNAL AGC SLOPE make provision for the time extrapolation referred to above.

The difference between the Pioneer nominal received spacecraft power level and that from the Echo Station listed under the RECEIVED POWER subheading is 4.97 db. The difference between the corresponding calibrated and normalized values is 0.39 and 0.13 db, respectively. The correction factors at the Pioneer and Echo Stations have opposite signs. This is typical for all the days that this CW power calibration method was applied at these stations. The correction factor from the Venus Station, however, did not retain a constant sign, but tended to change its sign randomly over almost all of the calibration period of several weeks. At the end of the experiment, when the detector was brought back to the Laboratory for evaluation, it was found to be intermittent. It is not known when the deterioration of the Venus detector started. This emphasizes the importance of daily data reduction and monitoring of results.

(a) PIONEER STATION

INPUT DATA

STATION 11

DATE 7-14-1965

DAY NO. 195

TIME 20 0

PRE-CAL REFERENCE 10.00 DB POST-CAL REFERENCE 10.00 DB ANT. EFF. 49.96 PERCENT

GFSK= -198.39 DB BWR= 11454.800 CPS ALPHA= .290 DB TS= 44.42 DEGREES

DATA POINT	AGC VOLTS	NOMINAL POWER DBM	ATTENUATOR DB	CAL-POWER DBM
1	-6.870	-110.000	43.860	-107.175
2	-6.520	-115.000	38.910	-112.129
3	-6.160	-120.000	33.920	-117.131
4	-5.750	-125.000	28.580	-122.514
5	-5.370	-130.000	23.810	-127.408
6	-4.960	-135.230		
7	-4.540	-140.230		
8	-4.130	-145.230		
9	-3.750	-149.230		
10	-3.370	-153.370		
11	-3.000	-157.370		
12	-2.590	-161.370		
13	-2.070	-166.370		

DATA POINT	SIGNAL AGC	NORMALIZED TIME	AIL ATT SKY	AIL ATT AMB
1	-2.68	0.00000	18.38	10.00
2			18.40	10.00
3			18.40	10.00
4			18.37	10.00
5			18.40	10.00

COMPUTED DATA

NOMINAL AGC CURVE		CALIBRATED AGC CURVE		RECEIVED SIGNAL AGC SLOPE	
A=-.11981E+03	PE= .36638E-01	A=-.11709E+03	PE= .15672E-01	A=-.26800E+01	PE= .00000E-99
B=-.13426E+02	PE= .44044E-01	B=-.13533E+02	PE= .19022E-01	B= .00000E-99	PE= .00000E-99
C= .49773E+00	PE= .12429E-01	C= .62734E+00	PE= .42721E-01		PEY= .00000E-99
	PEY= .88219E-01		PEY= .22274E-01		

CORRECTION FACTOR= 2.719 DBM

ERROR CONTRIBUTIONS

RECEIVED POWER

EC1= .42659E-02

NOMINAL=-160.513 DBM

EC2= .36677E-01

PE= .730 DB

EC3= .86621E-01

CALIBRATED=-157.793 DBM

EC4= .13834E+00

PE= .255 DB

EC5= .13923E+00

EC7= .21071E+00

NORMALIZED=-154.780 DBM

PE= .353 DB

Fig. 8. Mariner IV spacecraft received power calibrated with microwave noise standards

(b) ECHO STATION

INPUT DATA

STATION 12 DATE 7-14-1965 DAY NO. 195 TIME 1920

PRE-CAL REFERENCE 25.00 DB POST-CAL REFERENCE 25.04 DB ANT. EFF. 56.19 PERCENT

GFSK= -198.61 DB BWR= 9721.035 CPS ALPHA= .580 DB TS= 43.76 DEGREES

DATA POINT	AGC VOLTS	NOMINAL POWER DBM	ATTENUATOR DB	CAL-POWER DBM
1	-6.200	-110.000	54.760	-112.006
2	-5.860	-115.000	50.260	-116.514
3	-5.470	-120.000	45.430	-121.371
4	-5.050	-125.000	40.550	-126.334
5	-4.600	-130.000	35.800	-131.340
6	-2.680	-148.950		
7	-2.350	-153.150		
8	-1.990	-157.150		
9	-1.590	-161.150		
10	-1.250	-165.150		

DATA POINT	SIGNAL AGC	NORMALIZED TIME	AIL ATT SKY	AIL ATT AMS
1	-2.15	0.00000	33.56	25.00
2			33.56	25.00
3			33.55	25.00
4			33.56	25.00
5			33.57	25.00

COMPUTED DATA

NOMINAL AGC CURVE		CALIBRATED AGC CURVE		RECEIVED SIGNAL AGC SLOPE	
A=-.11951E+03	PE= .22137E+00	A=-.12137E+03	PE= .10002E-01	A=-.21500E+01	PE= .20000E-01
B=-.11603E+02	PE= .30728E+00	B=-.12193E+02	PE= .11791E-01	B= .00000E-99	PE= .00000E-99
C= .22609E+00	PE= .84469E-01	C= .86032E+00	PE= .24057E-01		PEY= .00000E-99
	PEY= .49938E+00		PEY= .14329E-01		

CORRECTION FACTOR= -1.864 DBM

ERROR CONTRIBUTIONS

RECEIVED POWER

EC1= .21329E-02

NOMINAL=-155.544 DBM

EC2= .36851E-01

PE= .792 DB

EC3= .74828E-01

CALIBRATED=-157.408 DBM

EC4= .13133E+00

PE= .397 DB

EC5= .13171E+00

NORMALIZED=-154.905 DBM

EC7= .30231E+00

PE= .466 DB

Fig. 8. Mariner IV spacecraft received power calibrated with microwave noise standards (cont'd)

The column of probable error contributions lists some of the important errors in db that make up the final answers, and is primarily a trouble-shooting and error-monitoring device. For example, EC1 is the measurement error, in db, associated with the Y-factors used in the determination of system temperature. EC2 is the probable error, in db, of the computed system temperature and includes EC1, nonlinearity errors in the precision IF attenuator (used in the Y-factor measurement), radiometer gain instability, and probable errors associated with the receiver and ambient temperatures. EC4 is the probable error, in db, of the calibrated power level of the test transmitter.

The probable error of the nominal received spacecraft power level can be separated into two parts. One is the error in the nominal test transmitter power level, the other being made up of all the error contributions common with the calibrated method. The probable error in the nominal test transmitter level has been estimated as 0.7 db. The probable error in the nominal received spacecraft power level is then, typically, approximately 0.8 db. The corresponding calibrated power level probable error is approximately 0.3 db. The error analysis flow with typical numbers is shown in Fig. 9.

Fig. 10 shows typical nominal and calibrated AGC curves which are the best second-order curves fitted to

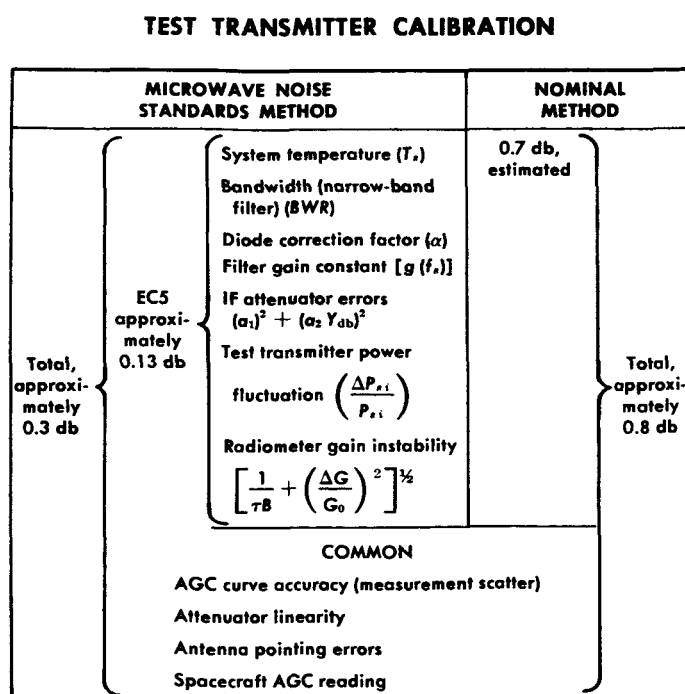


Fig. 9. Error analysis flow with typical numbers

the data points for the Pioneer Station for the day of Mars encounter.

Fig. 11 shows the best second-order curves fitted to the Pioneer and Echo data for 30 days, centered about the Mars encounter date. Both sections of the figure are drawn to the same scale and the ordinate values of received spacecraft power level correspond. The approximate average difference between nominal curves is 4 db, while the approximate average difference between normalized curves is 0.1 or 0.2 db.

Fig. 12 shows the averaged received spacecraft power level data points, normalized for 100% antenna efficiency, for both the Pioneer and Echo Stations, combined. There were 41 original data points. Points greater than 2σ were

Table 5. *Mariner IV* received power, normalized for 100% antenna efficiency as determined from Pioneer and Echo Station calibrated measurements

DAY	LEVEL, -dbm
185	-154.074
186	-154.177
187	-154.269
188	-154.352
189	-154.425
190	-154.488
191	-154.541
192	-154.584
193	-154.617
194	-154.641
ENCOUNTER 195	-154.654
196	-154.657
197	-154.651
198	-154.635
199	-154.609
200	-154.573
201	-154.527
202	-154.471
203	-154.405
204	-154.329
205	-154.244
206	-154.148
207	-154.043
208	-153.928
209	-153.802
210	-153.667
211	-153.522
212	-153.367

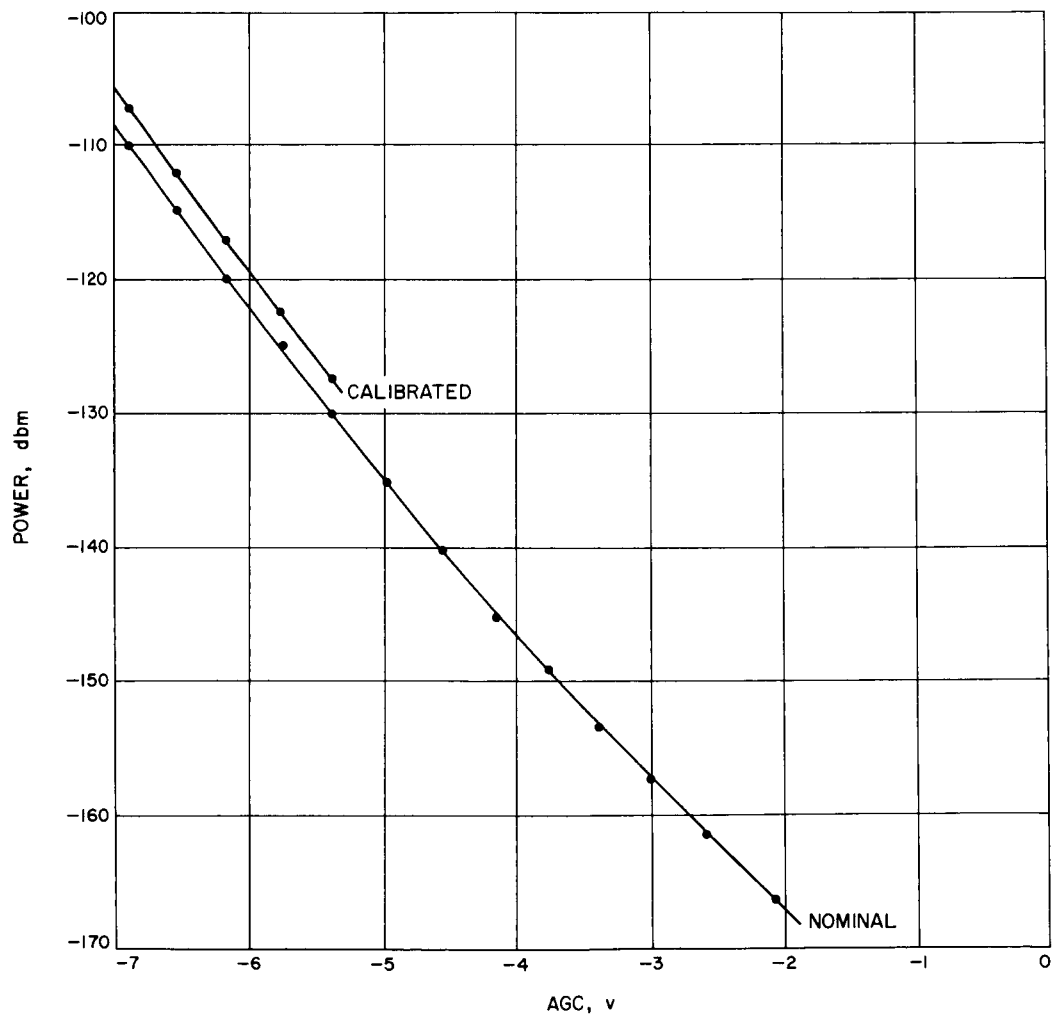
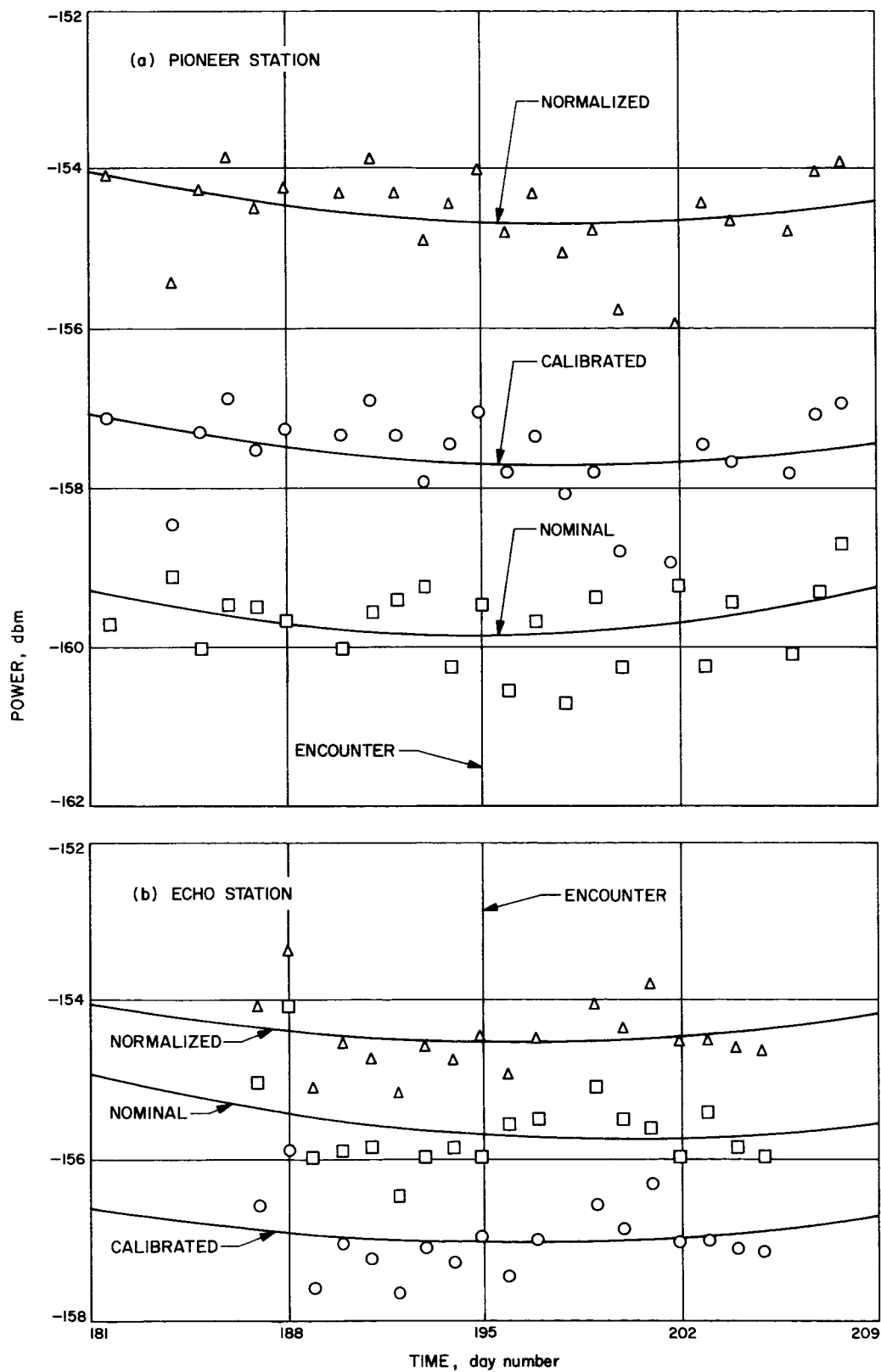


Fig. 10. Nominal and calibrated power versus AGC voltage, Pioneer Station, July 14, 1965

**Fig. 11. Mariner IV spacecraft received power**

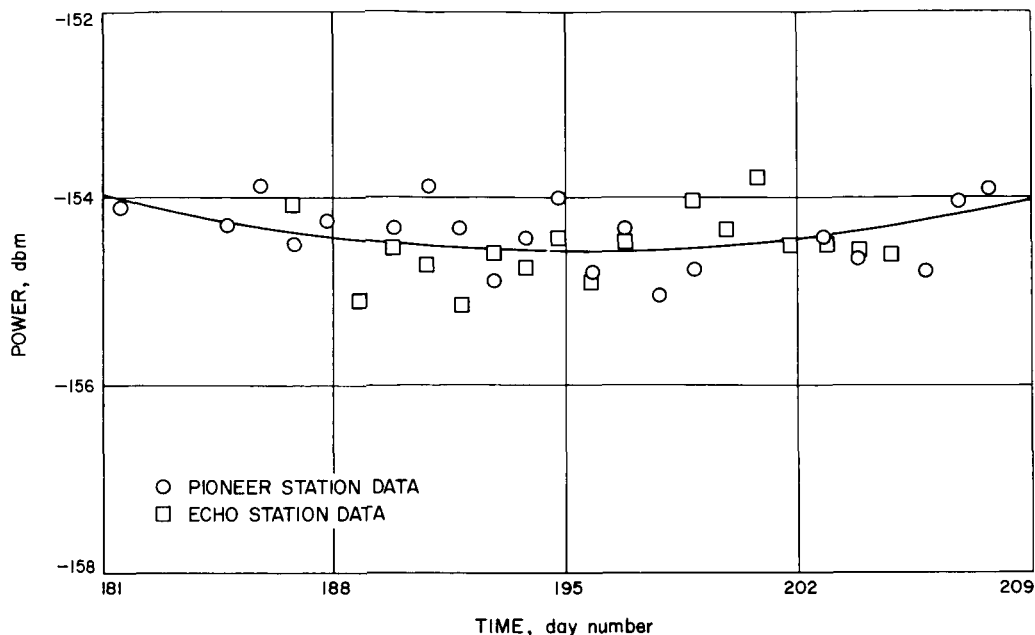


Fig. 12. Mariner IV spacecraft received power, normalized for 100% antenna efficiency, Pioneer and Echo Stations

removed (three from Pioneer, one from Echo) to result in the best fit curve for received power in dbm,

$$P_N = 35.209120 - 1.038851D + 0.004949706D^2 \quad (1)$$

where D = day number for the data for this time period. The standard deviation for the 37 data points was 0.35 db.

Table 5 lists the computed power from Eq. (1) by day number for the appropriate time period. The power level values in Table 5 do not take into account atmospheric loss. This effect will be investigated and may result in a further refinement of the calibrated data.

H. Simultaneous Lobing Radiometric Tracking System

B. Seidel

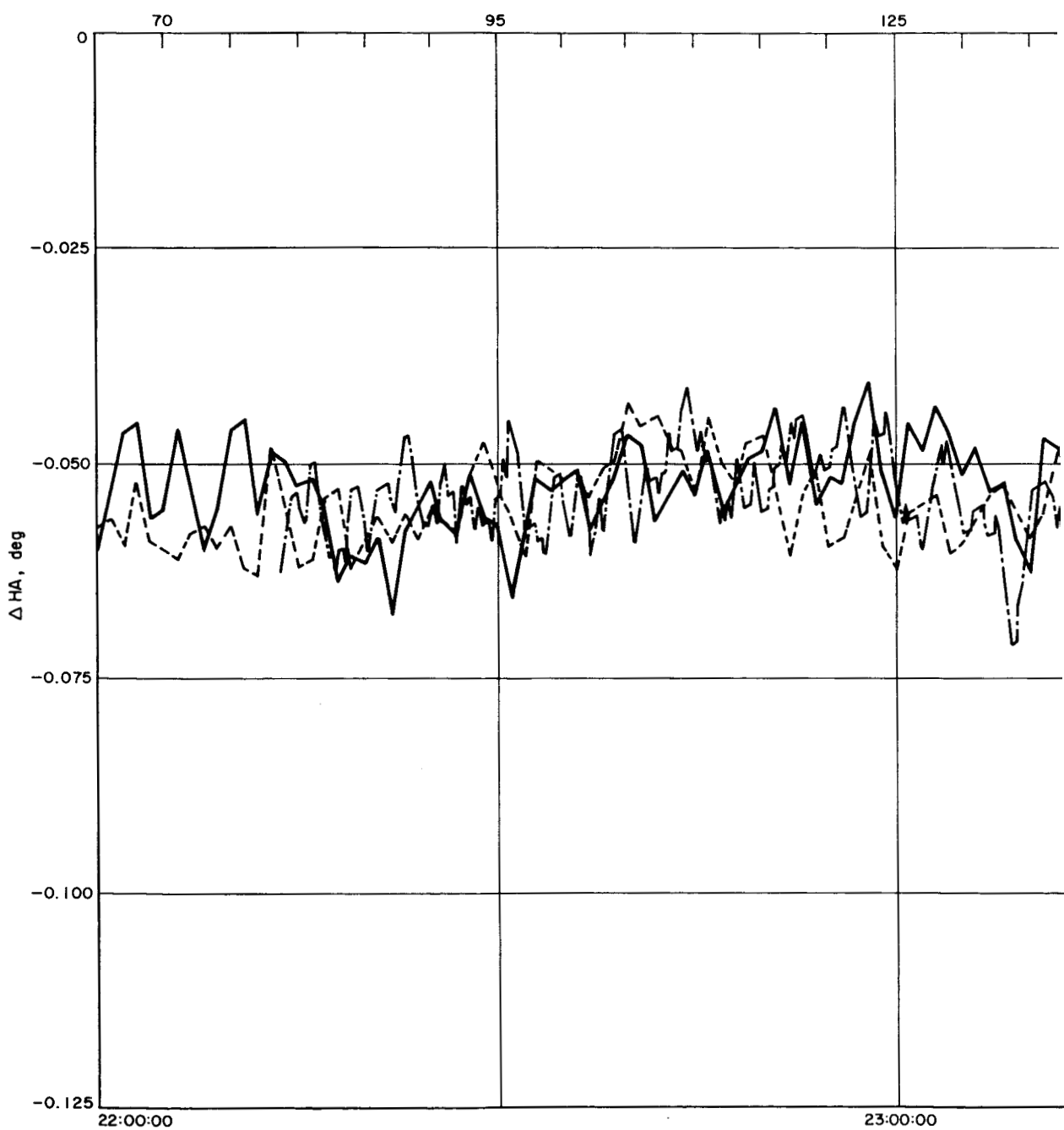
The S-band system modes of operation for the 210-ft diameter antenna will involve use of a simultaneous lobing angle tracking feed system. A radiometer which could be used in conjunction with the tracking feed would be a useful device for angle pointing and gain calibrations of the antenna system, using radio star

sources. This technique is especially important for the 210-ft antenna which does not have a collimation tower capability.

A prototype of such a radiometer is currently being evaluated using the Echo Station 85-ft diameter antenna. Results to date indicate that such a device is indeed feasible.

As previously reported (SPS 37-36, Vol. III), on October 5 and 6, 1965, the system was operated in an experiment designed to eliminate the necessity of a collimation tower when phasing the receiver for automatic tracking of a spacecraft. This experiment showed that the average difference between the phase shifter settings [hour angle (HA) channel] obtained from the collimation tower and the radio source was approximately 25 deg. In SPS 37-37, Vol. III, it was stated that the primary effect of this phase misalignment would be an increase in tracking jitter, and that it would be desirable to verify this, using a far-field moving source.

On January 23-24, 1966, the opportunity did arise and an experiment was performed using the Echo Station 85-ft antenna to verify the above. On this date, the Pioneer probe (PN-6) was tracked and the HA phase shifter was misaligned in 5-deg increments until tracking could no longer be accomplished. The phase shifter was then realigned and the procedure repeated for the opposite misalignment. Tracking data were taken at each



490

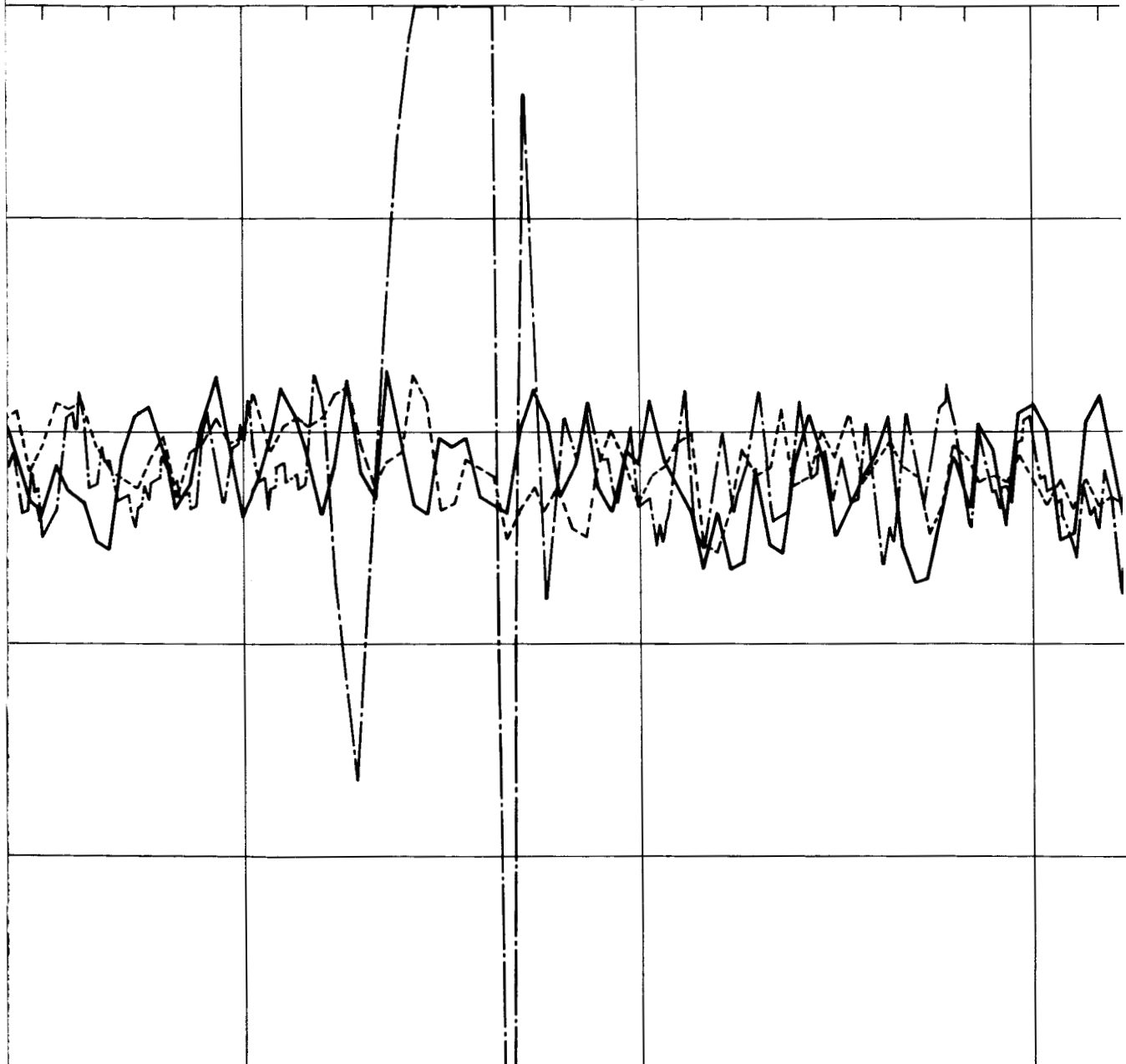
HA PHASE SHIFTER SETTING, deg

155

70

60

30



00:00:00

TIME, GMT

49-2

~~50~~ (2)

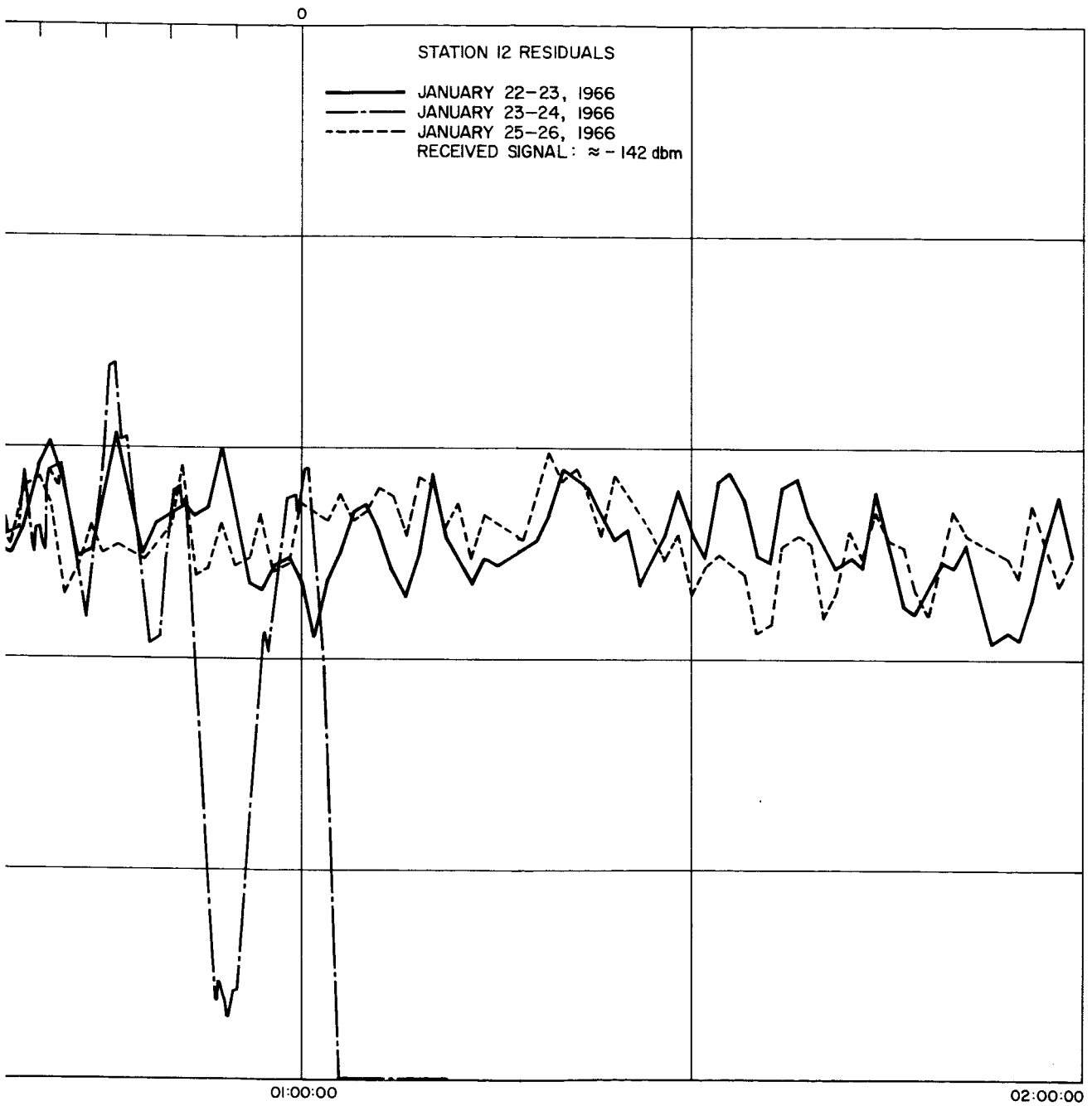


Fig. 13. Station 12 tracking residuals

49-3

~~50-3~~

setting of the phase shifter for 5 min using a 10-sec sample rate. The tracking residuals from this pass were then compared to those of both the previous and the following pass where proper phasing was maintained throughout the pass. All of these tracking residuals are shown overlaid in Fig. 13. The top scale in the figure (HA phase shifter setting) applies only to the tracking data of January 23-24, 1966, and the setting is incremented stepwise each 5 min.

These data indicate that: (1) the major portion of the tracking jitter is caused by the electromechanical dynamics of the antenna (i.e., no increase in tracking jitter with phase misalignment until the point where tracking cannot be accomplished); (2) the null depth of the feed is deep enough to cause no boresight shift with phase misalignment; and (3) the correct phasing of the receiver should have been at a setting of approximately 80 deg (the station had used a setting of 70 deg as the nominal proper setting). Tracking commitments permitting, this experiment will be repeated when the received signal from the spacecraft is at a lower level.

I. Microwave Maser Development

R. C. Clauss and W. H. Higa

Assembly techniques have been successfully used at S-band frequencies with the one-piece traveling wave maser (TWM) (SPS 37-37, Vol. III, p. 44). These techniques involve: (1) coupling signal power between the

coaxial transmission lines and the slow wave structure, and (2) adjusting the TWM bandpass to yield adequate slowing and tuning range.

1. TWM Coupling Technique

Coupling the signal power to the slow wave structure is accomplished by using a loop adjacent to the comb structure, as shown in Fig. 14. Adjustments are made by bending the loop, thereby changing the distance between the loop and the first resonant element. A screw located directly above the first element provides capacitive tuning. Fig. 15 is a block diagram of the test equipment used to indicate input and output match during the

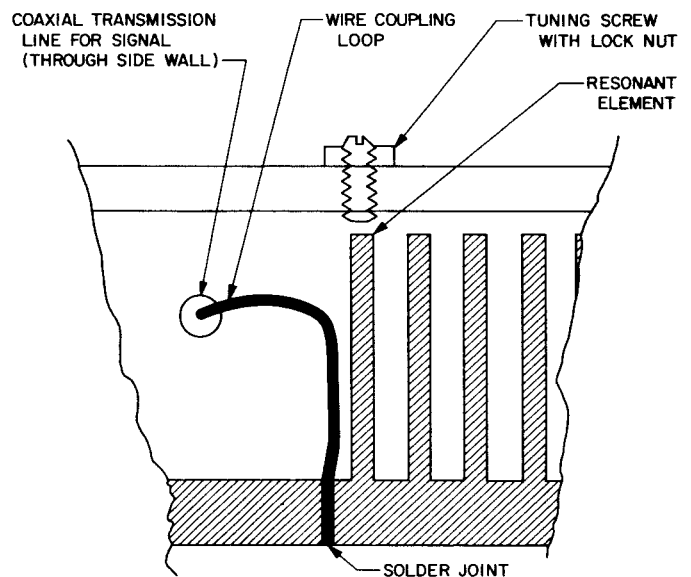


Fig. 14. TWM signal coupling loop

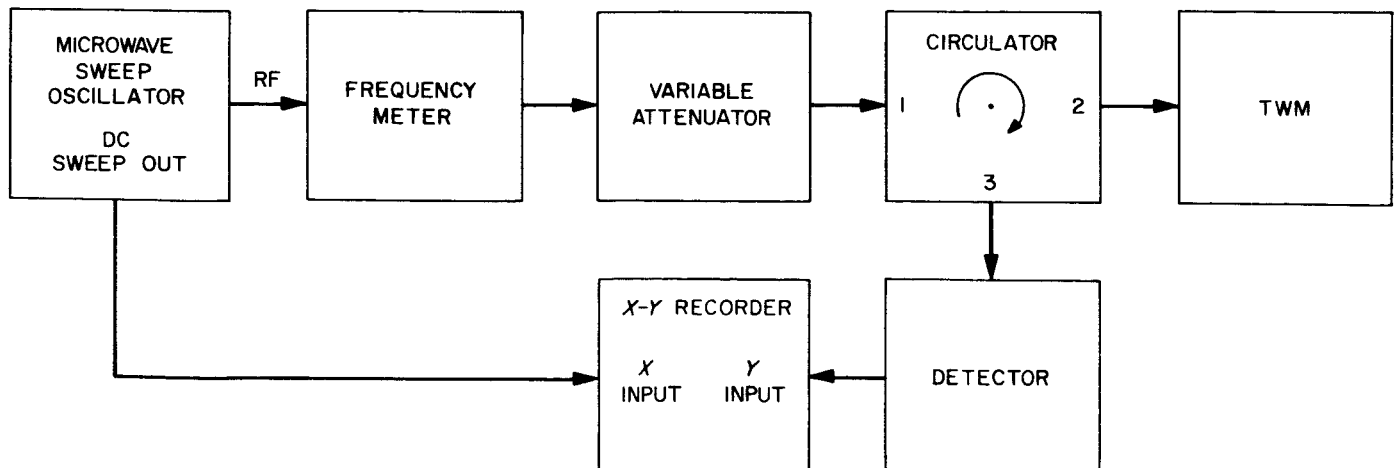


Fig. 15. Test setup for measuring reflected power

adjustment. Mismatched coupling at the TWM input can seriously degrade the equivalent input temperature of the amplifier. This noise temperature degradation is a function of both temperature and mismatch, as well as the equivalent input temperature of the TWM under matched conditions. The equivalent input temperature of a mismatched TWM, T_M , is given by

$$T_M = \frac{T_{M_0} + T_B \rho^2}{1 - \rho^2} \quad (1)$$

where

T_{M_0} = equivalent input temperature of TWM under matched condition

T_B = bath temperature

ρ = voltage reflection coefficient

The ratio of T_M/T_{M_0} is

$$T_M/T_{M_0} = \frac{1}{1 - \rho^2} + \frac{T_B}{T_{M_0}} \left(\frac{\rho^2}{1 - \rho^2} \right) \quad (2)$$

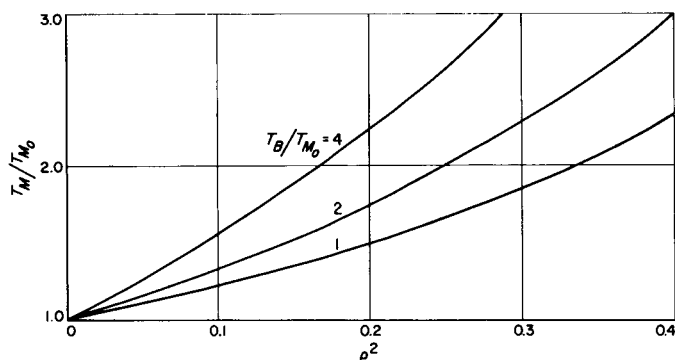


Fig. 16. Effect of mismatched input coupling on TWM equivalent input temperature

Fig. 16 shows the ratio T_M/T_{M_0} as a function of mismatch for three values of T_B/T_{M_0} . Fig. 17 is an X-Y recorder plot showing the reflected power from the TWM signal connections (Fig. 15). The matches shown are typical for a TWM which would cover a tuning range of approximately 130 Mc, centered at 2340 Mc. The VSWR from 2300 to 2400 Mc is approximately 1.4 to 1 and ρ^2 is 0.03.

2. TWM Bandwidth Adjustment

Bandpass adjustment of the TWM is accomplished by changing the geometry of the maser material. Ruby, the material used, has a dielectric constant which varies

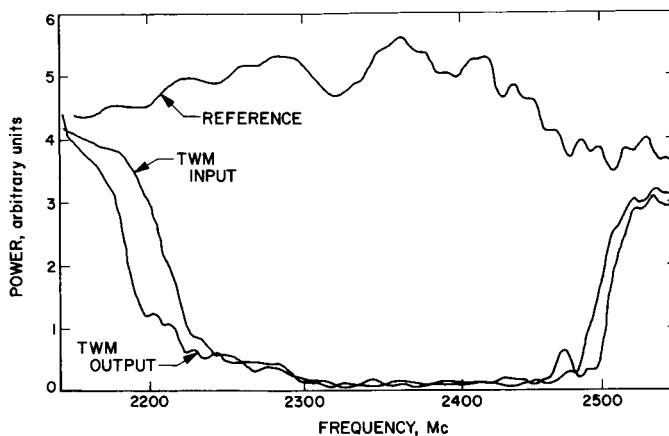


Fig. 17. Reflected power from TWM

from 10 to 12, depending on the C-axis orientation. Fig. 18 shows the end view of a TWM, with ruby, clamps, and isolators in a typical configuration. The clamps are made of beryllium copper shim stock and are copper plated to reduce resistive loss. In addition to its mechanical function, the height of the clamp is used to adjust the slowing factor which can be increased by reducing the height of the clamp. Increasing the depth of the bevel shown on the "forward-side" ruby

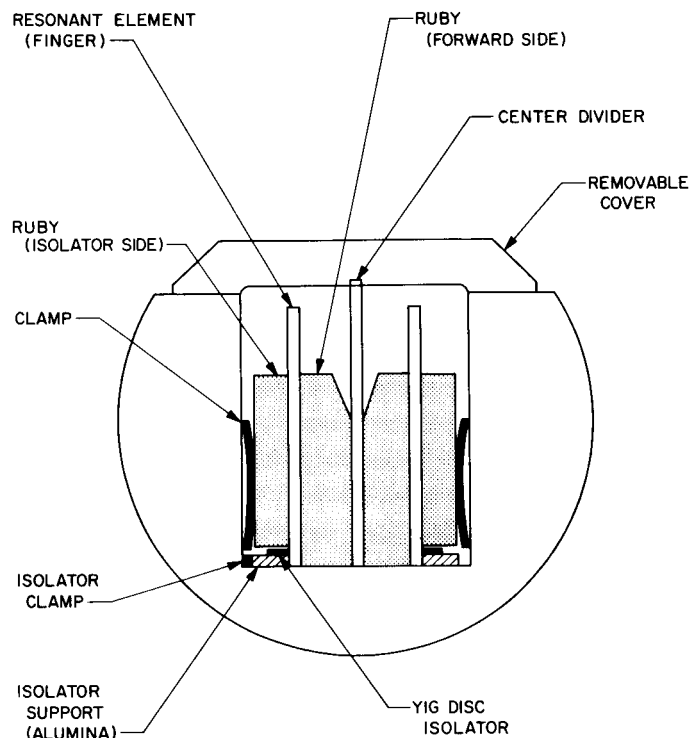


Fig. 18. End view of TWM (coupling loop omitted for clarity)

also raises the slowing factor. When the slowing factor is raised by adjusting the clamp or the ruby shape, the bandpass (tuning range) of the TWM is reduced.

The center frequency of the TWM can be shifted by adjusting the height of the ruby slab. At 2300 Mc, slab height of 0.475 in. is used with finger length of 0.720 in. The center frequency shifts at a rate of 4 Mc per 0.001-in. change in slab height. The ruby should always rest on the base of the structure where the RF magnetic field is maximum. These techniques have been found to be reliable and, with experience, not too difficult.

J. Venus Station Operations

E. B. Jackson and A. L. Price

1. Experimental Activities

The major activities (summarized in Table 6) during this reporting period were S-band planetary radar experiments, *Mariner* Mars 1964 tracking and command transmission, and radio star tracking.

a. Planetary radar. Experiments carried out with the S-band planetary radar system were open-loop ranging and mapping, closed-loop ranging, and total spectrum on Venus; also, total spectrum on Jupiter. The ranging data indicate that the actual round-trip range to Venus has continued to move into better agreement with the predicted round-trip range; e.g., whereas actual round-trip

range was some 5,560 μ sec shorter than prediction on December 13, 1965, it was approximately 30 μ sec longer than prediction on February 10, 1966, having crossed over several days after inferior conjunction on January 26, 1966.

b. *Mariner* Mars 1964. The monthly experimental reception from the *Mariner* spacecraft continued with signals being successfully received January 4 and February 2-3, 1966. Additionally, a command (DC-17) to change the look angle of the spacecraft Canopus sensor was transmitted February 3 after a 2-hr up-link transmission period designed to lockup the spacecraft RF and command loops. Subsequent to command transmission, the up-link RF transmission continued for another 15 min, and the Venus *Mariner* system was then switched to receive mode.

During the 38-min period of round-trip time after cessation of up-link transmission, the ground receive system searched (± 240 Hz) around the nominal two-way and the one-way receive frequencies without success. However, reception at the one-way frequency was successful as soon as the round-trip time had elapsed, thus definitely establishing that the spacecraft had not been transmitting at the one-way frequency during this round-trip time.

Although the spacecraft reached its maximum range from Earth during this reporting period, and is now closing the range, the range is still so great that signal levels are not significantly affected by the small decrease in range thus far effected. (Received carrier level February 3 was -178.1 dbm, not substantially different from the level November 1, 1965.)

2. Subsystem Performance

a. 100-kw transmitter. The R&D S/N 3 klystron which had been installed in *Mariner* Amplifier 1 (SPS 37-37, Vol. III, p. 51) was replaced because of apparent clogging of the collector cooling passages, as evidenced by inability of the cooling system to maintain required water flow at normal pressures. Otherwise, operation has been satisfactory, with minor lost-time periods because of protective circuitry actuating and shutting down the transmitter.

b. Receiving system. All three receiving systems were used. Venus experiments were conducted at both S-band (2388 MHz) and X-band (8448 MHz) frequencies, and *Mariner* IV was tracked with the *Mariner* receiver. However, since work on the *Mariner* receiver was still in

Table 6. Summary of Venus Station activity
(December 13, 1965–February 10, 1966)

Activity	Hours	Percent
Primary experiments		
Planetary radar (Venus)	382	26.52
Planetary radar (Jupiter)	148	10.28
Secondary experiments	81	5.62
Radio star tracking		
Mariner experiments		
Transmission, reception, and testing (includes time required to change Cassegrain feed cones)	91	6.33
Testing, calibration, construction, and scheduled maintenance	652	45.28
Holidays and scheduled nonoperating time	86	5.97
Total	1440	100.00

progress, *Mariner* reception was accomplished by cross-patching the 30-MHz output from the *Mariner* receiver into the R&D receiver for processing. The only equipment failure was a transistor in a frequency synthesizer used to supply the third local oscillator conversion frequency. The transistor was replaced, and operation is now normal.

Operation of the programmed local oscillator (PLO) continued to be acceptable, although several failures did occur—the most serious included a noisy VCO control potentiometer, faulty operation of the tape spooler in the rewind mode, and failure of the display lamp power supply; all have been repaired.

c. Central frequency synthesizer (CFS). The 35.2-MHz synthesizer module, needed for operation at X-band frequencies, was returned from the Laboratory (SPS 37-37, Vol. III, p. 52) and reinstalled in the CFS. Evaluation of the rubidium frequency standard standby battery system is continuing, with periodic voltage and specific gravity measurements being made to determine the correct float voltage and charging rate.

The CFS frequency counter failed during this period and was repaired on site.

3. System Improvements

a. Receiving system. Extensive modifications have been made to the Venus Station receiving system in an effort to provide three independent receivers: one for X-band

(8448 MHz), one for S-band R&D (2388 MHz), and one for the *Mariner* receive frequency (2297 MHz).

The X-band receiver is now contained in a separate single-bay cabinet, as is the *Mariner* receiver. The S-band R&D receiver was reduced in size from five to three cabinets by relocation of modules. Other changes to the R&D receiver included the reinstallation of a shortened "top hat" meter panel and modification of the control panel and instrumentation to allow easier operation. The X-band receiver now provides two output channels: one for ranging experiments (narrow band), and the other for spectrum analysis experiments (wide band). The R&D S-band receiver now provides three output channels: ranging, spectrum analysis, and main loop. Because of the data processing equipment, the spectrum analysis and ranging channels of both receivers are very similar.

The main-loop channel of the S-band R&D receiver can now provide doppler information in either of two modes. One mode utilizes the phase-locked loop of the main-loop channel. In this mode, the receiver first local oscillator frequency is tuned by both the programmed local oscillator (PLO) and the phase-locked loop. In the second mode of operation, the receiver first local oscillator is tuned only by the PLO, and a special 455-kHz phase-locked loop in the main channel measures the PLO tuning error with reference to actual received frequency. The addition of this latter 455-kHz loop allows doppler information to be recorded simultaneously while the receiver is being used in a CW mode for other open-loop experiments, such as total spectrum measurements.

References

1. Tausworthe, R., *Theory and Practical Design of Phase-Locked Receivers*, Vol. 1, Technical Report No. 32-819, Jet Propulsion Laboratory, Pasadena, California, February 15, 1966.
2. Tausworthe, R., "A Method for Calculating Phase-Locked Loop Performance Near Threshold," *Proceedings of the National Telemetry Conference* — 1966, Boston, Massachusetts, May 1966.
3. Posner, E. C., *The Application of Extreme-Value Theory to Error Probability Estimation in the Ranger Block III Command Detector*, Technical Report No. 32-705, Jet Propulsion Laboratory, Pasadena, California, January 15, 1965.

References (Cont'd)

4. Posner, E. C., and Ashlock, J. C., *Application of the Statistical Theory of Extreme Values to Spacecraft Receivers*, Technical Report No. 32-737, Jet Propulsion Laboratory, Pasadena, California, May 15, 1965.
5. Posner, E. C., "The Application of Extreme-Value Theory to Reliable Communication," *Technometrics*, pp. 517-529, 1965.
6. Drew, L., King, H., and Atwood, A., "A 320-Mc Broadband Amplifier," *Solid State Design*, Vol. 5, No. 10, pp. 19-22, Horizon House, Inc., Dedham, Massachusetts, October 1964.

V. Communications Development Engineering

A. Venus Station 1-Mw High Voltage Power Supply

R. E. Arnold

During this reporting period numerous tests were performed on the 1-Mw high voltage power supply installed at the Goldstone Venus Station. The purpose of the tests was to determine how the high voltage regulation and ripple characteristics could be improved. The results of these tests are summarized in this report.

1. System Description

Fig. 1 is a diagram of the present system. Although this system is capable of 55-kv, 1000-kw output, normal operation with 100-kw klystron transmitters has been in the 30- to 35-kv and 250- to 300-kw region. The power supply system is generally used in the closed-loop mode where a fraction of the high voltage is sampled through a resistive divider and compared with a reference voltage. The resultant signal is amplified by a vacuum tube am-

plifier which drives the input field windings of the amplidyne generator. The amplidyne supplies the field excitation to the main 400-cycle generator, thus regulating the high voltage. The power supply can also be operated in a manual open-loop mode by applying a DC current directly to the amplidyne control fields. This mode is used only for testing and in possible emergencies following a failure of the closed-loop regulation circuitry.

2. Electronic Regulator Amplifier

The electronic regulator amplifier is a vacuum tube device that uses two direct coupled cascaded amplifiers (one 6SN7) to drive a cathode coupled push-pull pentode amplifier (two 6L6's). Each pentode drives a field coil of the amplidyne. The regulator amplifier is powered by an internal unregulated 350-v power supply and a ± 105 -v regulated VR tube supply operated from a 60-cycle magnetic line regulator. Testing and design studies of the amplifier revealed the following deficiencies:

- (1) The internal unregulated 350-v power supply had a 5-v peak-to-peak 120-cycle ripple.

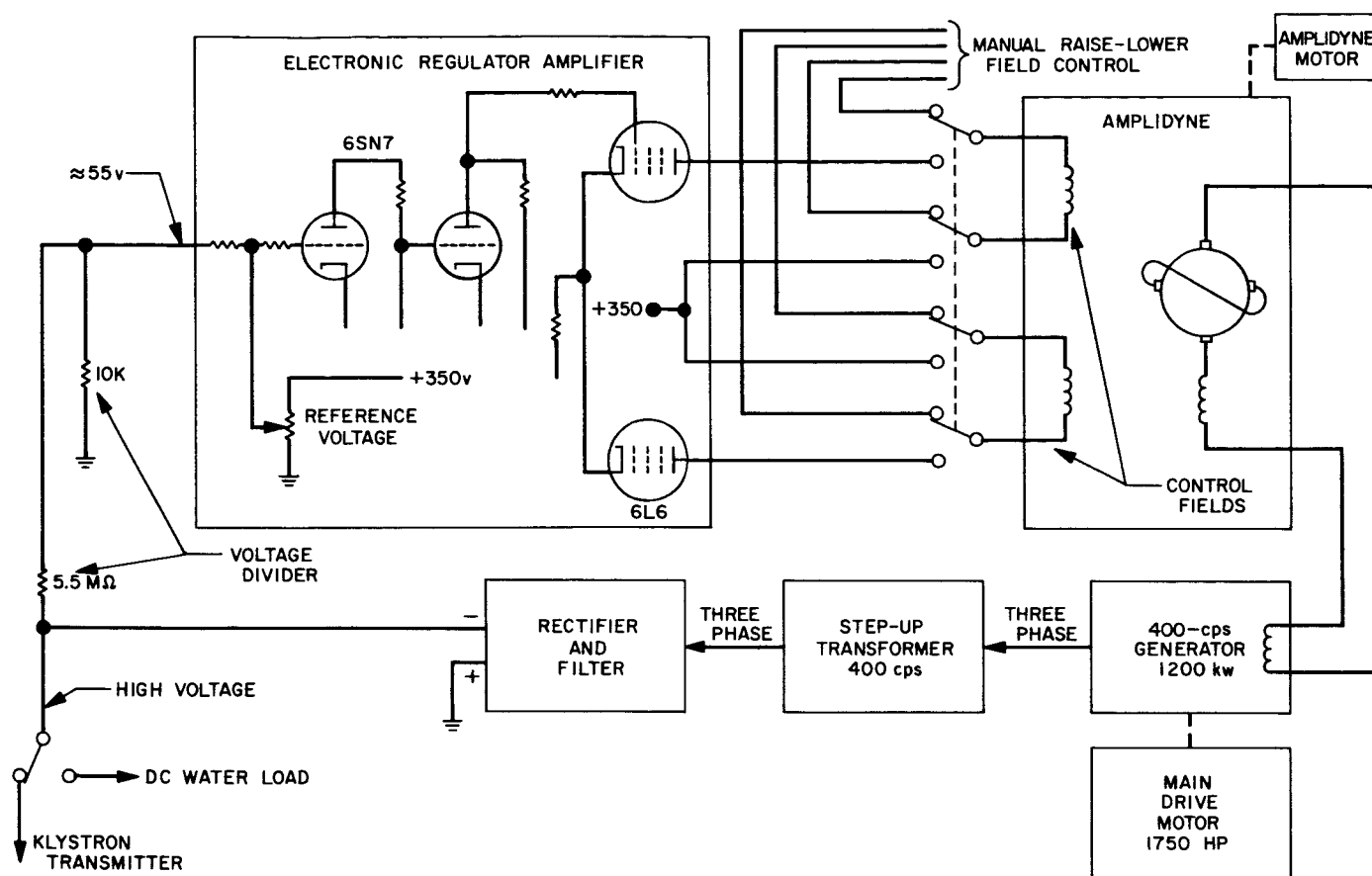


Fig. 1. Simplified diagram of 1-Mw DC power supply system

- (2) The reference voltage for the amplifier is furnished by the unregulated 350-v power supply. This results in both long- and short-term instability of the output beam voltage.
- (3) The amplifier introduces a 1.2-v peak-to-peak 60-cycle ripple on the 55-v DC output (the input to the amplifier) of the high voltage divider. This 60-cycle ripple is not directly related to the 120-cycle, 350-v power supply but appears to be magnetically coupled from the filament and/or 350-v power supply transformer.

In order to correct the first two deficiencies, external regulated power supplies were connected to the amplifier to replace the internal DC power supplies. Figs. 2 and 3 are strip chart recordings showing the high voltage ripple before and after the external supplies were connected. Ripple was reduced with the regulated power supplies, and the long-term stability was also improved. The beam voltage tended to drift approximately ± 50 v during a few minutes of recording when the internal

power supplies were used but remained centered on the recorder with the regulated supplies.

The final deficiency was not corrected because of the difficulty of completely isolating the amplifier chassis from 60 cycles. No attempt will be made to completely optimize the performance of the present regulator amplifier; rather, the unit will be replaced with a solid-state differential amplifier and regulated power supplies.

3. Amplidyne

The amplidyne is functionally a high gain DC current amplifier with low to moderate frequency response. Basically, it can be considered as two cascaded generators or amplifiers, the current output of the first stage driving the field of the second generator.

The inputs to the amplidyne are two field coils with the output current proportional to the difference of the current input to the two field coils. Fig. 4 shows

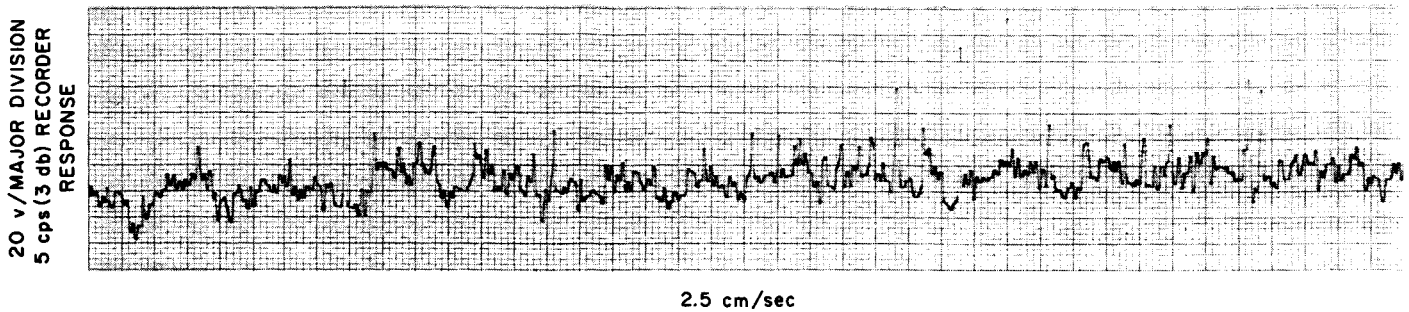


Fig. 2. High voltage ripple—with built-in amplifier power supplies

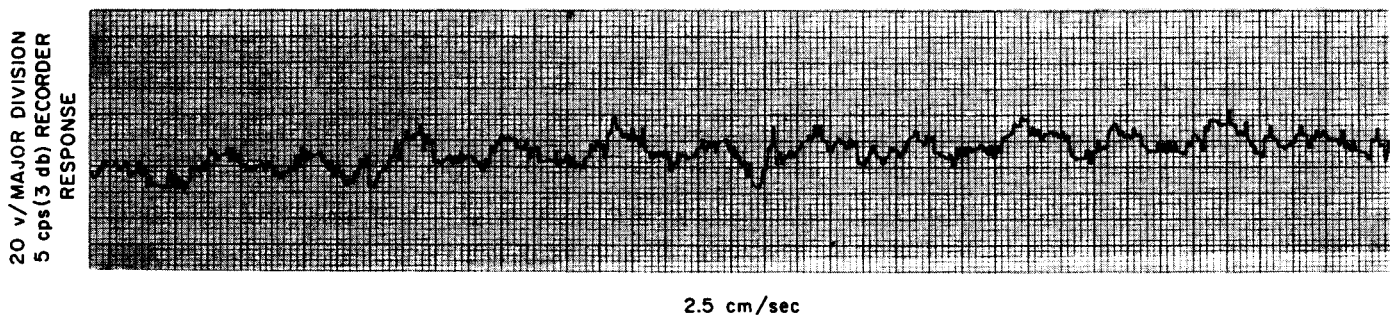


Fig. 3. High voltage ripple—with external regulated amplifier power supplies

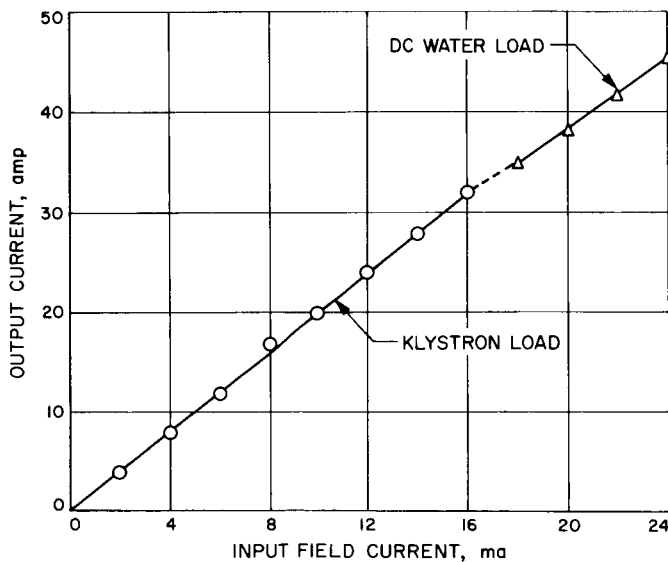


Fig. 4. Amplidyne current gain characteristics—400-cycle generator field load

the measured input current vs output current characteristic of the amplidyne when exciting the 400-cycle generator. The klystron was used as a load for the lower currents and the DC water load for the higher currents.

The amplidyne gain appears essentially linear through its range; the average current gain is 2000:1.

Fig. 5 shows the static gain characteristics of the amplidyne when its output was attached to a lamp load. The effective lamp resistances are shown for each test point. The lamp load was the only DC load with sufficient power handling capacities available at Goldstone. Each lamp was rated for 1500 w at 120 v, and up to eight lamps were connected in parallel for the test. Even though the light bulbs presented a nonlinear resistive load with respect to voltage, the current gain of the amplidyne (slope of line connecting the test points) is relatively constant. The slopes or gains increase with an increase in the number of light bulbs.

4. Generator Field Ripple vs Beam Voltage Ripple

In order to determine the effect of generator field ripple on the high voltage output ripple, the field of the 400-cycle generator was excited with the following supplies, and the corresponding high voltage ripple was recorded.

- (1) Amplidyne in the manual field control mode. The amplidyne fields are connected to the unregulated power supply built into the system.

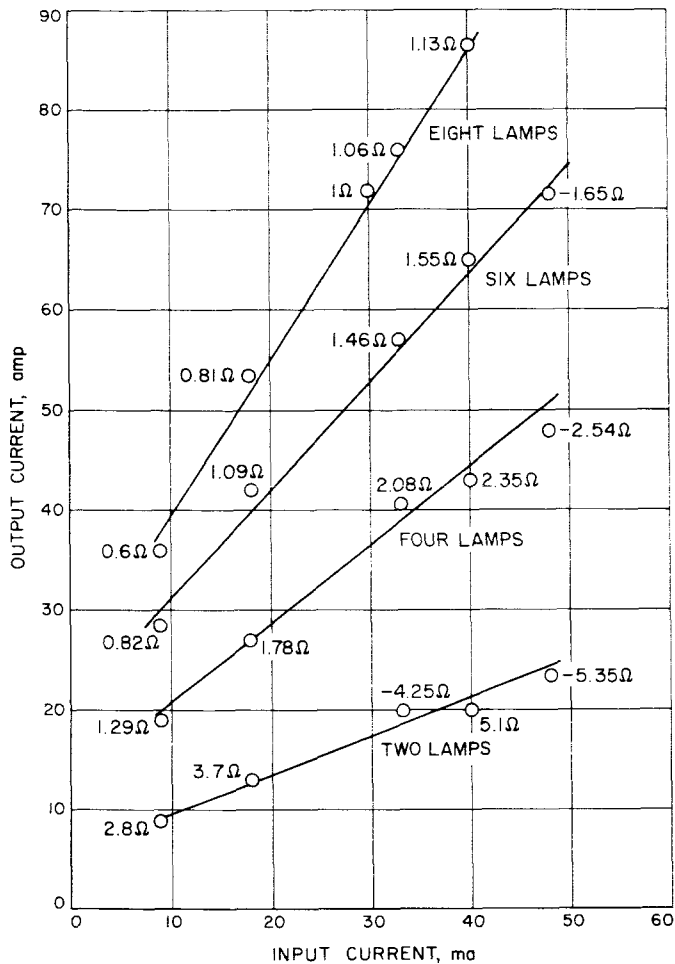


Fig. 5. Amplidyne current gain characteristics—lamp load

- (2) Amplidyne in the manual field control mode with an external, well-regulated power supply connected to the amplidyne fields instead of the unregulated power supply used in (1).

(3) An unfiltered three-phase full wave rectifier power supply using 60-cycle input power. The peak-to-peak ripple was 8 v at 360 cps.

(4) A well-filtered DC power supply with less than 0.1 v peak-to-peak ripple. The supply was normally used for the klystron focus magnet.

All tests were run at a nominal 28-v and 38-amp generator field current for a klystron beam voltage of 30 kv at 7.4 amp.

Fig. 6 is a strip chart recording using the amplidyne as described in (1). The peak excursions in the ripple are due to transients in the unregulated power supply providing the amplidyne field current.

Fig. 7 shows the high voltage ripple when a regulated power supply is used to excite the amplidyne fields as described in (2). Note the absence of any transients.

Fig. 8 shows the high voltage ripple with the three-phase unregulated supply as described in (3). The ripple characteristics have been improved by reducing the higher frequency components.

Fig. 9 shows the improvement that can be obtained when the generator is excited with a low ripple DC power source. Most of the higher frequency components have been eliminated. There is no effect in the lower frequency ripple.

From the tests it can be concluded that the higher frequency ripple is caused by generator exciter ripple, while the lower frequency components are attributed to some other cause. It is suspected that some form of mechanical modulation in the rotor of the 400-cycle

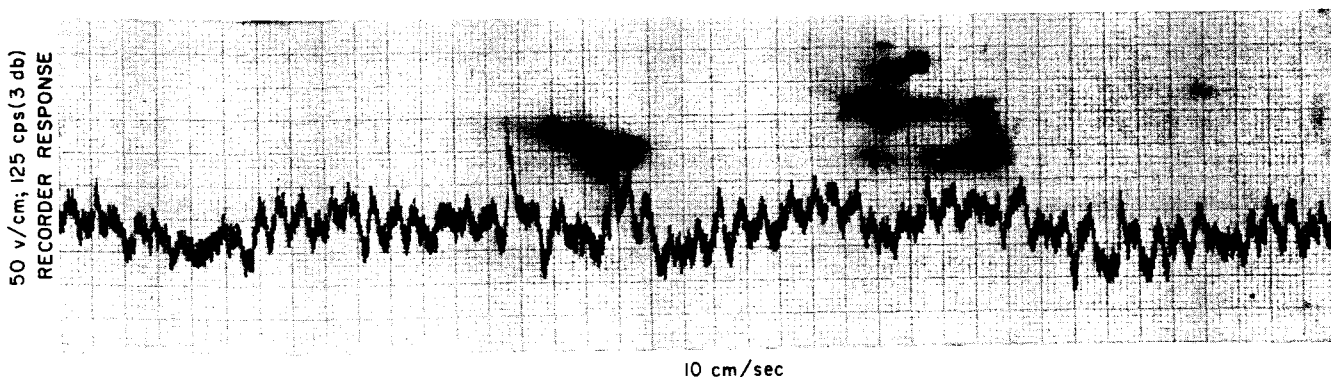


Fig. 6. High voltage ripple—manual field control mode using system unregulated power supplies

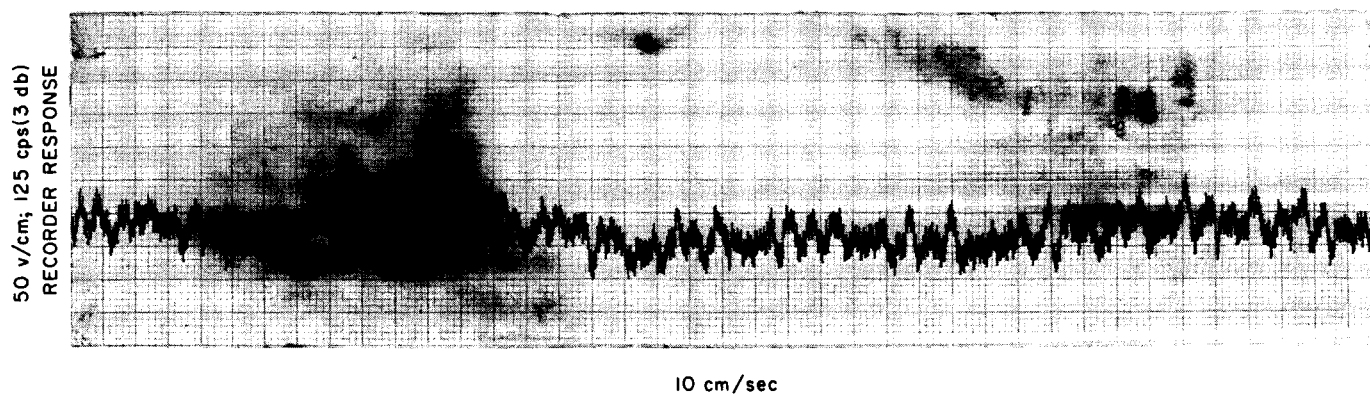


Fig. 7. High voltage ripple—manual field control mode using external regulated power supplies

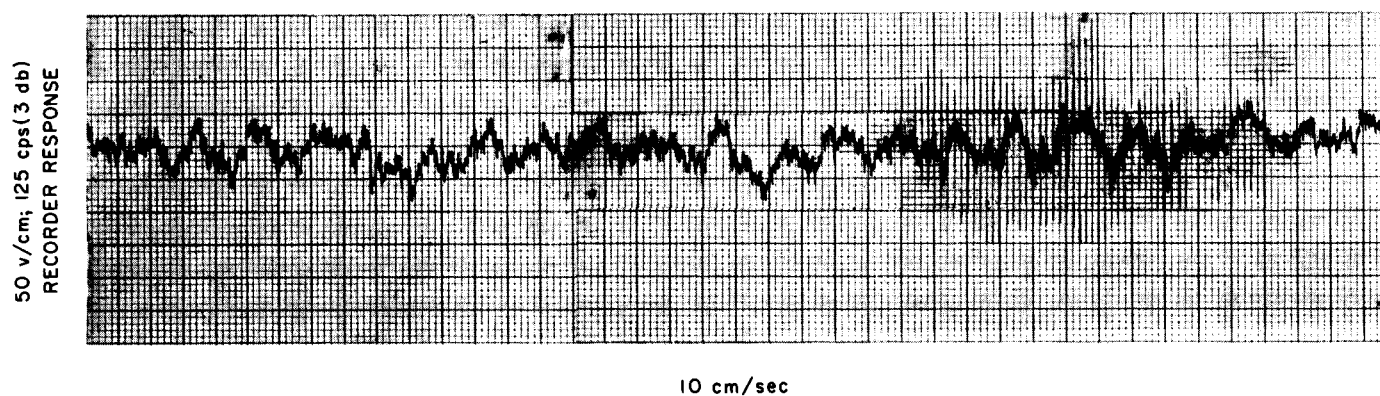


Fig. 8. High voltage ripple—external unfiltered power supply exciting 400-cycle generator field

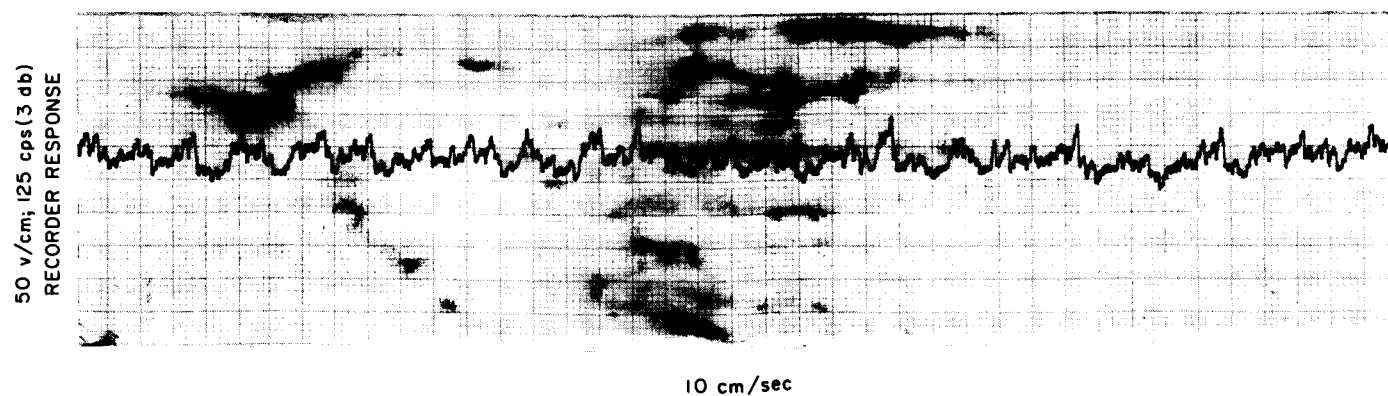


Fig. 9. High voltage ripple—external filtered power supply exciting 400-cycle generator field

generator is causing this low frequency ripple. Future investigations of this problem will require that the generator be instrumented to record mechanical vibration and shaft end play, and that the results be correlated with the high voltage ripple.

5. Amplidyne Step Response Time

The step response time of the amplidyne was checked with the amplidyne connected to lamp load. The voltage and current outputs of the amplidyne were changed 7 to 5%, respectively, by introducing a 1-ma step increase in the amplidyne input fields. Fig. 10 is an oscilloscope picture of the amplidyne voltage step response. The total response time is 0.5 sec.

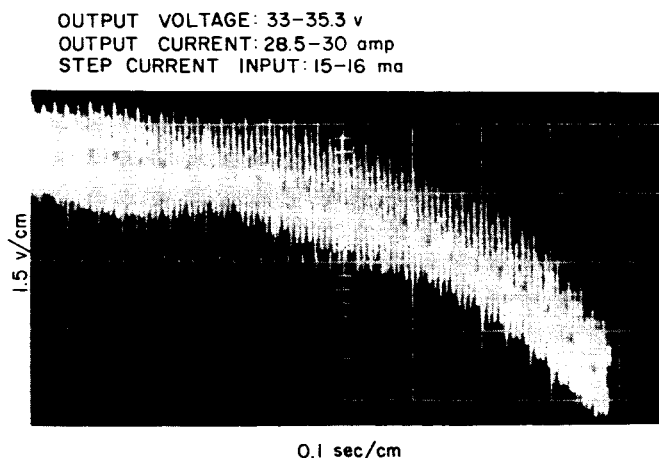


Fig. 10. Amplidyne step response time

The results of the amplidyne step response time tests and high voltage ripple tests indicate that the ripple can be reduced by decreasing the response time of the amplidyne to a point where the lower frequency components of the high voltage ripple are significantly decreased through the closed-loop regulation mode. However, a check with the amplidyne manufacturer revealed that the amplidyne response time cannot be decreased. The other alternative would be to replace the amplidyne with a programmable regulated-filtered 60- or 400-cycle line-operated, solid-state power supply. Such supplies are commercially available and have response times of 20-50 msec.

6. Conclusion

Since the results of the tests reported here indicate that the electronic regulator amplifier is unsatisfactory, it will

be replaced. The higher frequency of the high voltage ripple is caused by amplidyne ripple and the lower frequency is caused by mechanical modulation of the 400-cycle generator. Additional high voltage ripple reduction could be obtained by improving the 400-cycle generator and/or by replacing the amplidyne with a regulated-filtered, solid-state power supply. Both alternatives are currently being investigated.

B. Waveguide Transfer Switch

R. C. Chernoff

A two-position, four-port transfer switch for use with 100-kw S-band transmitters has been delivered and has undergone preliminary low power tests. This device will be used to switch the transmitter between the RF water load and the feed horn, or, in the case of a two-transmitter feed cone, it can be used to select the transmitter to be fed to the antenna as well as to terminate either of them in the water load (Fig. 11).

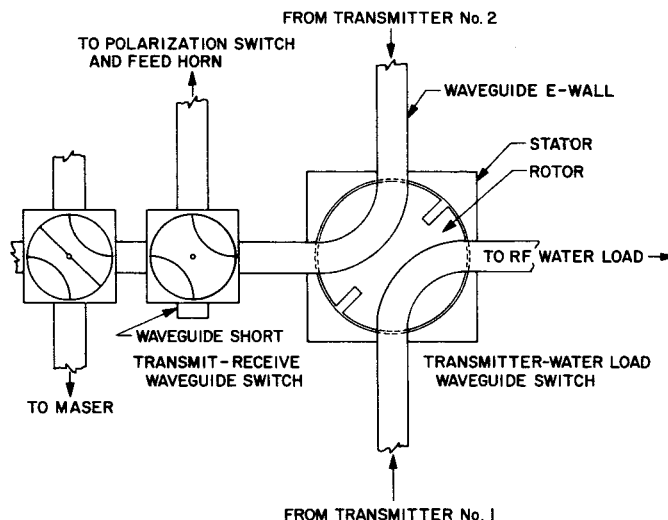


Fig. 11. Transmitter—feed horn switching diagram

The principal parameters of such a waveguide switch are: (1) power handling capacity, (2) insertion loss, (3) voltage standing wave ratio (VSWR), and (4) isolation between port pairs. The first three should be typical of the other waveguide components of the transmitter-feed horn system. The last parameter, isolation, must be large enough to satisfy the following requirements: (1) the

power coupled into the maser during transmitting must be well below the level which would permanently or temporarily degrade its performance, and (2) the klystron beam noise power coupled into the maser during the receive cycle must be below receiver threshold. Receiver and transmitter are isolated by two waveguide switches during both transmit and receive cycles (SPS 37-18, Vol. III, pp. 24-27). It is not yet feasible to eliminate klystron beam noise as a possible source of interference by substituting beam-keying for the presently used drive-keying, but this may be attempted when the new X3060 klystrons, which incorporate a modulating anode, are put into service (SPS 37-33, Vol. III, pp. 88-89).

The specification for this switch are as follows:

RF power	125-kw CW maximum
Insertion loss	0.020-db maximum 0.015-db design objective
VSWR	1.02:1.00 maximum
Isolation	80-db minimum
Frequency range	2.1 to 2.4 GHz

The switch is of conventional design consisting of two 90-deg E-plane bends machined into a solid rotor, and a stator to which input and output waveguide are connected. Low power measurements of insertion loss have been made; the results are given in Table 1.

Table 1. Waveguide switch insertion loss at 2.388 GHz

Port	Loss, db
Port 1 to Port 2	0.0118
Port 2 to Port 3	0.0104
Port 3 to Port 4	0.0132
Port 4 to Port 1	0.0138

These measurements were made with an insertion loss test set essentially identical to that described in SPS 37-30, Vol. IV, pp. 234-238. The values of Table 1 are the averages of three readings made at each port pair. This number of readings is not enough to establish the probable error of the measurements, but since the largest variation within any one set was 0.0020 db, it is clear that the maximum insertion loss specification of 0.020 db is met. However, it is less certain

that the "design objective" insertion loss of 0.015 db is met for port pairs 3-4 and 4-1, and this question can only be resolved by a much longer series of measurements.

C. 455-kc Doppler System

R. B. Crow

A new method of obtaining S-band doppler in the bistatic configuration (transmit at Venus Station and receive at Mars Station) has been developed. However, all required equipment is not currently available for bistatic operation, and the 455-kc doppler system has been used in a monostatic configuration (transmit/receive at Venus Station with a 50% duty cycle). One desirable feature of this system becomes immediately apparent: the 455-kc doppler loop can be locked and doppler data gathered simultaneously with other "open loop" experiments.

The 455-kc doppler loop (Fig. 12) has the same loop bandwidth as the carrier tracking loop (Fig. 13), and has been designed to utilize modules that are normally part of the latter. A tape containing the ephemeris doppler is inserted into the programmed local oscillator (PLO), as is shown in Fig. 12. The ephemeris doppler of the PLO differs from the tape by the amount of loop error. The PLO error is printed out to allow data correction. The PLO is offset by the amount of the anticipated doppler so that the receiver is tuned on its nominal center frequency. The received signal can now be used to obtain the error between the predicted doppler and the actual doppler.

The bistatic doppler radar system (Fig. 14), which is scheduled for installation in the near future, will have the following advantages over the monostatic operation:

1. Continuous transmission and reception can be employed, thereby increasing the received time by a factor of two.
2. The increased gain of the 210-ft antenna at the Mars Station can be used.

Table 2 shows the measured bandwidth and jitter for both the carrier tracking loop and the 455-kc doppler loop as installed at the Venus Station. Jitter measurements were also taken at the output of the doppler balanced mixer.

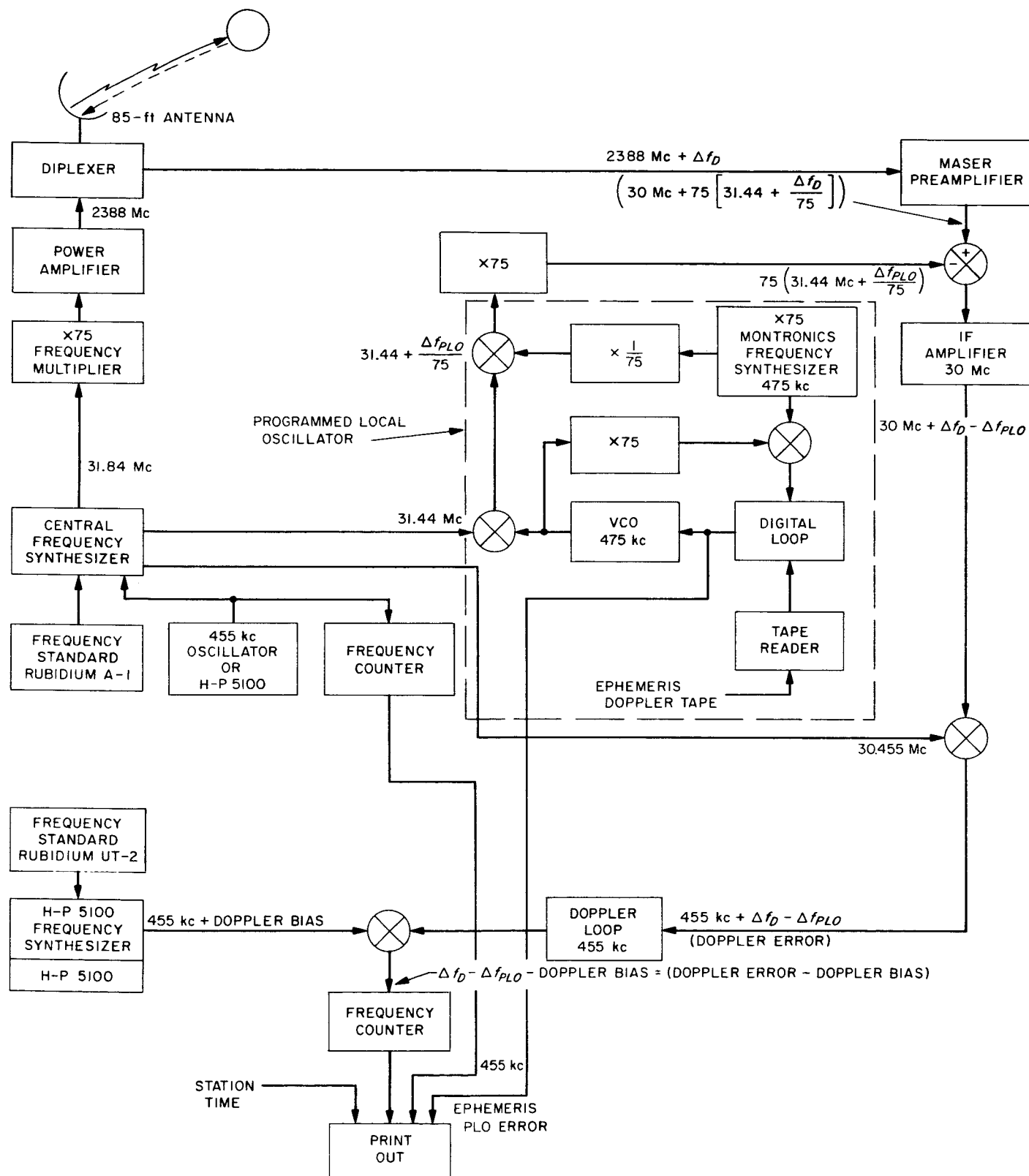


Fig. 12. Monostatic doppler radar system at the Venus Station

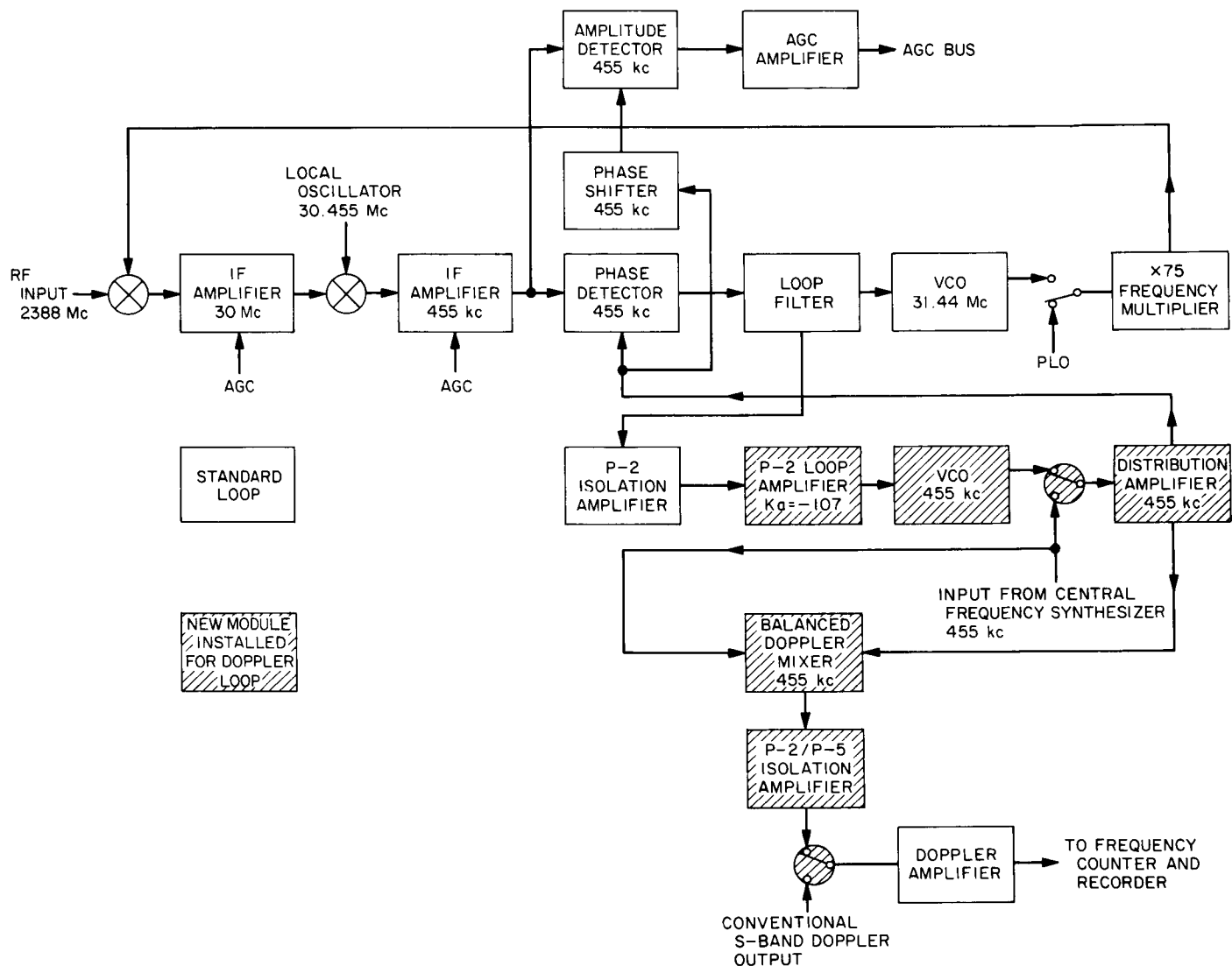


Fig. 13. Block diagram showing the addition of the 455-kc doppler loop to the standard planetary radar receiver

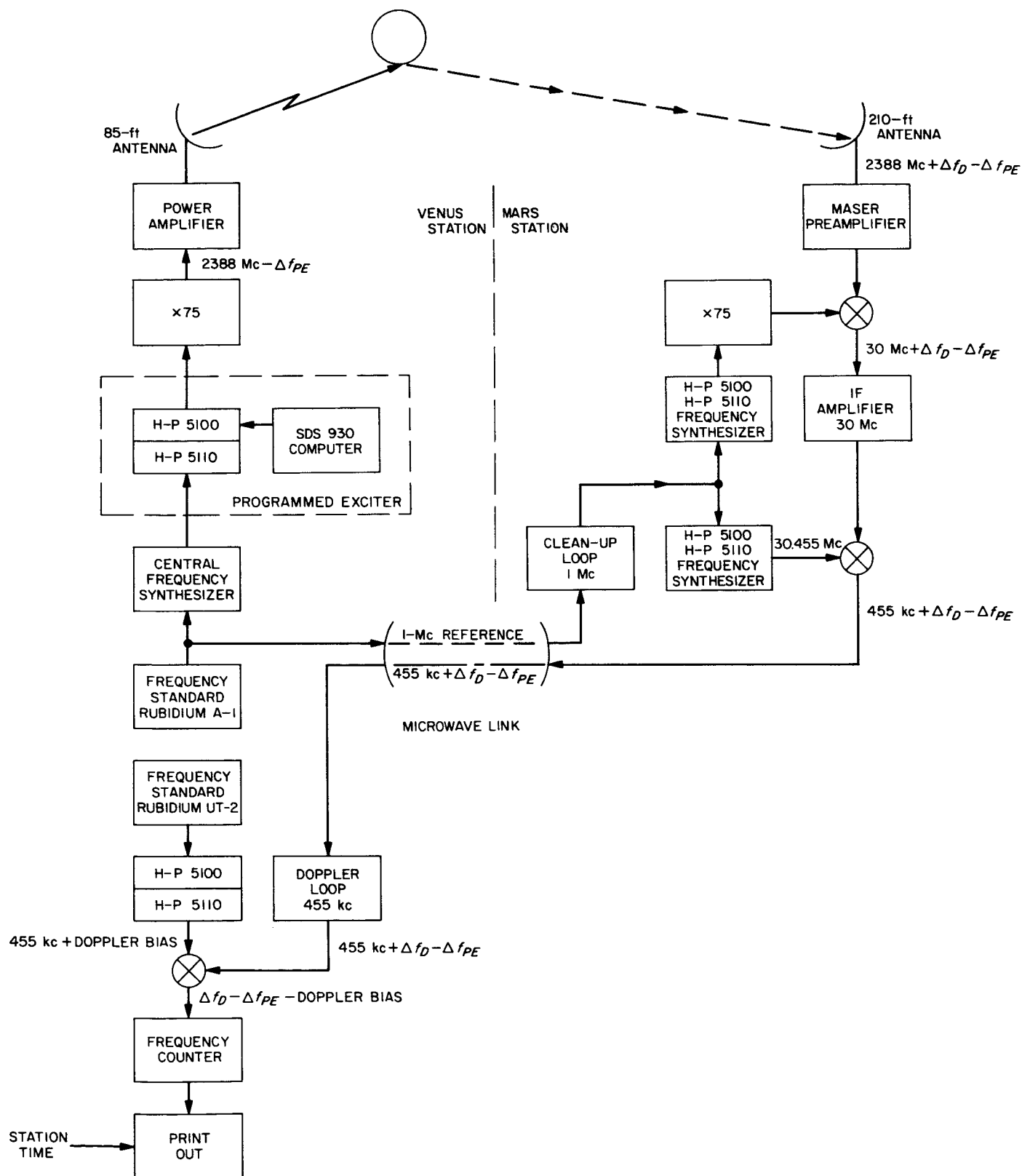


Fig. 14. Bistatic doppler radar system

Table 2. Measured bandwidth and jitter for both carrier loop and 455-kc doppler loop at the Venus Station

Item	Design $2B_{L_0}$, cps	Measured $2B_{L_0}$, cps	Degrees, rms
Standard carrier loop	2 4 8	1.85 3.78 7.66	3.6 2.5 1.2
455-kc doppler loop	2 4 8	1.98 3.78 7.62	2.3 1.5 1.1
Output of doppler balanced mixer	2 4 8		0.4 0.66 1.0

It is interesting to note that the 455-kc doppler loop showed a phase lock over a reasonable period of time during the January 1966 reception of *Mariner IV*. The received signal level at this time was -177.8 dbm (system temperature of 29°K and $2B_{L_0} = 2$ cps).

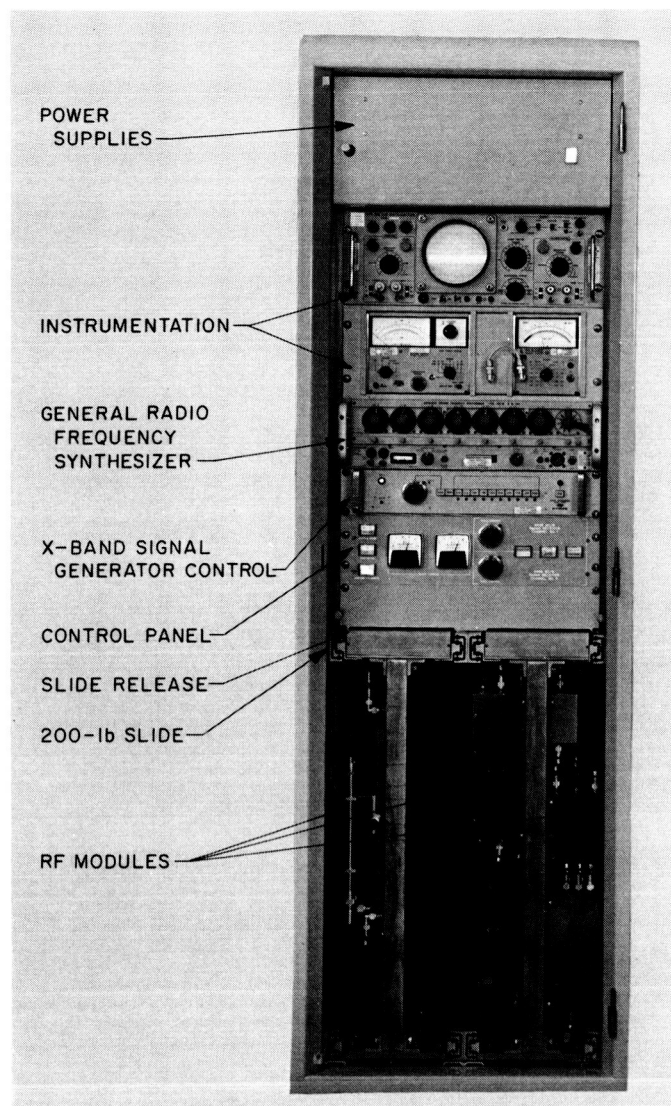
D. Venus Station *Mariner IV* Post-Encounter Receiver, X-Band Lunar Radar Receiver, and S-Band Planetary Radar Receiver

C. F. Foster

The three receiver systems at the Venus Station—the 8448 Mc and the 2295 Mc (SPS 37-35, Vol. III, pp. 42-45), and the 2388 Mc (SPS 37-31, Vol. III, pp. 72-76)—have been separated, both physically and electrically, to eliminate time loss because of system interdependence and to provide increased experiment support by allowing simultaneous operation of all three.

1. Design Modifications

A single bay cabinet was constructed for the 8448-Mc receiver. This cabinet is of the general design used for the 2295-Mc receiver (Fig. 15). To gain necessary space and to provide ease of servicing, several improvements

**Fig. 15. 8448-Mc receiver**

have been incorporated in this cabinet (Figs. 15 and 16). The large, 500-lb slides were replaced with a smaller, 200-lb version. The slide release was moved from the bottom to the top slide. The voltage distribution was accomplished by means of a special retractable cable (Fig. 17); this provided additional panel space and also allowed improved routing of power cables.

The 8448-Mc receiver modules were removed from the 2388-Mc receiver system and were mounted in the new cabinet along with the additional modules required (see shaded area of Fig. 18). Since the 8448-Mc receiver controls had been shared with the 2388-Mc receiver, a new control panel was constructed. This new panel (Fig. 19) provides remote *on-off* switching of the antenna-mounted

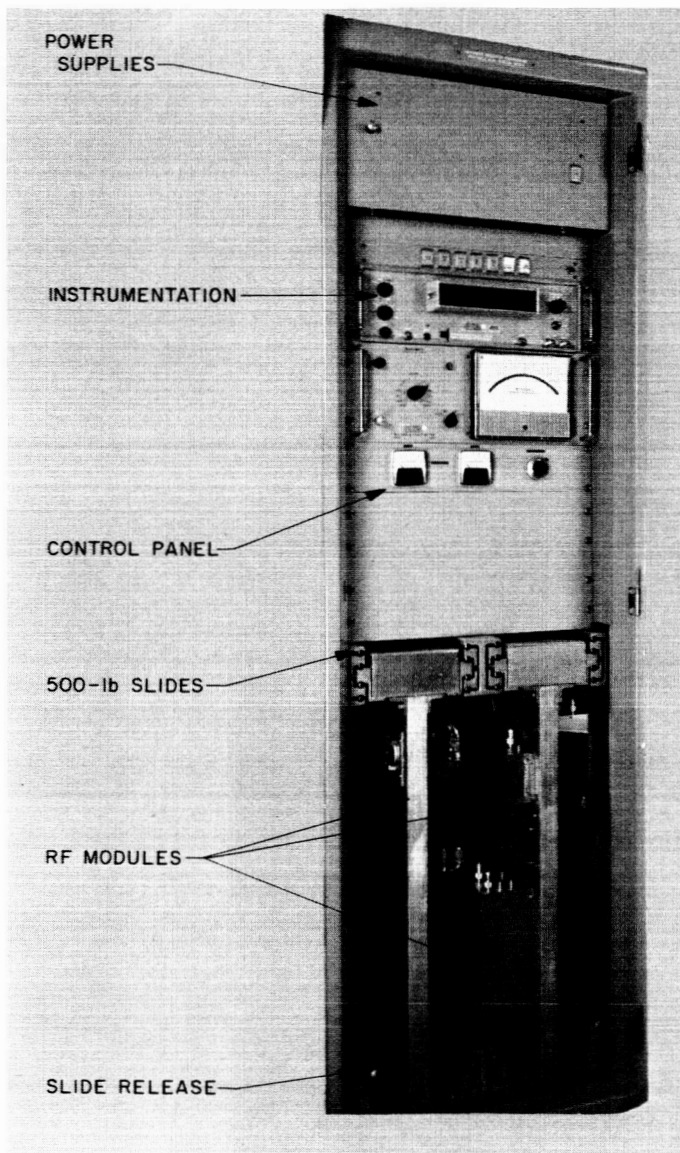


Fig. 16. 2295-Mc receiver

converter, remote operation of the antenna-mounted system calibration probe, visual indication of the converter mixer current, system mode indication, instrumentation selection, and manual gain for channels 1 and 2.

The DC power supplies are mounted at the top of the cabinet, and receiver instrumentation is mounted in the center of the cabinet, along with a frequency synthesizer (for the coherent reference signal used in the third conversion), a remote control panel which adjusts the level of the X-band signal generator located in the antenna (SPS 37-34, Vol. III, pp. 59-60), and the new 8448-Mc receiver control panel. The lower section of the cabinet contains all the RF modules.

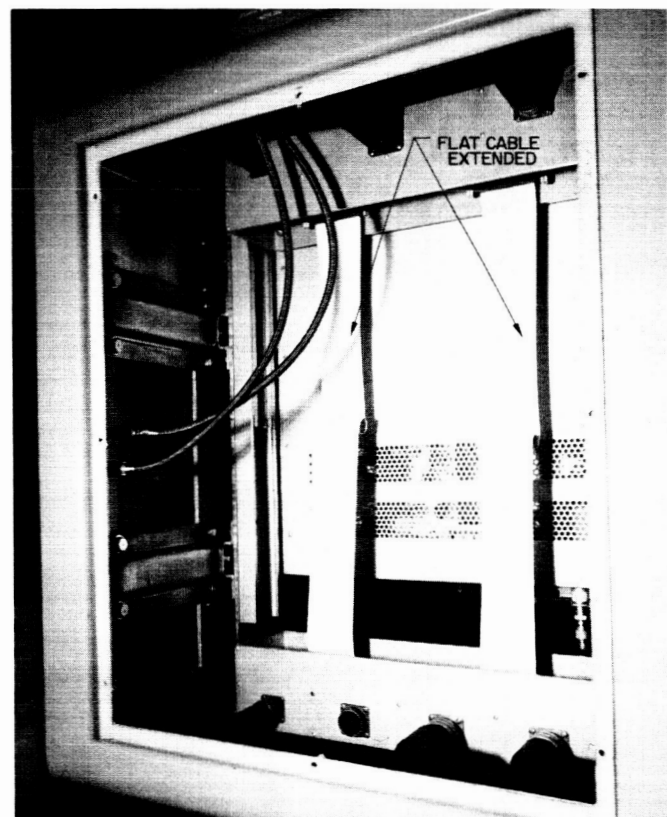
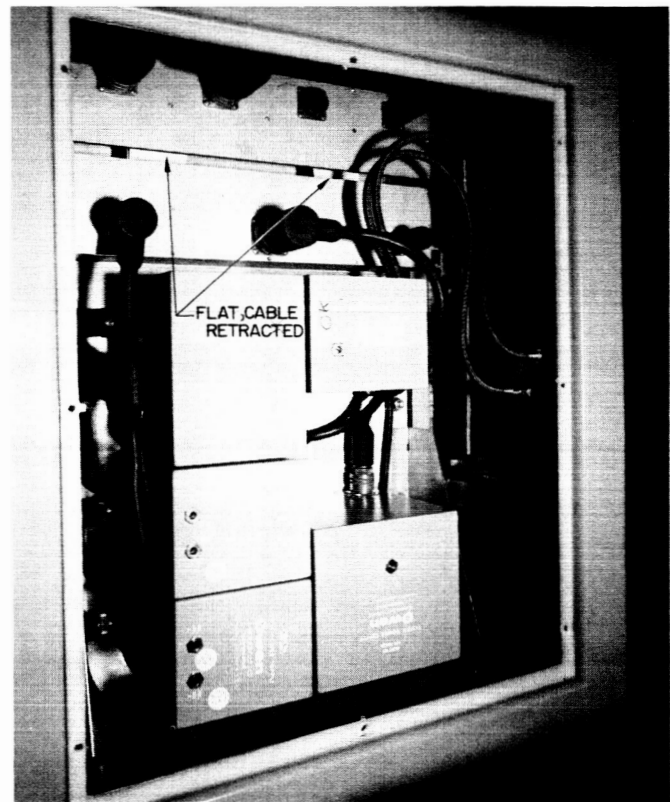


Fig. 17. 8448-Mc power distribution

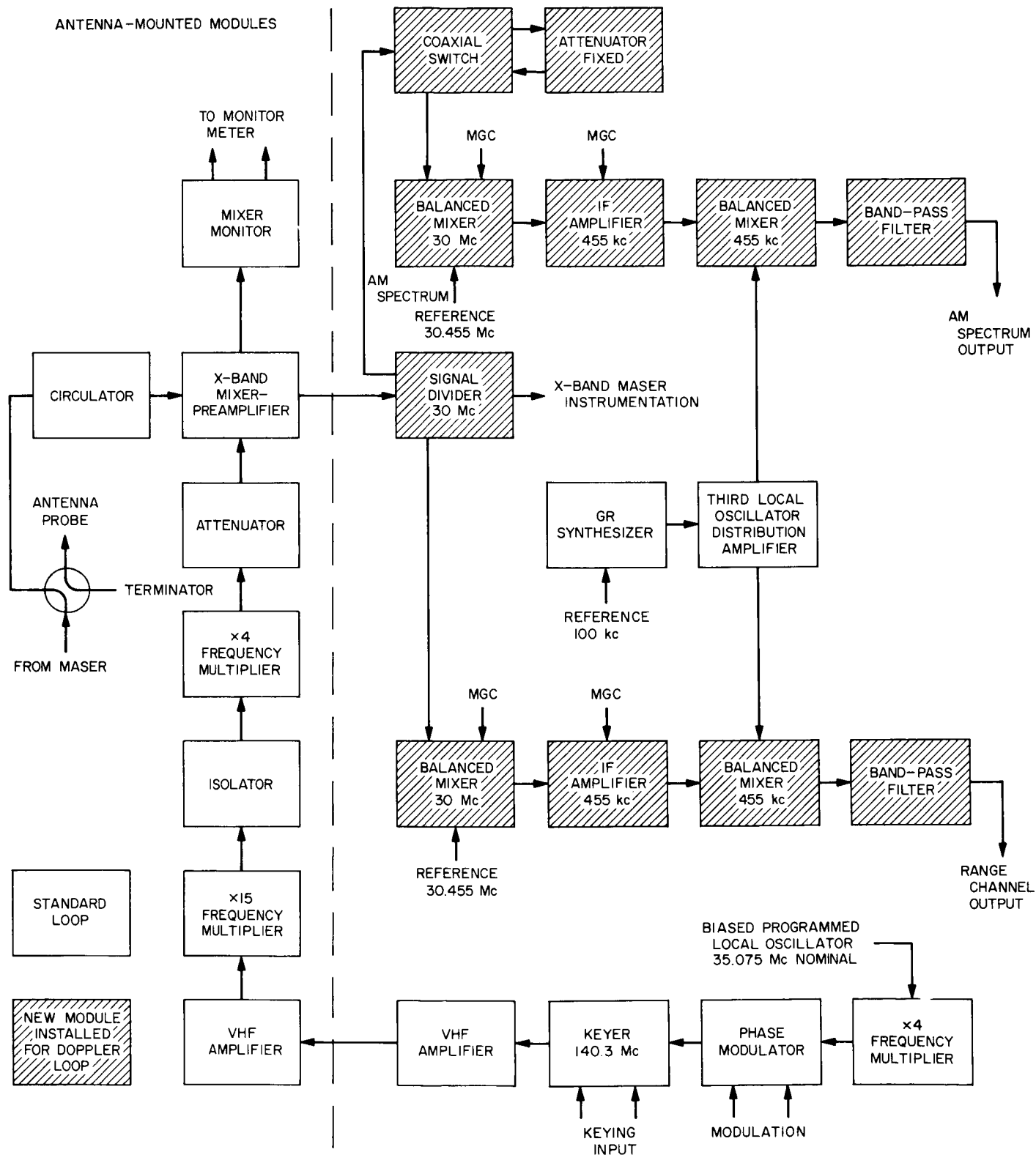


Fig. 18. 8448-Mc receiver block diagram

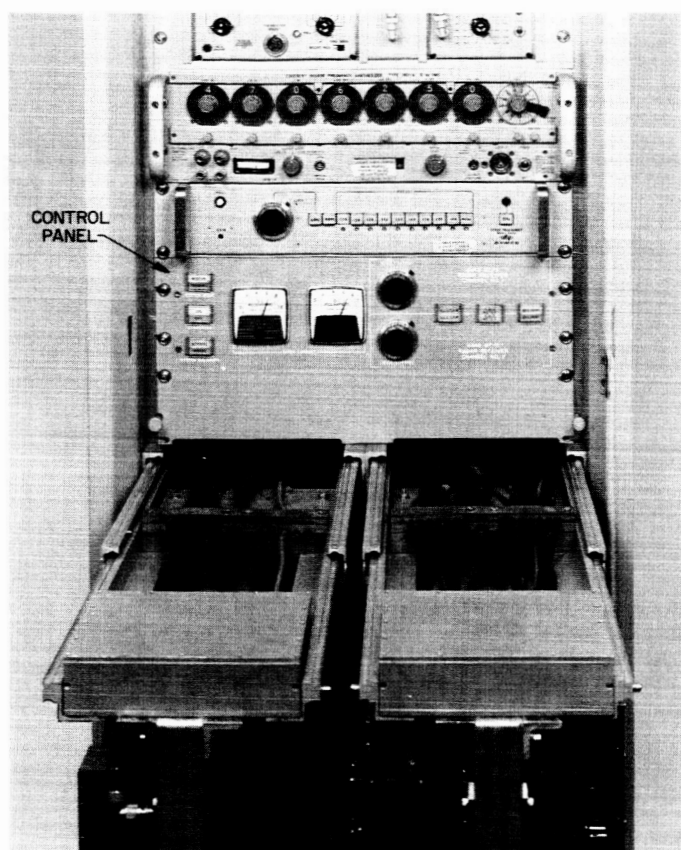


Fig. 19. 8448-Mc receiver control panel

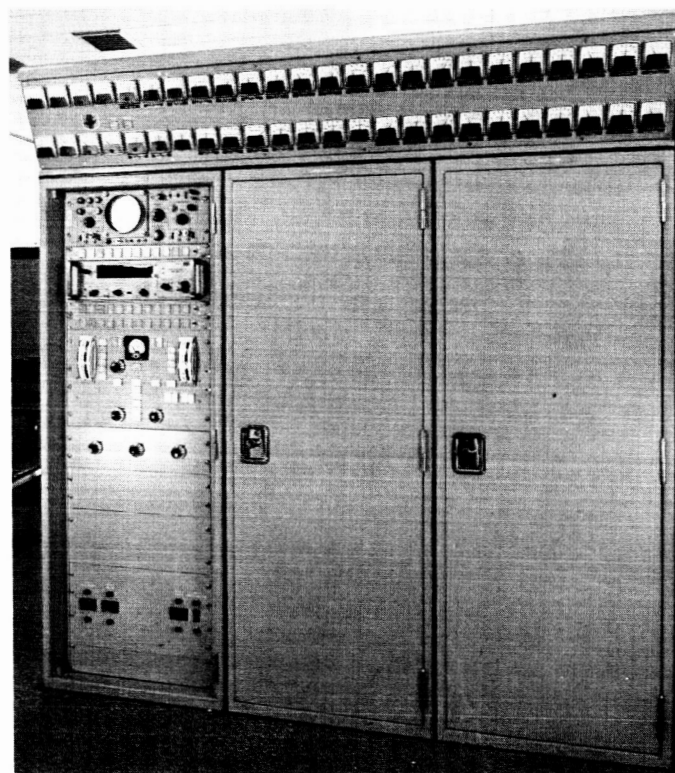


Fig. 20. 2388-Mc receiver

The Mod IV receiver system (SPS 37-31, Vol. III, pp. 72-76) contained the 8448-Mc receiver, the 2388-Mc receiver, and parts of the 2295-Mc receiver. The modules and controls associated with the 8448- and 2295-Mc receivers were removed, and two bays of the Mod IV were removed along with a section of the top hat. It was not possible to return the 2388-Mc receiver to JPL at the time of modification, as it was being used to support the Venus mapping experiment. Therefore, the sheet metal work was accomplished at the Venus Station. The top hat meter panel was shortened, and all meters not in use were removed. The modules were relocated in two of the remaining bays and the system was rewired (Fig. 20). The original 2388-Mc receiver has been changed, as is shown in Fig. 21, to provide for future experiments. One significant change is the inclusion of a simple system for injecting receiver noise into the amplitude-modulated spectrum channel during transmit time for calibration. The local oscillator drive is turned off during transmit time, and the coaxial relay switches a variable attenuator from the 30-Mc signal line. As this attenuator was set up to a precise level during the receive time, the autocorrelator receives the same noise

level during transmit as during receive. A 455-kc phase-locked doppler loop which was also installed is reported in detail elsewhere in this volume.

Work completed on the 2295-Mc receiver consisted of the removal of cables connecting this receiver with the Mod IV, the removal of modules used for *Mariner* back-up, and the installation of the new modules required for a single wide-band total power channel (Fig. 22) now being used once a month to receive the *Mariner* spacecraft. The arrangement of the cabinet remains the same, with power supplies at the top, instrumentation in the center, and RF modules mounted on the lower section. A new control panel was constructed which provides remote metering of the antenna-mounted mixer current and a control for manual gain.

2. Testing and Evaluation

Because of extensive module relocation, a coherent leakage check was made on all systems using the Venus Station autocorrelator; results were well within the design specifications. The synchronous channel in the 2388-Mc system was subjected to field tests, and it was determined that no changes had occurred because of

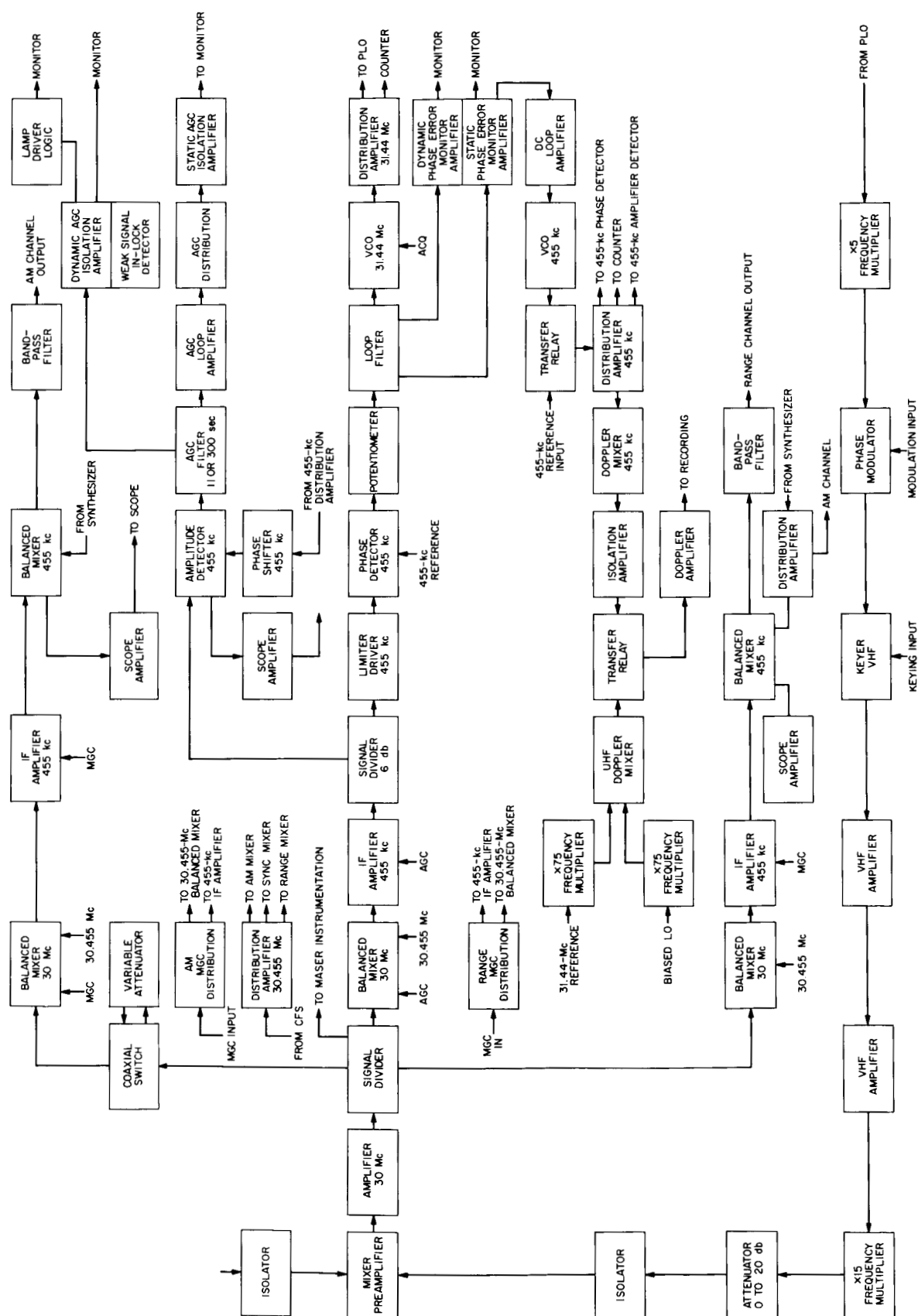


Fig. 21. 2388-Mc receiver block diagram

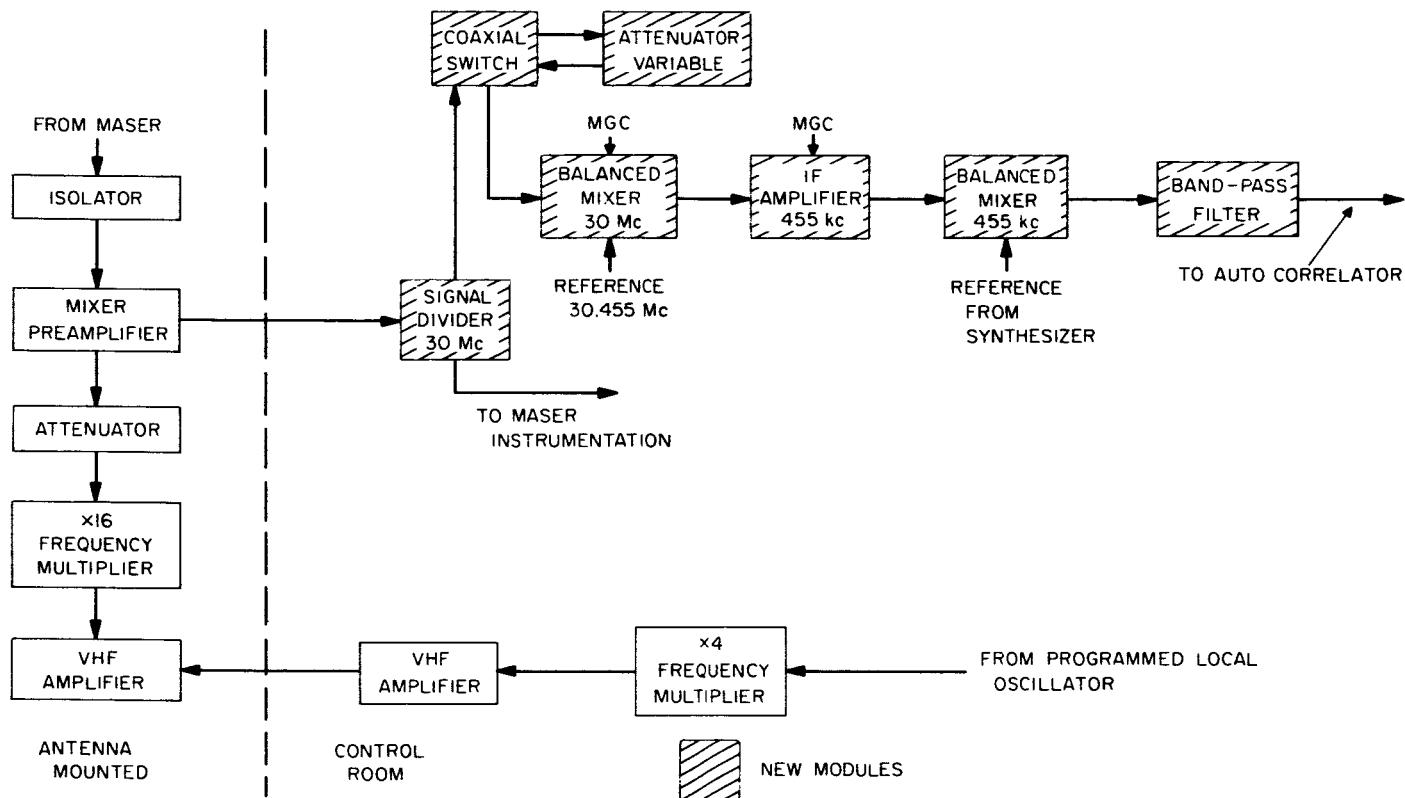


Fig. 22. 2295-Mc receiver block diagram

module relocation. Because of module construction and redesign (SPS 37-36, Vol. III, pp. 36-37), the overall bandwidth of the open loop channels was measured. The results of these measurements are shown in Figs. 23 and 24.

The 2295-, the 8448-, and the 2388-Mc receivers, which had previously shared controls and modules, have been successfully modified and now contain separate controls and instrumentation, as well as the additional modules

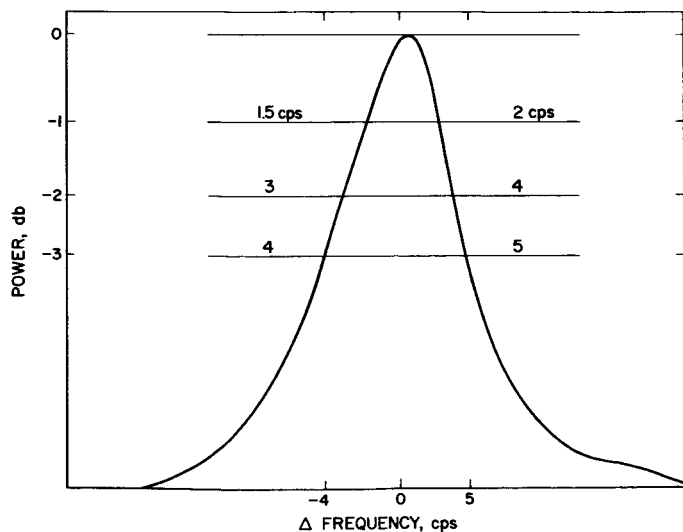


Fig. 23. Range channel bandpass

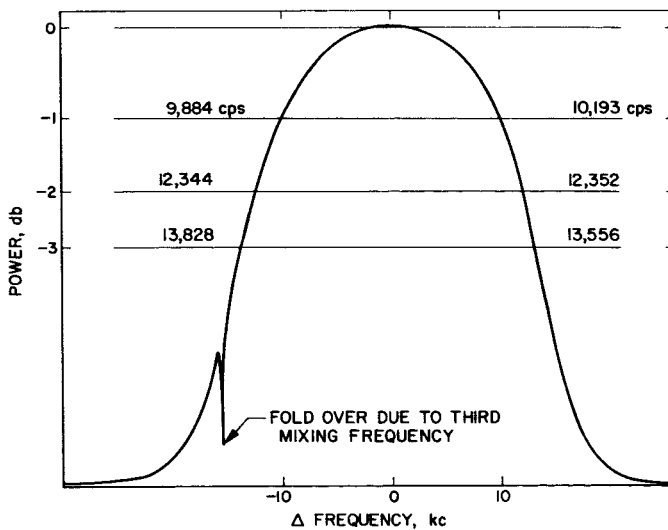


Fig. 24. Amplitude-modulated channel bandpass

necessary to provide the Venus Station with three completely independent receivers (with the exception of cables running from the control room to the 85-ft antenna). Additional cables have been ordered and are now at the Venus Station awaiting installation.

E. DSN/MSFN 20-kw Transmitters

R. L. Leu

The JPL Manned Space Flight Network (MSFN) transmitter backup requirement is simultaneous radiation of two 10-kw carriers from an 85-ft antenna, as shown in Fig. 25. To meet the objective, two 20-kw outputs will be combined in a short-slot hybrid, resulting in a 3-db power loss to each carrier. The 20-kw transmitters will utilize the 5K70SG klystron developed for the MSFN and will meet the Goddard Space Flight Center (GSFC) requirements, with the exception of the incidental phase modulation resulting from beam voltage ripple.

1. Combiner

Initially, two types of combiners were considered: a 3-db short-slot hybrid, and a low loss combiner. The 3-db hybrid is small, simple, and practical, but results in a

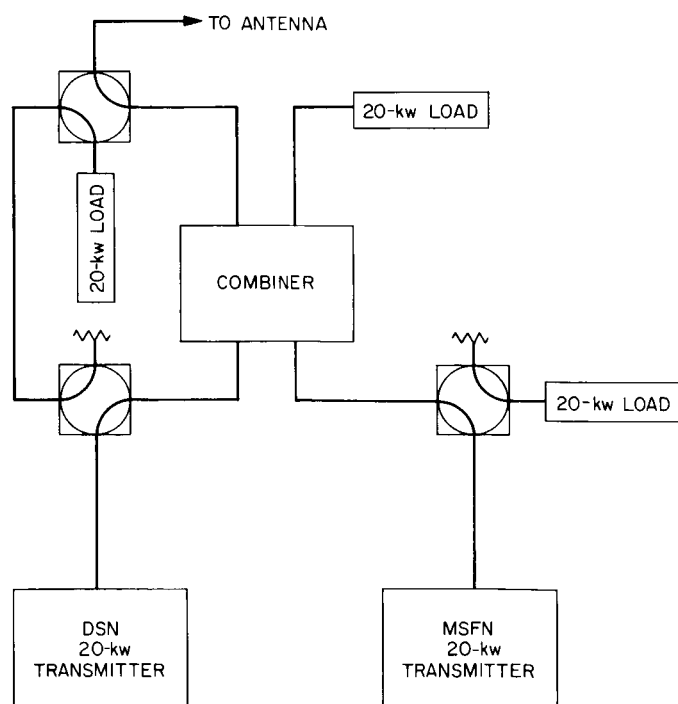


Fig. 25. DSN/MSFN dual transmitter configuration

3-db power loss for each input signal. The lost power is dissipated in an RF water load. The low loss combiner consists of two 3-db short-slot hybrids interconnected by two waveguide runs. One waveguide run is very short (2-3 ft); the other is in excess of 80 ft. The input hybrid receives two signals separated by a fixed frequency increment. The output hybrid combines the signals into a common output.

The input hybrid divides half the power of each signal into each of the two waveguide runs. The long waveguide length serves as a delay line for phasing the dual frequency signals in each arm to combine at the second hybrid in a common output port. A servo-driven 360-deg line stretcher is incorporated in the 80-ft arm to compensate for temperature changes and slight frequency deviations. Because of the large size of this unit, repackaging would be required and difficulties would be encountered in placing it in the antenna structure. The cost of the unit, plus that of repackaging, prohibits the use of the combiner.

2. Power Amplifier

The 5K70SG klystron was developed for the *Apollo* program to meet the performance specifications imposed by GSFC. However, this klystron has proved more efficient and has a higher gain than that originally intended for use in the existing 10-kw transmitters. The only specification which will not be met is phase-modulation generated by beam voltage ripple. The GSFC requirement is that the power in the incidental phase-modulated sidebands be 50 db below the carrier. The high voltage power supplies which are part of the DSN transmitters have a maximum beam voltage ripple of 20 v peak-to-peak, which could result in incidental phase-modulated sidebands 39 db below the carrier at ± 2400 cps. This does not include the 60-cps modulation of the 400-cps motor generator output. To meet the -50-db sideband requirement with the 5K70SG klystron phase-pushing figure of 0.10 deg/v would require reduction of the high voltage power supply ripple to 5.5 v peak-to-peak and provision of a filter for the 60-cps modulation. Filters to achieve this low ripple would result in energy storage too high for the klystron to withstand in the event of arc.

The JPL DSN/MSFN 20-kw transmitter specification for incidental phase modulation and stability will be 1-deg rms above 1 cps, resulting in total sideband power 35 db below the carrier. Using the high voltage power supply ripple and klystron phase-pushing figure as a guide, the 1-deg rms phase contribution by the 20-kw transmitter is a realistic number.

VI. Tracking Stations Engineering and Operations

A. Station Control and Monitor Console Subsystem

G. Jenkins

The station control and monitor console (SMC) subsystem provides a central point for station operations, as well as a writing surface and means for inter- and intra-station communications. System and subsystem status is displayed by means of lights, relays, and meters. For a detailed description, see SPS 37-31, Vol. III, pp. 9-13.

Evaluation revealed the need for certain modifications in the prototype SMC which was built by Hughes Aircraft Co., Fullerton, California, and installed at the Pioneer Station (DSIF 11). To provide better visibility, the five-bay console was reduced in height. Also, in order to shield some of the overhead light and to make the displays more readable, bezels were installed in the antenna position panel and in the GMT clock panel

(Fig. 1). It was further indicated that the count down clock should display seconds in addition to minutes. Redesign of the count down clock is now in process, and the first unit is scheduled for delivery by September 1966.

The contract for ten production-type SMCs was awarded to Resdel Inc., of Pasadena, California. The first full production unit was delivered to JPL in September 1965 and shipped to the Spacecraft Guidance and Command Station at Ascension Island (DSIF 72). However, because of scheduling difficulties, this unit is not operational at present. The second production unit was shipped to the Spacecraft Monitoring Station at Cape Kennedy (DSIF 71). The cognizant development engineer observed the installation at this site and reported that no major problem areas were discovered and that installation and checkout were routine.

All of the production units have been delivered to the DSIF sites, and those at the Pioneer (DSIF 11), Echo (DSIF 12), Tidbinbilla (DSIF 42), and Spacecraft Monitoring (DSIF 71) Stations are operational.

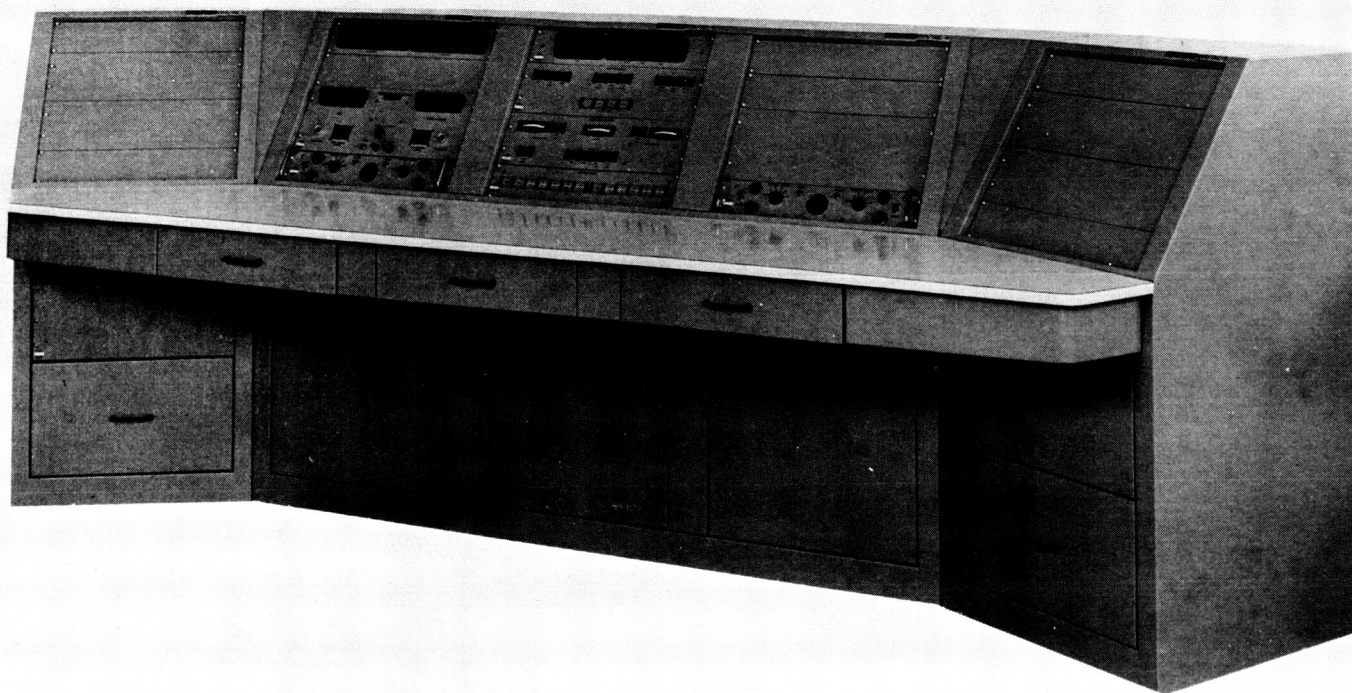


Fig. 1. Station Control and Monitor Console (SMC) Subsystem 8

B. Antenna Pointing Subsystem

W. C. Frey

1. Introduction

The antenna pointing subsystem (APS) is a new subsystem that will provide the DSIF stations with the capability to point antennas under computer control, in addition to the existing automatic tracking and manual control modes of operation. The subsystem computes spacecraft and celestial body ephemerides from parameter inputs and provides position error signals to the servo assembly of the antenna mechanical subsystem (ANT). In addition to this primary function, the APS accepts inputs of rate and position offsets from a subsystem control panel, positions the antenna to preselected coordinates for calibration purposes, and displays selected data on the subsystem control panel.

APS equipment will add the following capabilities to the DSIF: (1) improved spacecraft acquisition time, (2) effective angle search patterns for spacecraft acquisition

for nonstandard trajectories, (3) tracking when received signal strength is too low for auto track operations, (4) programmed corrections to eliminate antenna structural and radio boresight shift pointing errors, and (5) more flexibility and precision in control of antenna movement.

2. Implementation

The subsystem consists of a computer with associated peripheral equipment, a control panel located on the servo operator's console, and an interface equipment rack. The APS operates in a closed position loop in conjunction with the ANT servo assembly and the antenna angle position readout assembly. The APS will use the Scientific Data Systems (SDS) 910 computer, presently located in the digital instrumentation subsystem (DIS), as the central processor.

The APS will be implemented in two steps: (1) the interim antenna pointing subsystem, and (2) a full capability antenna pointing subsystem (APS I).

a. Interim antenna pointing subsystem. The equipment configuration for this phase will include the 910 computer, a control panel, and portions of the DIS computer input/output equipment. Use of the DIS input/output equipment for APS interface to other subsystems will eliminate the design and procurement time involved in providing a special rack of APS input/output equipment. Although the interim subsystem will operate with reduced control and display capabilities, flight project requirements can be met. During this time the 920 computer in the DIS will perform Phase I system monitoring. Since the input/output equipment must be shared by the Phase I system monitoring and the APS, the capabilities of the DIS will be reduced. Therefore it is necessary that the interim APS terminate use of the DIS I/O hardware before the DIS Phase I system monitor configuration reverts to the DIS Phase II configuration, where full capabilities are required.

The interim APS will use the existing Venus Station prototype program to carry out the antenna pointing function. This program will be modified to meet the new equipment configuration and to provide noninterference operation with the 920 DIS Phase I system monitoring program.

b. Full capability antenna pointing subsystem (APS I). The equipment configuration for the APS I will include the 910 computer, a control panel, and a rack of APS input/output interface equipment. The APS I will be introduced at each station before the DIS Phase I system monitoring configuration is changed to the DIS Phase II configuration. Since the APS I will contain its own interface equipment rack, the DIS will be restored to its full input/output capability. The SDS 910 computer will be functionally separated from the DIS/SMC II subsystem and connected to the APS interface rack for all input/output operations. The APS I will conform to the assembly configuration and functional capabilities listed in Section 3.

3. Functional Description

The APS will be programmed to perform ephemeris computations and provide antenna position errors to the servo assembly.

a. Ephemeris computation. The subsystem program accepts two types of data: (1) time-dependent samples of angles in local coordinates, and (2) time-independent or time-varying samples of apparent geocentric coordinates.

Time-dependent samples of angles in local coordinates. The principal functions of the subsystem in this mode are as follows:

1. Accept an input of a precomputed paper drive tape by the computer photo reader. The tape consists of time tagged samples of local hour angle and declination of the trajectory of the object to be tracked.
2. Synchronize tape pull time with station time.
3. Reject samples with improper format or disallowed characters.
4. Perform linear interpolation between tape samples to continuously update the ephemeris.

Time-independent or time-varying samples of apparent geocentric coordinates. The principal functions of the subsystem in this mode are as follows:

1. Accept inputs of one set of time-independent geocentric coordinates (apparent right ascension and declination) from the subsystem control panel for tracking stars.
2. Accept inputs of three sets of time-varying geocentric coordinates from the subsystem control panel for planetary and spacecraft tracking.
3. Perform a three point interpolation computation for time-varying geocentric coordinates, using Lagrange's formula to solve for the values of right ascension and declination corresponding to station time.
4. Compute sidereal time for a given station time.
5. Calculate the ephemeris in local coordinates using the above information of right ascension, declination, sidereal time, and station longitude.
6. Compute elevation refraction correction.
7. Update the ephemeris by computing a set of coordinates every second.
8. Perform linear interpolations between 1-sec coordinate values to continuously update the ephemeris.

b. Servo error signals. The subsystem program performs the following functions to provide servo error signals:

1. Accept inputs of actual antenna position from angle encoding assembly every 20 msec.

2. Compute angular difference between actual antenna position and desired ephemeris position every 20 msec for each antenna axis.
3. Output from the computer the digital angular difference to a digital-to-analog converter every 20 msec for each antenna axis.

4. Schedule

It is anticipated that the first interim APS will be installed and operational at the Goldstone Echo Station (DSIF 12) in June 1966. The remaining stations in the net are scheduled for installation at one-month intervals. All stations, with the exception of the Spacecraft Monitoring Station (DSIF 71), will be equipped with antenna pointing hardware.

Plans call for installation and checkout of the first APS I at the Goldstone Mars Station (DSIF 14) in May 1966; the remaining systems are calendared for operation at one-month intervals beginning April 1967.

C. Telemetry and Command Processors, Phase II

A. Burke

1. Objectives and Basic Configurations

The telemetry and command data processors, Phase II (TCP II) are the major assemblies in the telemetry and command data handling subsystem, Phase II (TCD II). The primary objective of the TCP II is to provide the DSIF stations with a subsystem that will process, edit, alarm-monitor, and format spacecraft telemetry data, and can also perform the required processing and verification of spacecraft commands. A secondary objective is to provide additional computing to the stations when not involved in flight project support.

It was necessary to limit the TCP II configurations to those which would meet existing requirements on the DSIF. Therefore, three basic configurations were established:

- TCP II. Two Scientific Data Systems (SDS) 920 computers and a dual communications buffer.

TCP II A. One SDS 920 computer and a dual communications buffer. The digital instrumentation system (DIS) 910 computer is used as a backup.

TCP II B. The DIS SDS 910 computer with the DIS SDS 920 computer as backup. (Originally, this was identified as the TCD I.)

Table 1 shows the DSIF TCP II configuration for each station and also indicates actual or estimated operational dates.

Table 1. DSIF TCP II configuration

DSIF identification	Configuration	Operational date
11	TCP II A	September 1966
12	TCP II	February 1966
41	TCP II	March 1966
42	TCP II A	September 1966
51	TCP II B	October 1965
61	TCP II	March 1966
62	TCP II A ^a	November 1966
71	TCP II	March 1966
72	TCP II	April 1966

^aPresently installed at DSIF 61 for Surveyor support, but will be transferred to DSIF 62 when the station becomes operational.

2. Internal Operation and Functional Description

The principal elements of the subsystem are two SDS 920 computers, associated peripheral equipment for input/output, interface equipment for data transfer, and communications buffers for on-line communications with the Space Flight Operations Facility (SFOF). The subsystem is composed of two completely independent sections, designated alpha and beta, providing a fully redundant data processing capability. In the event of failure in any portion of either section, the alternate unit may assume the responsibility for performing the required functions. The TCP II provides the DSIF with an on-site computing capability for support of mission dependent equipment (MDE). Decommutated telemetry data, presented in parallel to the subsystem, are processed (edited, formatted, etc.) and transmitted, via the communications buffers, to the SFOF. Command data received from the SFOF are verified and presented to the MDE for transmission to the spacecraft.

3. Assembly

a. Subsystem computers. The subsystem contains two SDS 920 general purpose digital computers, each equipped with 8192 words of random access magnetic core memory. The 920 computer uses a fixed-word length of 24 information bits plus a parity bit. The machine cycle time is 8 msec. All memory locations are directly addressable. The memory is nonvolatile and retains stored data in the event of power failure.

b. Communications buffers. The communications buffers provide the subsystem with a capability for transmitting and receiving data via full duplex teletypes and with a send-only mode for transmitting via a high-speed data line. The communications buffers are composed of two completely independent assemblies, alpha and beta, for operation with the respective alpha and beta computer assemblies.

c. Teletype communications equipment. Three full duplex teletype communications channels for alpha and beta, each capable of transmitting and receiving simultaneously, interface with common carrier transmission lines. Standard five-level baudot code characters are transmitted and received at either 60 or 66.7 words per minute, as determined by the terminal equipment in

use at each station. The equipment contains connect/disconnect and error detecting circuitry in addition to the communications hardware.

The major subassemblies of TCP II are shown in Fig. 2.

D. Antenna Engineering

F. W. Stoller

The 30-ft antenna and its support items have been installed at the Spacecraft Guidance and Command Station (DSIF 72, Ascension Island), and checkout has been completed. Included among the support items are the electronics room, air-conditioning assembly, optical tracking aid (OTA) assembly, 100-ft and 30-ft collimation towers, acquisition-aid horns, cassegrain cone, cassegrain service trailer, hyperbola, and cable wrap-up. The installation has met or exceeded all specification requirements.

Portions of the installation are depicted in Figs. 3-8. Fig. 3 shows the early stages of the antenna erection,

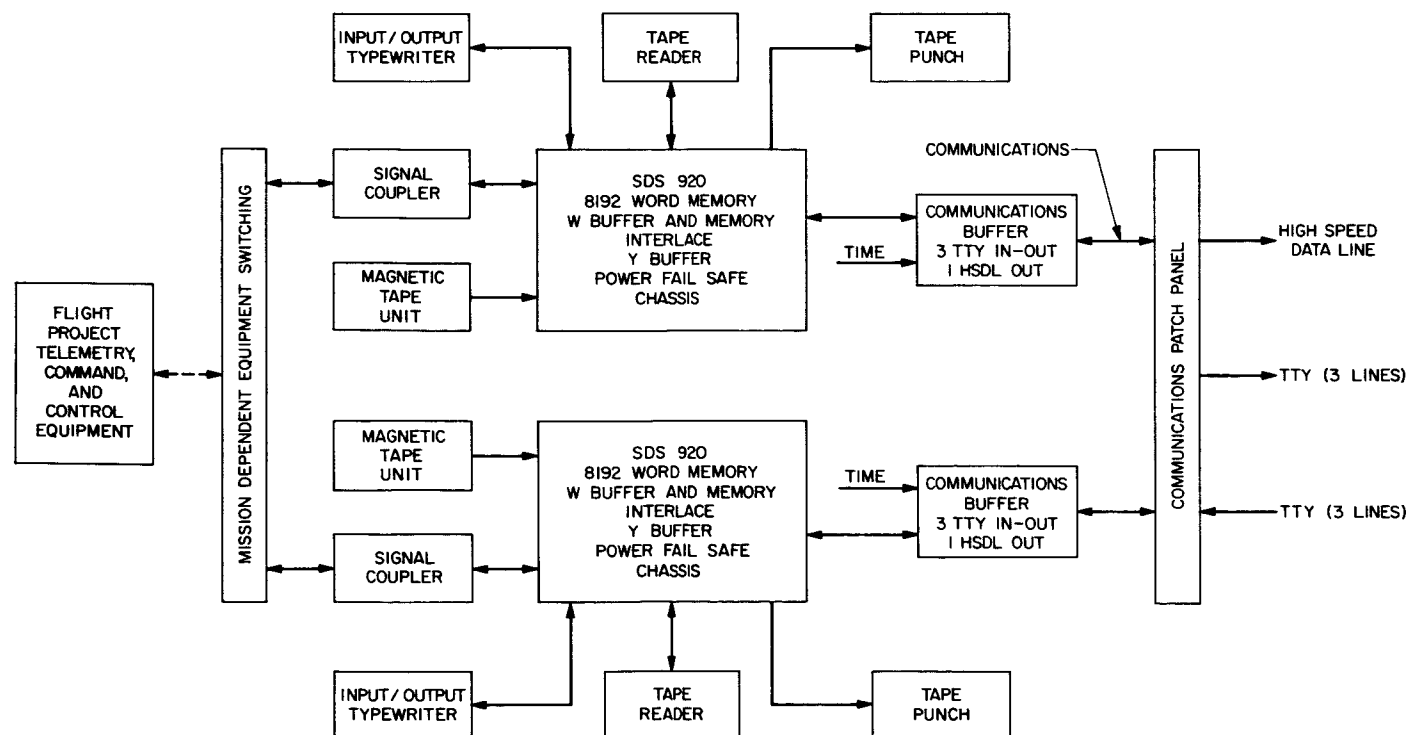


Fig. 2. Major subassemblies of TCP II



Fig. 3. Early stages of the 30-ft antenna erection

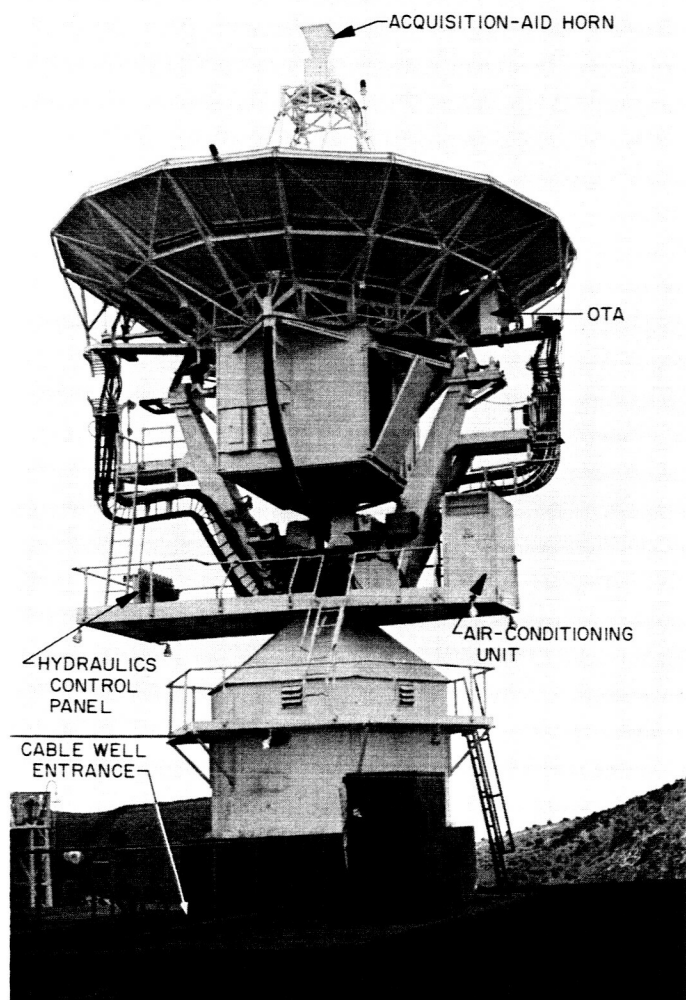


Fig. 4. Completed 30-ft antenna and supporting hardware

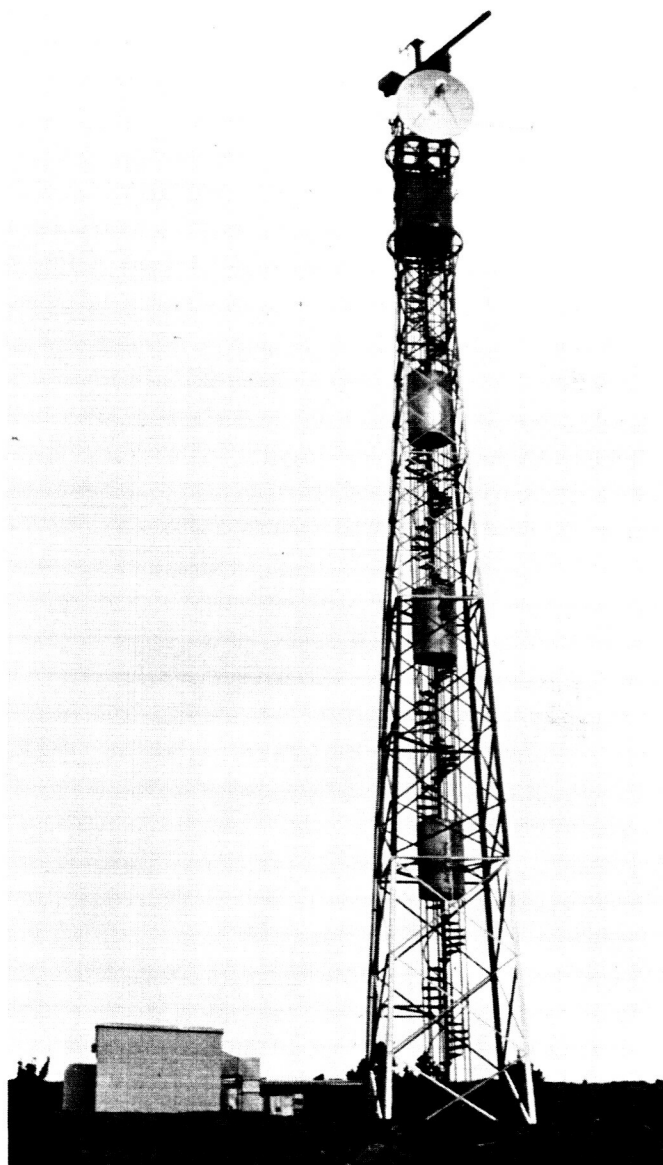


Fig. 5. Completed 100-ft collimation tower

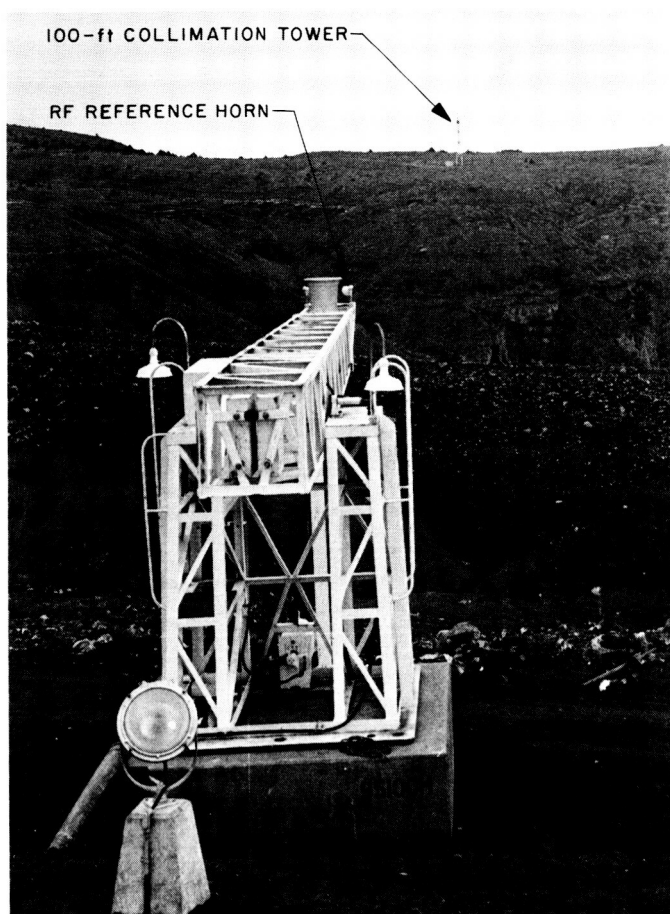


Fig. 6. Completed 30-ft collimation tower in stored position

with Green Mountain and the incoming fog visible in the background. The completed 30-ft antenna and its OTA assembly, electronics room, air-conditioning unit, hydraulic control panel, acquisition-aid horn, and cable well entrance are shown in Fig. 4. The completed 100-ft collimation tower is pictured in Fig. 5. Fig. 6 shows the completed 30-ft collimation tower in stored position, its RF reference horn, and its position relative to the 100-ft collimation tower. Fig. 7 is a photograph of the 30-ft antenna and the collimation tower, showing their relationship to each other and to the hydromechanical building. Fig. 8 is a close-up view of the completed cassegrain cone, hyperbola, encoder, acquisition-aid horns, and OTA installations—all of which are new designs.

The five cassegrain cones (three for the MSFN and two for the DSN) and their five service trailers have been completed and delivered to JPL, as have the three

cassegrain cone special overseas shipping containers for the MSFN cones.

The design and mock-up of the new 85-ft ha-dec cable wrap-up unit have been completed and checked out, and the engineering change requirements (ECRs) have been approved. The apropos configuration of the wrap-up are being implemented for the MSFN stations at DSIFs 11, 42, and 61, and for the DSN at DSIF 62 (the Pioneer, Tidbinbilla, Robledo, and Cebreros Stations, respectively). As funding and scheduling permit, the remaining stations will follow.

An integrity study is being initiated at JPL to resolve the bolt and joint maintenance problems existing throughout the DSN. An investigation will be made to evaluate the following: (1) types of bolts to use, (2) protective coatings to use, (3) proper torqueing and installation procedures for bolts, (4) nut lubrication procedures to ensure proper bolt-tensioning levels, (5) design concepts causing joint slippage problems, and (6) material coatings of surfaces. This study program is currently in the planning, setup, and hardware-procurement stages. Start of actual testing of bolts and materials is planned for April and expected to take approximately eight months. An additional two months will be required for data reduction and publication of a final report.

The 85-ft ha-dec antenna and the 100-ft collimation tower for the Cebreros Station (DSIF 62), along with all support items such as drive skids, servo-hydraulics, optical targets, air-conditioning units, hyperbola, cassegrain cone, cassegrain service trailer, cassegrain assembly shipping containers, and OTA assembly, have been fabricated and are currently in the checkout and packaging phases in preparation for shipment to Madrid. Erection is currently scheduled to begin on May 2, 1966.

The retrofit hardware for the Goldstone Echo Station (DSIF 12) is now in fabrication, with delivery planned for April 1966. The upgrade hardware for the Woomera Station (DSIF 41) is also in fabrication and will be ready for delivery in May 1966. In both cases the hardware will be delivered to the respective stations and stored pending available antenna time to implement installation.

Procurement for the upgrade hardware for the Goldstone Pioneer (DSIF 11), Woomera (DSIF 41), and Johannesburg (DSIF 51) Stations is now in process. It is expected that these items will be fabricated and shipped by October 1966 and stored on site, with installation to follow the "DSIF Master Schedule" delineations.

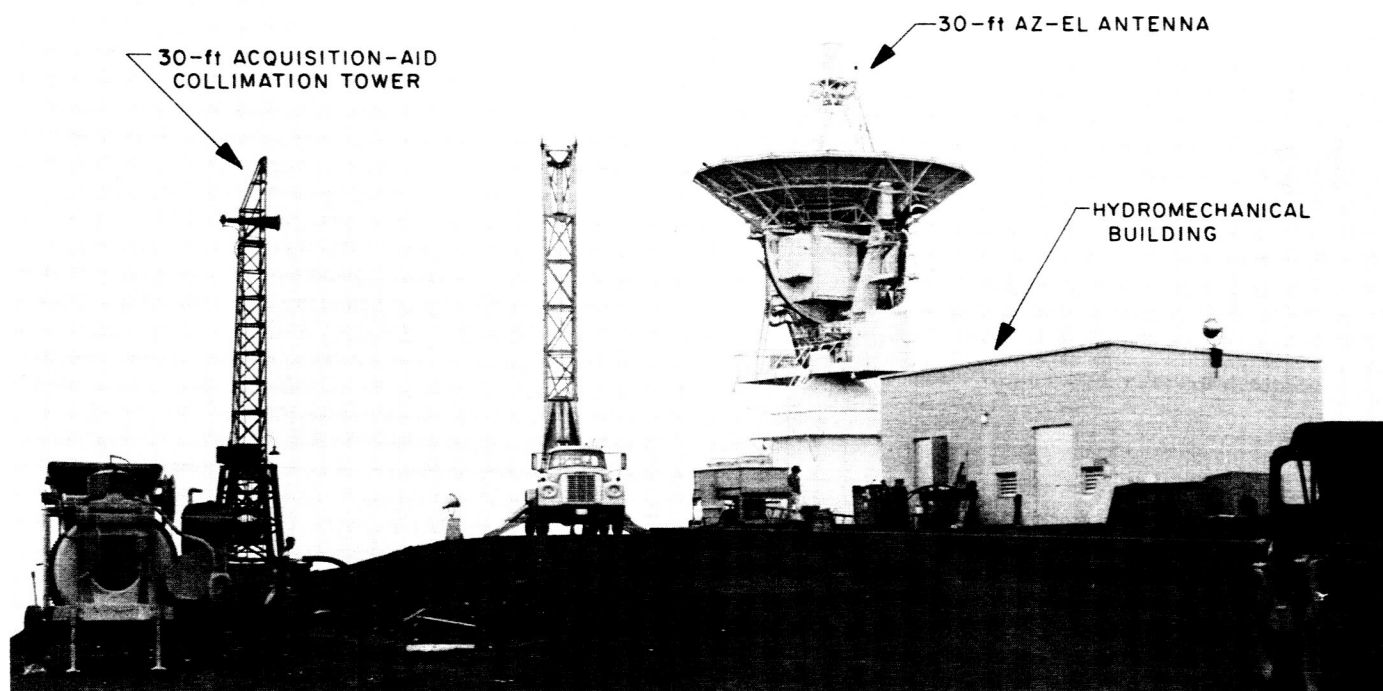


Fig. 7. Relative positioning of the 30-ft and 100-ft collimation towers

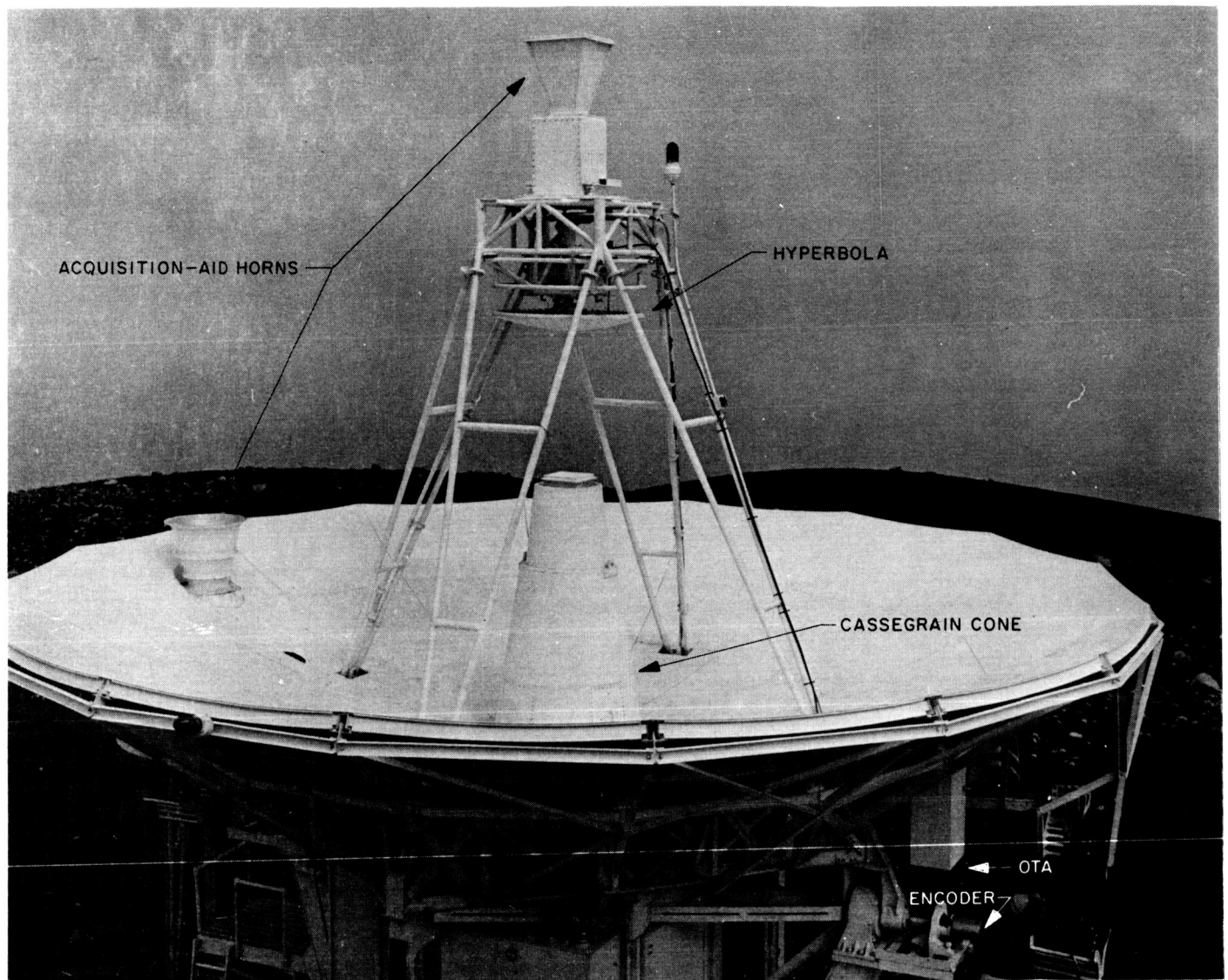


Fig. 8. Completed cassegrain assembly installation

E. Demonstration Doppler Monitor Program

F. B. Leppia

To demonstrate that doppler monitoring can be performed, the Systems Data Analysis Group has written a computer program using the Scientific Data Systems (SDS) 920 digital computer located in the digital instrumentation system (DIS). This effort was undertaken as a feasibility study for the primary purpose of checking monitoring techniques on the DIS computer system. The secondary purpose was to determine whether a computer program written in Fortran II could be used efficiently in a real-time environment. One symbolic routine was required to honor the tracking data handling (TDH) interrupt and input tracking data to the DIS.

The monitoring of doppler data consists primarily of:

1. Testing for good continuous legal doppler data

2. Converting raw doppler counts to one second count
3. Comparing observed doppler with predicted doppler
4. Rejecting blunder points through tolerance testing
5. Computing mean and standard deviation of the good doppler residuals
6. Flagging of bad data.

In order to monitor doppler data, a mainline program was written to accept input parameters, initialize various constants, and control the logical flow of computations throughout execution of the program. Fig. 9 is a basic flow chart of the computer program. Several subroutines which were written are described:

1. CLEAR — Clear all residual buffers and flags to zero
2. SHIFT — Shift all residual buffers and flags one position to accept new data

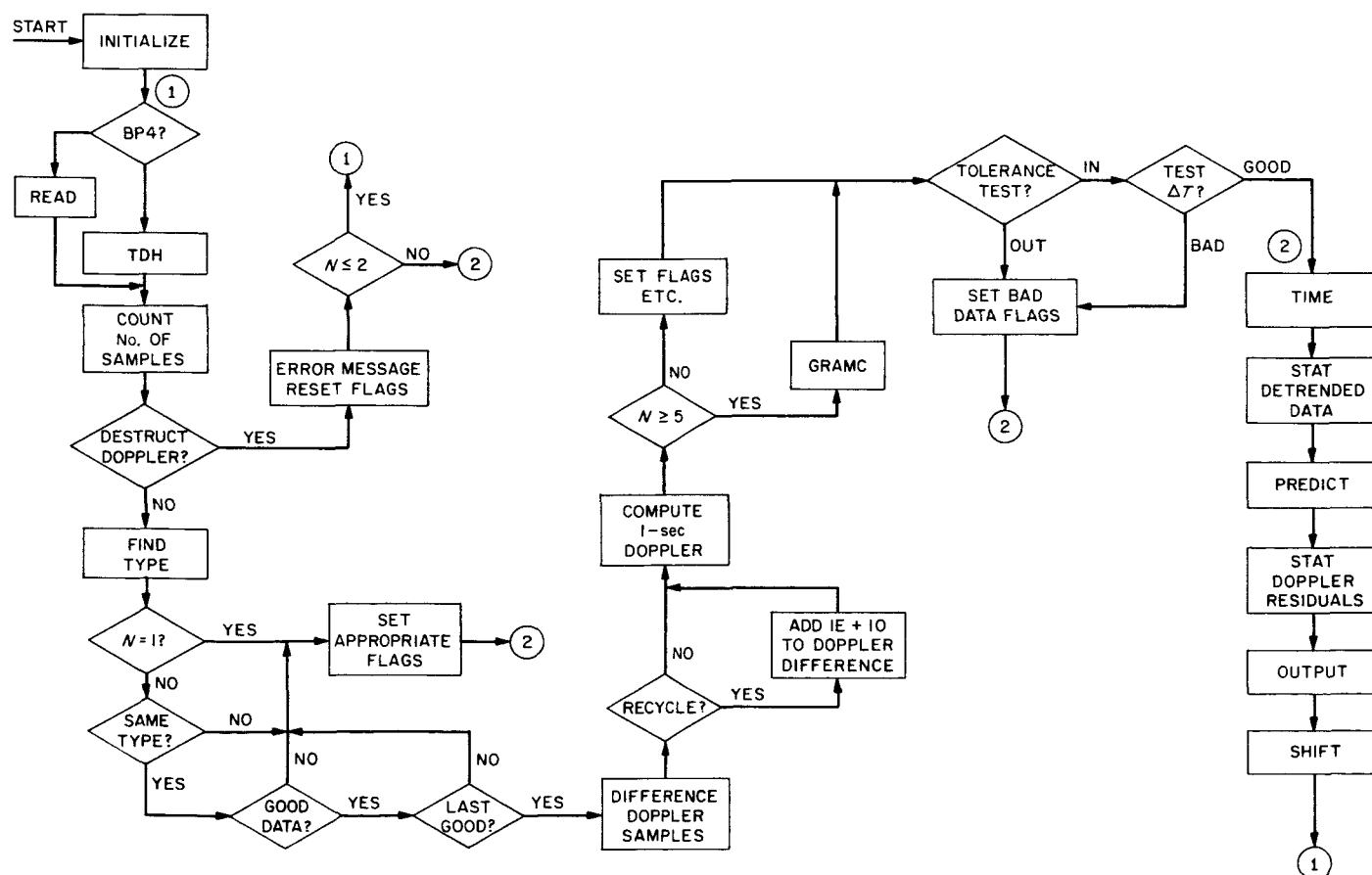


Fig. 9. Flow chart of doppler monitor program

3. STAT — Compute mean and standard deviation of N samples eliminating flagged bad points
4. READ — Read tracking data from IBM cards (for checkout purposes only)
5. GRAMC — Detrend doppler data by five-point Gram-Chebyshev second-order polynomial
6. PREDICT — Compute predicted doppler through interpolation of predicts on magnetic tape, form residuals, do tolerance test
7. INTERPOL — Interpolate to compute one-second doppler with equally or unequally spaced time points
8. TIME — Format GMT for output with leading zeros and adjust GMT for middle of interval sampling
9. FINDTYPE — Compute flag for one-, two-, or three-way doppler
10. TDH — Wait for sample interrupt from TDH, then input day, GMT, data condition code (DCC), doppler, and convert raw data to engineering units for computation.

To eliminate as many problems as possible before attempting execution in a real-time environment, all basic monitoring techniques were tested and checked on an SDS 930 computer. This machine has a high-speed output device capable of outputting intermediate computational steps in a convenient manner. The program was then operated in a real-time environment during the early portion of the *Pioneer A* mission. After eliminating some problems in the TDH subroutine, it was discovered that a 10-sec sample rate could not be handled without cutting down the output message. This problem was traced to a total processing time in excess of 11 sec; the typed output alone required more than 5 sec. This problem was solved by the most convenient method—that of cutting the line down about 20 characters. An alternative solution would have been to modify the Fortran-type subroutine to take advantage of the interlace option on the DIS which allows for easy overlap of input/output simultaneously with computation. Another solution would have been to summarize output messages at certain time intervals, thereby eliminating output at every sample time. This is especially useful at 1-sec sample rates.

It is felt that, in general, the basic techniques used for doppler monitoring can be used to good advantage on the SDS equipment in the DIS. However, the use of Fortran II does not seem satisfactory because any input/output subroutines would have to be rewritten and computation time must be reduced with the use of symbolically coded multi-precision fixed-point subroutines.

F. Goldstone Operations

J. Orbison

Construction has begun on a building to house the Goldstone termination of a telephone microwave system (Fig. 10). This system, being installed by the California Interstate Telephone Company, will provide 60 channels of microwave voice circuits plus 30 channels of open wire carrier. Scheduled for a fall completion date, the microwave system will provide a more flexible system for both incoming and off-station calls.

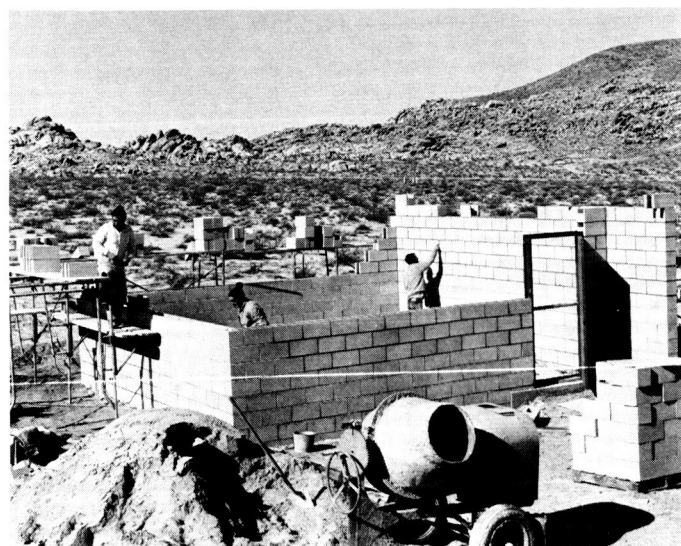


Fig. 10. Goldstone microwave terminal building

1. Pioneer Station

a. S-band system testing. The Cebreros Station (DSIF 62, Madrid) S-band system (Fig. 11), located in the west annex building, is being operationally tested and is scheduled for shipment to Madrid in late spring. Personnel selected for installation and operation of the

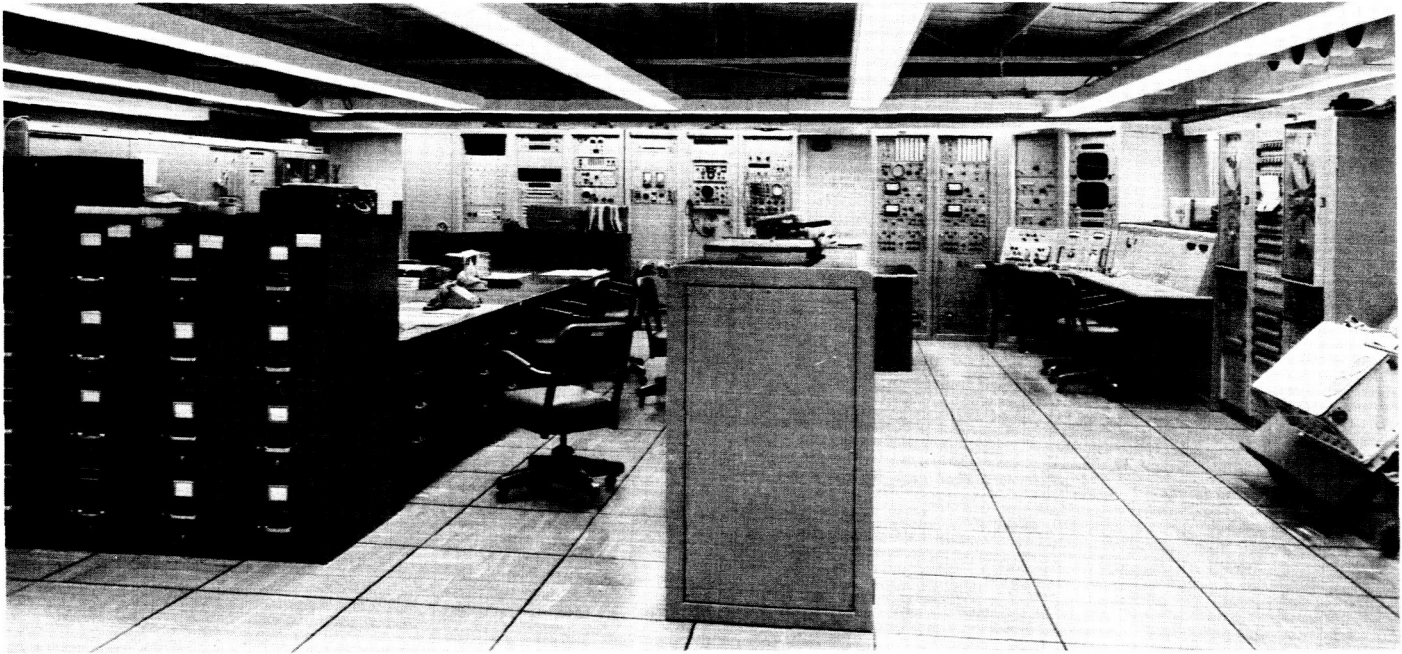


Fig. 11. Cebreros Station (DSIF 62, Madrid) S-band system test installation

system are assembling at the Pioneer Station where a dual S-band system and *Surveyor* ground operation equipment training program is in progress.

b. Construction. A 350-kw diesel generator (Fig. 12) has been installed west of the generator building, and will be used for backup to the commercial electrical power during the powerhouse modification and change-over.

2. Mars Station

The Rohr-conducted training program for the Mars Station (DSIF 14) servo group is continuing, and covers the operation and maintenance of the antenna mechanics. DSIF personnel assisted in the installation of the alidade limit switches, pressure switches, flow interlock switches and other devices. As part of the training, they assisted Rohr personnel in the evaluation of the hydrostatic bearings tests.

Subsystems of the S-band system are being installed in the second floor control room of the pedestal. Currently installed and being tested are the digital instrumentation subsystem (DIS) and the tracking data handling (TDH) subsystem. The off-antenna portions of the surveillance television have been installed and tested, and are operational from the servo control console. Ap-

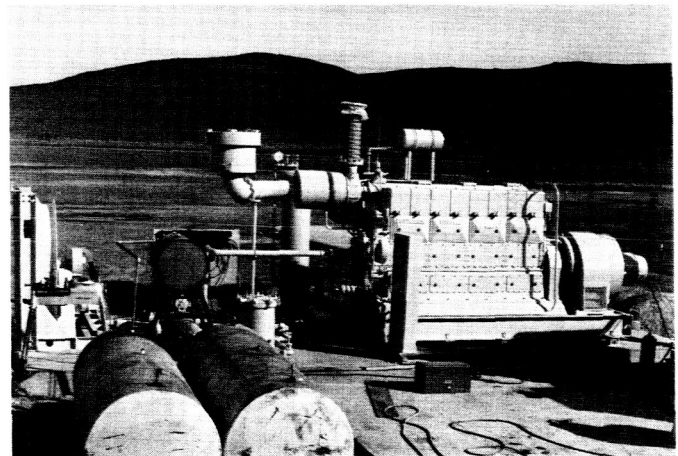


Fig. 12. Pioneer Station backup diesel generator

proximately 75% of the documentation for the S-band system is on hand and is being microfilmed for storage.

Cable trays in the control room under-floor plenum have been modified to incorporate the arrangement of the above-floor rack locations. Cable trays on the antenna, into the reflector hub, and through it into the cassegrain cone are being installed. Microwave cables from the equipment room in the southeast corner of the powerhouse have been installed in the cable tunnel and into the pedestal.

A JPL research and development receiver which uses a standard Goldstone duplicate standard (GSDS) cryogenic cooled maser has been installed in the alidade control

room. This receiver is being prepared for use by the Mars Station in tracking the solar occultation experiment of the *Mariner IV* spacecraft during March and April.

VII. Flight Project Activities

A. Pioneer VI Trajectory Characteristics

R. A. Wallace

Pioneer VI was launched from the Air Force Eastern Test Range (AFETR), Cape Kennedy, Florida, December 16, 1965, at 07:31:20.380 (GMT). Using tracking data available through January 31, 1966, an orbit was fitted to 7009 data points from the Tidbinbilla, Johannesburg,

Goldstone (Pioneer and Echo), and Robledo tracking stations. The heliocentric trajectory characteristics are given in Table 1 for the solar ellipse established at the time of perihelion (about launch + 155 days).

These elements indicate that the trajectory is close to the nominal with a more desirable perihelion and less desirable inclination to the ecliptic than the nominal (nominal: perihelion 0.82491 AU, and inclination 0.06598 deg; ideal: perihelion 0.800 AU, and inclination 0.0 deg).

**Table 1. Pioneer VI heliocentric conic elements
(ellipse at time of perihelion)**

Perihelion	0.814320 AU*
Inclination to the ecliptic	0.16931 deg
Period	311.327 days
Aphelion	0.98362 AU
Semi-major axis	134.485×10^6 km
Eccentricity	0.09416
C3 (twice total energy per unit mass)	$-986.855 \text{ (km/sec)}^2$
Longitude of the ascending node	260.346 deg
Argument of perifocus	2.77756 deg
Time of perihelion	02:54:07.768, May 20, 1966
*1 astronomical unit = 149.59850×10^6 km.	

B. Pioneer VI Orbit Determination Results

J. E. Ball

The DSN has tracked the *Pioneer* spacecraft since injection into its heliocentric orbit. The data from the tracking network are processed by the Orbit Determination Program and results of its computations are given in Table 2, which lists orbit parameters between the end of the first phase of Step 2 orientation which ended at

Table 2. Summary of Pioneer VI monthly orbit (December 18, 1965 to January 23, 1966)

Items	Pre Step 2 orientation orbit	Post Step 2 orientation Orbit 1	Post Step 2 orientation Orbit 2	Post Step 2 orientation Orbit 3	Post orientation Orbit 4
Date orbit computed (injection conditions)	December 19	December 21	December 30	January 18	February 13
Epoch	16 Dec. 1965, 07 ^h 56 ^m 03 ^s .925 — 141.315.85	18 Dec. 1965, 04 ^h 18 ^m 00 ^s .000 430.947.37 — 25.176.090 — 39.396.166 2.1568228 4.7167202 — 0.74061370 — 0.69998336	18 Dec. 1965, 04 ^h 18 ^m 00 ^s .000 430.947.78 — 25.174.259 — 39.426.897 2.1568193 0.025740099 — 0.10906484	18 Dec. 1965, 04 ^h 18 ^m 00 ^s .000 430.933.43 — 25.173.116 — 39.414.496 2.1568350 0.025705716 — 0.10888780	18 Dec. 1965, 04 ^h 18 ^m 00 ^s .000 430.935.31 — 25.174.536 — 39.394.712 2.1568385 0.025691275 — 0.10878262
Position of probe, geocentric equatorial true of date $\begin{cases} X \text{ (km)} \\ Y \text{ (km)} \\ Z \text{ (km)} \end{cases}$					
Velocity of probe, geocentric equatorial true of date $\begin{cases} DX \text{ (km/sec)} \\ DY \text{ (km/sec)} \\ DZ \text{ (km/sec)} \end{cases}$					
CC3 data in solution	Data from Dec. 16 10 ^h to Dec. 17 22 ^h 269 points of 60-sec data	Data from Dec. 18 04 ^h to Dec. 20 21 ^h 855 points of 60-sec data	Data from Dec. 18 04 ^h to Dec. 27 20 ^h 309 points of 600-sec data	Data from Dec. 18 04 ^h to Jan. 1 11 ^h 744 points of 600-sec data	Data from Dec. 18 04 ^h to Jan. 31 09 ^h 833 points of 600-sec data and 1918 points of 60-sec data and 348 points of 600-sec data and 1394 points of 60-sec data and 618 points of 600-sec data and 950 points of 60-sec data and 882 points of 60-sec data and 66 points of 600-sec data
Sta 3 (Tidbinilla; DSIF-42)					
Sta 5 (Johannesburg; DSIF-51)					
Sta 12 (Goldstone, Echo; DSIF-12)					
Sta 2 (Goldstone, Pioneer; DSIF-11) Sta 13 (Robledo; DSIF-61)					
Type of solution	No a priori, estimated X, Y, Z, DX, DY, DZ, KE, RI (3), LA (3), LO (3), RI (5), LA (5), LO (5), RI (12), LA (12), LO (12).	No a priori, estimated X, Y, Z, DX, DY, DZ, KE, RI (3), LA (3), LO (3), RI (5), LA (5), LO (5), RI (12), LA (12), LO (12).	No a priori, estimated X, Y, Z, DX, DY, DZ, KE, RI (3), LA (3), LO (3), RI (5), LA (5), LO (5), RI (12), LA (12), LO (12).	No a priori, estimated X, Y, Z, DX, DY, DZ, G, RI (3), LA (3), LO (3), RI (5), LA (5), RI (12), LA (12), LO (12).	No a priori, estimated X, Y, Z, DX, DY, DZ, G, AU, RI (13), LO (13), RI (3), LO (3), RI (4), LO (4), RI (2), LO (2).
Geocentric conic ^a Epoch of pericenter passage	16 Dec. 1965, 07 ^h 56 ^m 03 ^s .925 — 141.315.85	16 Dec. 1965, 07 ^h 55 ^m 46 ^s .311 — 141.081.43	16 Dec. 1965, 07 ^h 55 ^m 47 ^s .398 — 141.081.34	16 Dec. 1965, 07 ^h 55 ^m 50 ^s .824 — 141.081.95	16 Dec. 1965, 07 ^h 55 ^m 50 ^s .813 — 141.082.73
SMA (km)	1.0490803	1.0497645	1.0497670	1.0497803	1.0497780
ECC	2.8206438	2.8253277	2.8253252	2.8253127	2.8253017
C3 (km ² /sec ²)	6935.8190	7020.8527	7021.1958	7023.1060	7022.8217
RCA (km)	127°.26066	157°.06816	157°.06758	157°.06557	157.06496
TA (deg)	30.135354	30.288802	30.307487	30.346739	30.349315
INC (deg)	5.7050075	5.6455298	5.6462572	5.6294139	5.6237146
LAN (deg)	192°.34165	192°.55067	192°.54871	192°.56721	192.57281
APF (deg)					

Table 2. Summary of Pioneer VI monthly orbit (December 18, 1965 to January 23, 1966) (cont'd)

Items	Pre Step 2 orientation orbit	Post Step 2 orientation Orbit 1	Post Step 2 orientation Orbit 2	Post Step 2 orientation Orbit 3	Post orientation Orbit 4
Date orbit computed (injection conditions)	December 19	December 21	December 30	January 18	February 13
Heliocentric conic ^a					
Epoch of pericenter passage					
SMA (km)	SMA: semi-major axis	15 May 1966, 16 ^h 24 ^m 30 ^s .750	15 May 1966, 16 ^h 23 ^m 15 ^s .625	15 May 1966, 16 ^h 24 ^m 03 ^s .750	15 May 1966, 16 ^h 41 ^m 30 ^s .250
ECC	ECC: eccentricity	0.13107383 × 10 ⁰	0.13107381 × 10 ⁰	0.13107373 × 10 ⁰	0.13114427 × 10 ⁰
C3 (km ² /sec ²)	C3: twice total energy per unit mass	0.12298570	0.12298576	0.12298643	0.12292235
RCA (km)	RCA: radius of closest approach	-1012.5142	-1012.5143	-1012.5150	-1013.4310
TA (deg)	TA: true anomaly	0.11495362 × 10 ⁰	0.11495360 × 10 ⁰	0.11495344 × 10 ⁰	0.11502371 × 10 ⁰
INC (deg)	INC: inclination of probe orbit plane to equator of date	-178.79447	-178.79367	-178.79433	-178.79358
LAN (deg)	LAN: longitude of ascending node	0.22315511	0.22337421	0.22293579	0.22271626
APF (deg)	APF: argument of pericenter	262.99644	262.99597	262.99103	262.99147
	σ: 1 sigma value	1.6723214	1.6720034	1.6768289	1.6764946
Change in injection conditions (current minus preceding)	(Current minus 1800Z orbit)				
ΔX (km)	1.799	-5.59	-5.59	-8.35	1.88
ΔY (km)	-0.791	1.831	1.831	1.143	-1.420
ΔZ (km)	4.533	-30.731	-30.731	12.401	19.784
ΔDX (km/sec)	-0.0000078	-0.0000035	-0.0000035	0.0000157	0.00000350
ΔDY (km/sec)	0.00002234	-0.0000145	-0.0000145	-0.000034383	0.000014441
ΔDZ (km/sec)	0.00006281	0.0001048	0.0001048	0.00017704	-0.00010518
Statistics on parameters					
σX (km)	2.860	8.577	3.800	6.704	3.952
σY (km)	1.115	7.276	4.909	6.051	3.408
σZ (km)	4.031	46.578	25.773	24.929	13.372
σDX (km/sec)	0.00071322	0.000017727	0.000008990	0.0000064717	0.000003330
σDY (km/sec)	0.000073745	0.000052024	0.000022767	0.000024037	0.000006339
σDZ (km/sec)	0.000303902	0.000268520	0.000145168	0.0000638938	0.000027005

^aOsculating elements at injection epoch.

9^h 47^m on December 16 (injection + 1^h 50^m), and the beginning of the final (second) phase of the Step 2 orientation which started at 22^h 10^m on December 17. The table also contains a listing of three updates of the post Step 2 orientation orbit and defines the latest *Pioneer VI* orbital parameters.

C. Pioneer VI High Frequency Doppler Noise

W. D. Chaney

High frequency doppler noise estimates for the *Pioneer VI* mission were obtained by fitting, by least squares, a third- to tenth-order polynomial to the doppler data. The order of the polynomial was dependent upon the number of points available. The raw, continuous-count, doppler data had been reduced to cycles/second by the equation:

$$D_j = \frac{C_i - C_{i-1}}{K_m(t_i - t_{i-1} + R_i - R_{i-1})}$$

where

C_i and C_{i-1} are the observed continuous count from the doppler counter

t_i and t_{i-1} are the time for the observations C_i , C_{i-1} ,
 R_i and R_{i-1}

R_i and R_{i-1} are the digital resolver outputs at t_i and t_{i-1}

K_m is the effective doppler multiplier

DSIF-12 is the only station using the experimental digital resolver (installed on Pass 15). For all other stations R_i and R_{i-1} are set to zero. The purpose of the digital resolver is to provide higher resolution of the doppler count by counting the elapsed time from the counter readout pulse to the next zero crossing (Fig. 1).

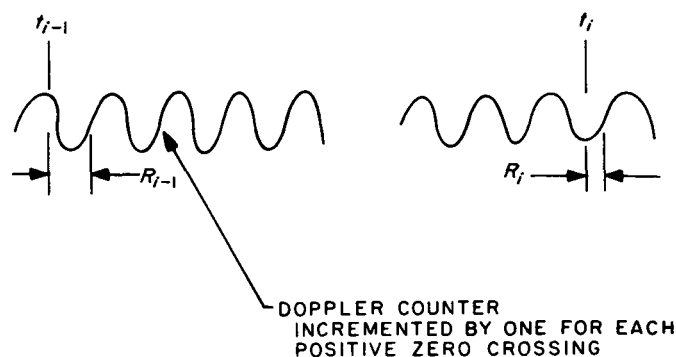


Fig. 1. Elapsed time from counter readout pulse to the next zero crossing

The value of K_m for the DSIF stations to date has been:

Station No.	$K_m =$
11	2
12	2 before Pass 15, $K_m = 1$ subsequent pass
41	1
42	2
51	1
61	1

Fig. 2 (a-d)¹ shows the high frequency noise estimates as determined from rms of the residuals formed by differencing the curve-fitted doppler from the observed doppler. The lines on the plots join the rms noise estimates of the two-way (C-2) doppler points. Three-way² (C-3) doppler points have not been joined by lines.

For all stations, there has been a significant increase in the noise estimate from the beginning of the mission. The rms noise estimate at the start of the mission was ≈ 0.005 cps³ increasing to approximately 0.010 cps on Pass 25. The increase in noise can most probably be attributed to rubidium standard noise as the round-trip light time increased. Fig. 3 presents the round-trip light time versus day number.

¹Fig. 2 (a-d) is from a JPL internal publication by J. Heller, R. Ball, and A. Caticchio.

²Three-way doppler is the terminology used for doppler data taken at a receiving station remote from a transmitting station. The transmitting station is coherently locked to the spacecraft transponder but the receiving station is using its own internal frequency standard for the receiver reference frequency.

³1 cps = 6.5 mm/sec for the DSIF S-band system.

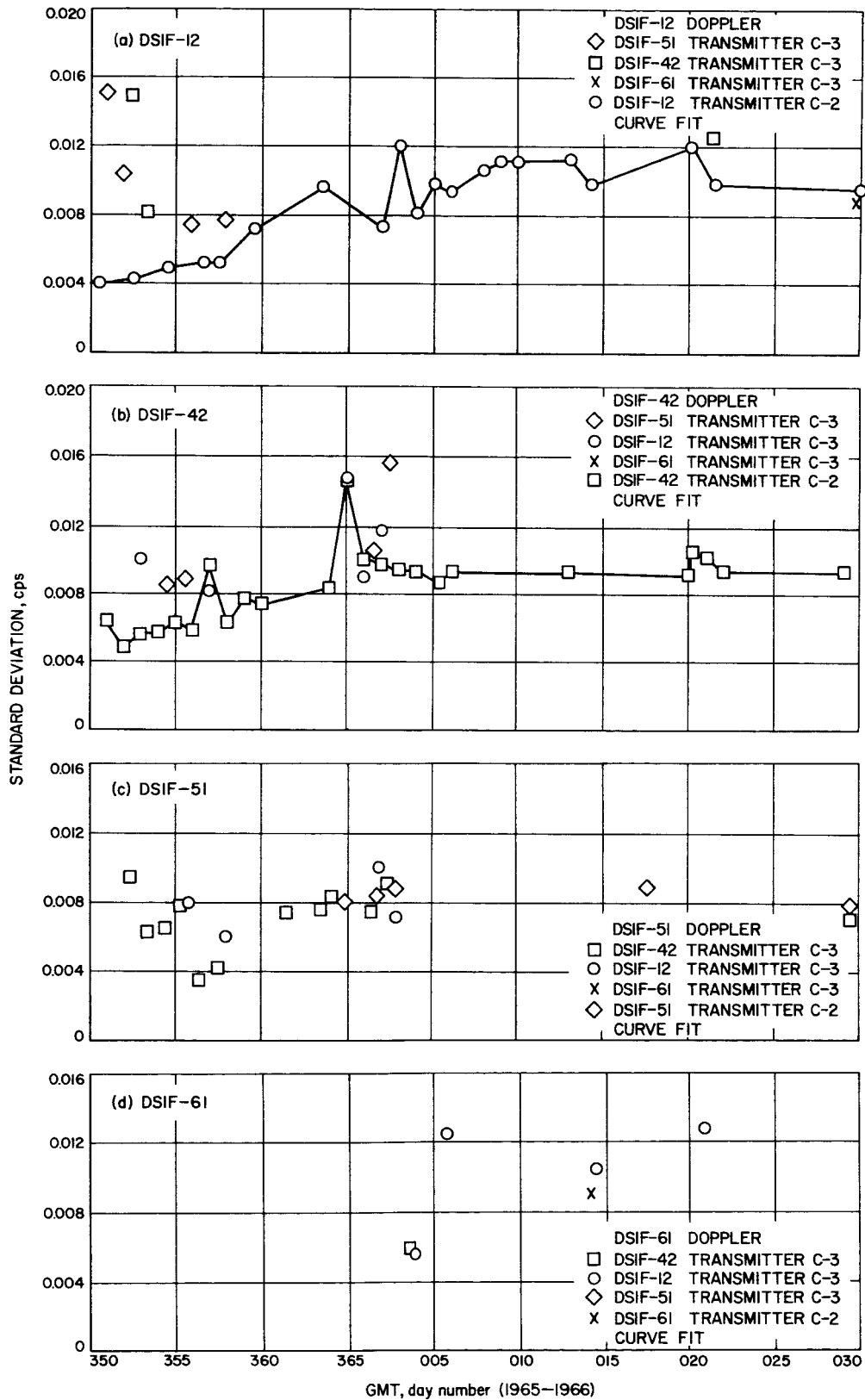


Fig. 2. High frequency noise versus day number

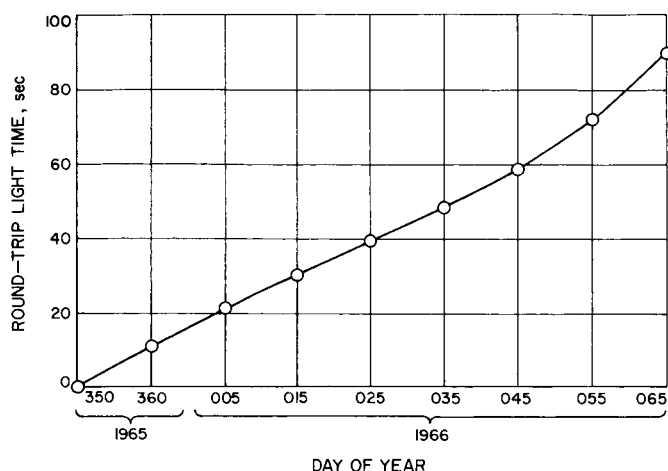


Fig. 3. Pioneer VI round-trip light time versus day number

Long-term effects, such as those due to atmosphere and ionosphere, cannot be estimated because of the curve-fit technique.

D. Lunar Orbiter Project: Introduction and Early Flight Path Analysis

J. P. Brenkle

The *Lunar Orbiter* Project consists of five flights. The first launch is presently scheduled for the third quarter of calendar year 1966, and subsequent flights are scheduled on 3-mo centers. A *Lunar Orbiter* mission has an expected lifetime of 1 yr which is divided into two phases: the first, the primary photographic phase, will last for approximately 35 days followed by the extended seleno-detic phase that will continue for a total of 1 yr.

The *Lunar Orbiter* spacecraft will be launched by an *Atlas/Agna* vehicle from Cape Kennedy. The launch profile is similar to a *Ranger* mission; however, 90-hr approximate flight time will be used (Figs. 4 and 5). The *Lunar Orbiter* will be capable of two midcourse maneuvers. After deboost into the initial lunar orbit, which has an apolune of 1850 km and a perilune of approximately 200 km, DSIF tracking data will continue to be processed in the SFOF. Sufficient tracking data and orbit determination analysis must be accomplished to determine the orbital parameters and a rough evaluation of the lunar harmonics must be made on the first mission before a

transfer maneuver can be achieved. This analysis is necessary to insure that the *Lunar Orbiter* can photograph the ten distributed targets (Fig. 6) and will not impact the lunar surface before all photographs have been read out.

After approximately 3 to 6 days in the initial orbit, a transfer maneuver will be executed which will place the *Lunar Orbiter* in a 1850-km apolune and 46-km perilune orbit at an inclination of approximately 12 deg to the lunar equator. This orbit will pass over the 10 photo targets in approximately 9 days (Fig. 7). Prime photo data will be read out between picture-taking sequences. After all the targets have been photographed, a complete read-out of all pictures will be accomplished before the photographic mission is considered completed.

The DSN has the major responsibility for the tracking and data acquisition support of *Lunar Orbiter* flights. In addition to the DSN support, there are also AFETR and Manned Space Flight Network (MSFN) tracking and data acquisition support requirements. To avoid establishing new interfaces between the *Lunar Orbiter* Project, the DSN, AFETR and MSFN, the DSN has been assigned the responsibility for the flight path activities during the acquisition phase of the mission which normally will be completed within 4 to 6 hr after launch.

The DSN portion of the *Lunar Orbiter* flight path analysis and command (FPAC) team will be responsible for:

- (1) Receipt and evaluation of *Lunar Orbiter* frequency data received at DSIF-71 spacecraft monitoring station, and reporting of spacecraft frequency parameters to the AFETR Real Time Computer Center (RTCC) for use in DSIF predicts generated by the RTCC.
- (2) Computation of DSIF prediction data based on expected and actual lift-off time.
- (3) Receipt and evaluation of AFETR-furnished tracking, trajectory, and performance data, and for DSIF prediction data furnished by the AFETR Real Time Computer Center.
- (4) Backup computation of the parking orbit and transfer orbit based on AFETR raw tracking data and backup computation of DSIF prediction data.
- (5) Receipt and evaluation of DSIF tracking data, determination of spacecraft orbits, generation of DSIF prediction data, and computation of trajectory data for DSN and for general information.

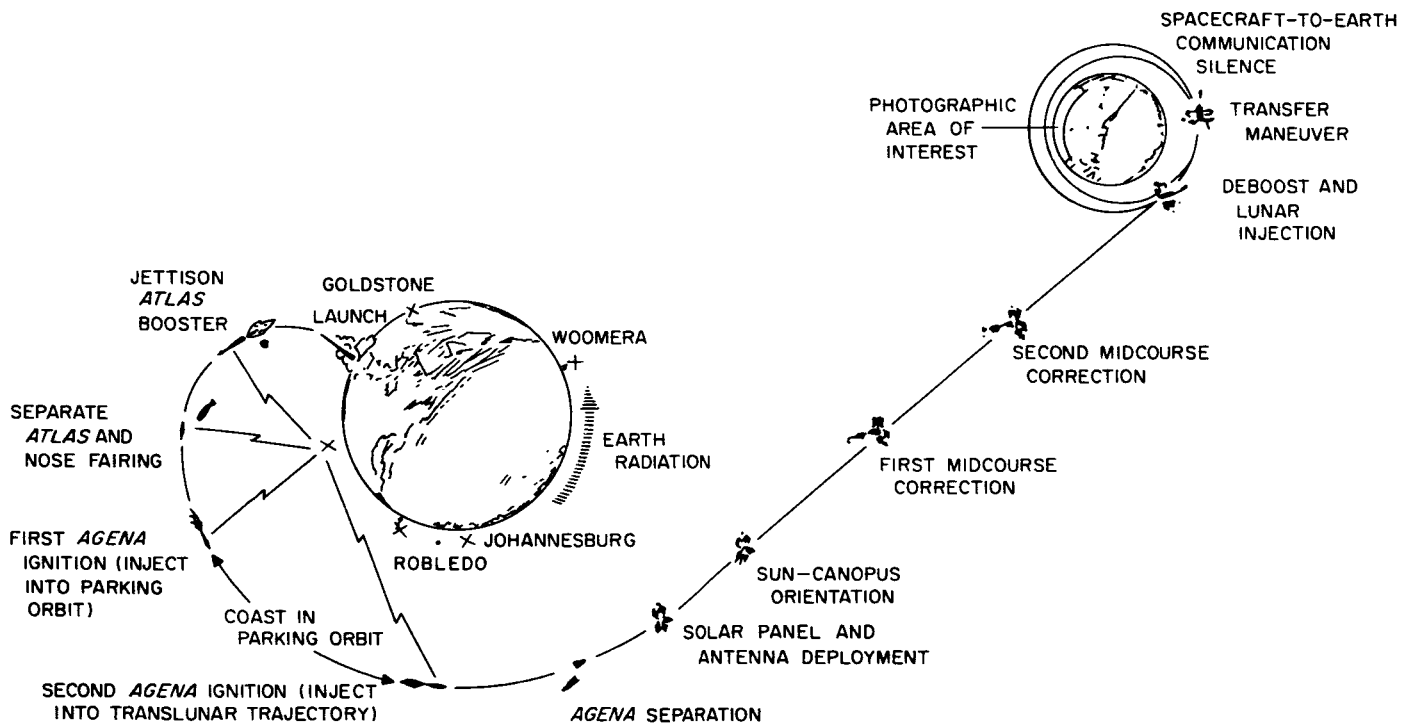


Fig. 4. Lunar Orbiter flight profile

		SUN OCCULTATION		INJECTION AND TRANSFER ΔV , m/sec	WAITING TIME, days
		AT TRANSLUNAR INJECTION, min	AT LUNAR ARRIVAL, min		
JUNE	11	53	28	884-906	8.5
	12	53	30	826-849	7.5
	13	54	32	764-786	6.4
	14	54	39	715-723	5.4
	15-16	53	50	681-715	4.3
	16-17	49	66	735-794	3.3
	17-18	49	91	875-932	2.3
JULY	11	59	28	840-865	8.0
	12	58	31	785-799	6.9
	13	55	35	741-754	5.9
	14-15	50	43	743-779	4.8
	15-16	45	55	822-863	3.8
	17	40	72	950-987	2.7
AUG	9	62	27	851-864	8.4
	10	56	29	809-817	7.4
	11	51	33	789-812	6.4
	12-13	45	39	815-843	5.3
	13-14	40	47	883-912	4.3
	15	37	61	986-1014	3.2

Fig. 5. Planning Mission P-4 launch periods

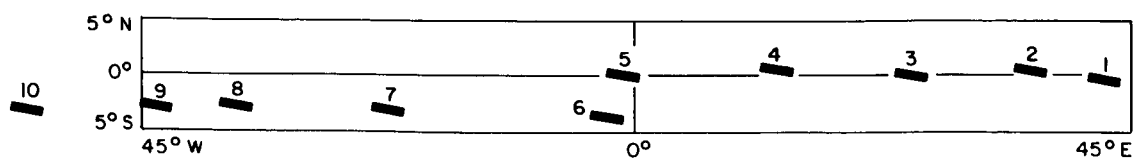


Fig. 6. Planning Mission P-4A photo targets

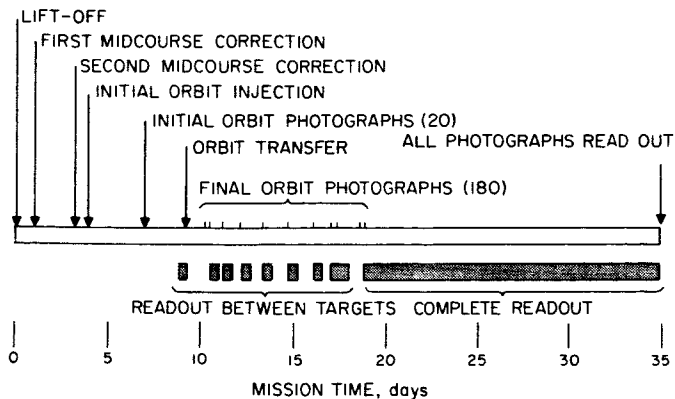


Fig. 7. Planning Mission P-4A event sequence summary

- (6) Furnishing the best estimate of the spacecraft orbit to the project portion of the FPAC team and providing a statement concerning the quality of the DSIF tracking data.

After the first 4 to 6 hr of the missions, the DSN will continue to monitor and validate the DSIF tracking data. The DSN will also participate and consult in the selection of data weights and blocks, interpretation of results, analysis of anomalies, and general assistance in the application of flight path technology.

The tool required to carry out the above functions is a series of computer programs. These FPAC user programs are made up of a series of links or IBM 7094 core loads which are linked together by source decks. All user programs will be operated on the primary computer string during the acquisition phase. Some of these programs, plus those peculiar to the *Lunar Orbiter* project, will also be run on the backup computer string during the acquisition phase. To provide maximum operational flexibility, both computer strings will be loaded with an identical set of computer programs and both will receive all AFETR and DSIF tracking and telemetry data.

These programs and procedures are a direct adaptation of those used by the *Ranger*, *Mariner*, *Surveyor* and *Pioneer* FPAC teams and indicate that all space flight projects have similar procedures during launch and acquisition phases. This similarity will be exploited in the future to avoid the establishment of new interfaces and training of new operational teams for each project. The DSN portion of the *Lunar Orbiter* project is the first step toward establishing a mission-independent launch-to-space flight operational interface.

E. Sensitivities of a Lunar Orbiter to the Lunar Gravity Harmonics

A. Liu

1. Introduction

One of the major objectives of the *Lunar Orbiter* Project is the accurate determination of the oblateness of the Moon and the values of the higher harmonics of the lunar gravitational field.

The determination of these constants, which describe the mass distribution of the Moon, will be useful in answering questions regarding the origin of the Earth-Moon system, the internal composition of the Moon, and provides fundamental physical constants and parameters.

Knowledge of the size of these gravity parameters would be valuable in planning future lunar missions, such as *Apollo*, and would aid in verifying the trajectory analysis for *Apollo*. Finally, the process of determining the gravity harmonics led to an accurate trajectory which could be used in locating the terrain that was photographed.

In order to estimate the degree of precision to which a set of gravitational harmonic parameters can be determined from a set of observations, it is necessary to know the sensitivity (partial derivatives) of the data with respect to changes in the parameters.

Hence it is important before embarking on the selenodesy experiment to have some assurance that the motion of the satellite will be sensitive to the harmonics in the gravitational field in a fashion susceptible to measurement. Further, these partial derivatives are central to the estimation of the lunar gravity harmonics.

2. Partial Derivative (PARD) Program Description

JPL has been using the computer program PARD, received from Prof. W. M. Kaula of U.C.L.A., for the calculation of the partial derivatives of Kepler elements, M , a , e , i , ω , Ω , with respect to a set of gravity harmonic coefficients, C_{lm} , S_{lm} .

The lunar gravity potential V can be written as a harmonic expansion in terms of a linear combination of

the gravity coefficients, C_{lm} , S_{lm} , as

$$V = \frac{kM}{r} \times \left[1 + \sum_{l=2}^{\infty} \left(\frac{a_e}{r} \right)^l \sum_{m=0}^l P_{lm}(\sin \Phi) \{ C_{lm} \cos m\lambda + S_{lm} \sin m\lambda \} \right]$$

where a_e is the equatorial radius, M is the mass of the Moon, k is the gravitational constant, r , Φ , λ are spherical coordinates of the satellite, $P_{lm}(\sin \Phi)$ is the associated Legendre polynomial of degree l and order m . We rewrite V as:

$$V = kM \left[\frac{1}{r} + \sum_{l=2}^{\infty} \left(\frac{a_e}{a} \right)^l \sum_{m=0}^l \sum_{p=0}^l F_{lmp}(i) \sum_{q=-\infty}^{+\infty} G_{lpq}(e) \times \left(\left\{ \begin{matrix} C_{lm} \\ S_{lm} \end{matrix} \right\}_{l-m \text{ even}} \cos \{(l-2p)\omega + (l-2p+q)M + m(\Omega - \theta)\} \right. \right. \\ \left. \left. + \left\{ \begin{matrix} S_{lm} \\ C_{lm} \end{matrix} \right\}_{l-m \text{ odd}} \sin \{(l-2p)\omega + (l-2p+q)M + m(\Omega - \theta)\} \right) \right]$$

where a , e , i , M , ω , Ω are the Keplerian elements referenced to the lunar equator and θ is the lunar sidereal time. $F_{lmp}(i)$, $G_{lpq}(e)$ are defined in Ref. 1. A first-order solution to the lunar orbit may be obtained by writing the Lagrange planetary equation (Ref. 2) in terms of the lunar potential and integrating only the angle variables, delaying any consideration of the interaction between the elements to a second-order theory. The resulting solution appears in the form of:

$$\Delta s_i = \sum_{p,q} \frac{K_{ilmpq}(a, e, i)}{\Psi_{ilmpq}} \left[\left\{ \begin{matrix} C_{lm} \\ -S_{lm} \end{matrix} \right\}_{l-m \text{ even}} \cos \Psi_{ilmpq} + \left\{ \begin{matrix} S_{lm} \\ C_{lm} \end{matrix} \right\}_{l-m \text{ odd}} \sin \Psi_{ilmpq} \right]$$

where $\Psi = (l-2p)\omega + (l-2p+q)M + m(\Omega - \theta)$ and s_i represents one of the set of Kepler elements, $s(M, a, e, i, \omega, \Omega)$. We may write the partial derivative of

any one of the Keplerian elements, s_i , for a specified set of l, m , as:

$$\frac{\partial s_i}{\partial (C_{lm}, S_{lm})} = \sum_{p,q} \frac{K_{ilmpq}(a, e, i)}{\Psi_{ilmpq}} \left\{ \begin{matrix} \cos \\ \sin \end{matrix} \right\} (\Psi_{ilmpq})$$

We observe that the general form of these partial derivatives consists of an amplitude, K_{ilmpq} , and phase angle, Ψ_{ilmpq} . Because of the effect of oblateness of the lunar equator, and the perturbation of the Earth upon the satellite, the phase angle will change with time in a secular fashion, so that we would expect the partial derivatives to have secular, long- and short-period terms.

3. Numerical Results for the Lunar Orbiter Mission

Partial derivatives were calculated by PARD with a set of nominal *Lunar Orbiter* initial conditions. These were:

$$a = 2686 \text{ km}$$

$$e = 0.33$$

$$i = 15 \text{ deg}$$

$$\Omega = 359.861 \text{ deg}$$

$$\omega = 348.766 \text{ deg}$$

$$M = 0.0$$

$$T_o = \text{June 29, 1966; 1 hr, 33 min, 5 sec}$$

The amplitude and phase angles of the partial derivatives are shown in Table 3 for zonal harmonics up to the sixth order and all tesseral and sectorial harmonics up to the fourth order. M , i , ω , Ω , are in radians.

Several general features are apparent from Table 3:

- (1) The even zonal harmonics, 20, 40, 60, all have secular terms.
- (2) The eccentricity is unsensitive to changes for the second-order tesseral harmonics, 21, 22.
- (3) The fourth-order sectorial harmonic, 44, does not appreciably perturb any of the Kepler elements.

Since we are interested in the long-term effect of these partials, periodic terms less than the period of the satellite have been ignored. The shortest periodic terms to be considered arise from the tesseral harmonics which cause periodicities of fractions of the period of the revolution of the Moon.

Table 3. Amplitude of sensitivity coefficients

<i>l</i>	<i>m</i>	No. of terms	Coefficient of		Amplitude of					<i>M, ω, Ω</i> function	<i>e, i</i> function
			ω	$\Omega - \theta$	∂M	∂e	∂i	$\partial \omega$	$\partial \Omega$		
2	0	1	0	0	-0.350	0	0	-0.754	0.398	Secular	
3	0	2	1	0	-507	183	-253	-281	963	cos	sin
			-1	0	-507	-183	253	-281	963	cos	sin
4	0	3	0	0	0.029	0	0	0.922	-0.538	Secular	
			2	0	-30.2	-10.7	14.8	-16.0	57.2	sin	cos
			-2	0	30.2	-10.7	14.8	16.0	-57.2	sin	cos
5	0	2	1	0	709	-222	306	-501	-738	cos	sin
			-1	0	709	222	-306	-501	-738	cos	sin
6	0	3	0	0	0.044	0	0	-0.780	0.543	Secular	
			2	0	90.3	30.5	-42.2	-3.94	-139	cos	sin
			-2	0	-90.3	30.5	-42.2	3.94	139	cos	sin
2	1	1	0	1	-102	0	-139	-359	-484	cos	sin
2	2	1	0	2	-13.7	0	37.5	120	-139	sin	cos
3	1	2	1	1	-143	-81.7	-3.98	592	-192	sin	cos
			-1	1	-15.9	8.52	-23.4	-43.7	87.6	sin	cos
3	2	1	1	2	105	-58.3	-86.3	-27.5	-266	cos	sin
3	3	1	1	3	28.5	15.7	45.8	82.6	-165	sin	cos
4	1	2	0	1	32.4	0	189	3.38	468	cos	sin
			2	1	48.9	-21.5	14.3	-57.4	-39.0	cos	sin
4	2	2	0	2	20.4	0	-238	-500	814	sin	cos
			2	2	153	66.6	-3.25	406	-119	sin	cos
4	3	2	0	3	-8.62	0	-150	409	-549	cos	sin
			2	3	222	-95.4	-72.9	-220	-198	cos	sin

Figs. 8-22 are plots of partial derivatives of Keplerian elements e, i, ω, Ω , with respect to gravitational harmonics. The periodicity due to the rotation of the Moon is the

outstanding feature in Figs. 12-22; however, a long period trend is also noticeable in these figures by examining the maximum and minimum points of each cycle. The secular effects of the even zonal harmonics is quite distinctive in Figs. 8-11.

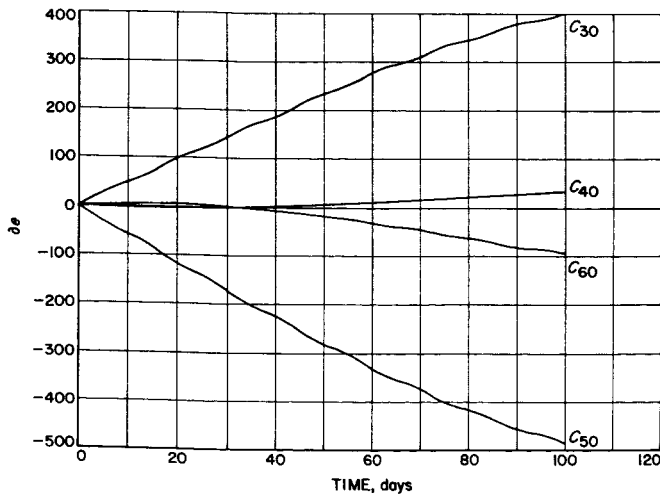


Fig. 8. Sensitivity of eccentricity with respect to zonal harmonics

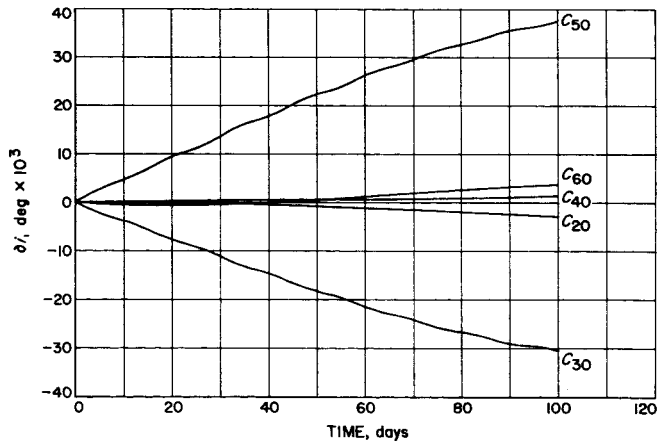


Fig. 9. Sensitivity of inclination with respect to zonal harmonics

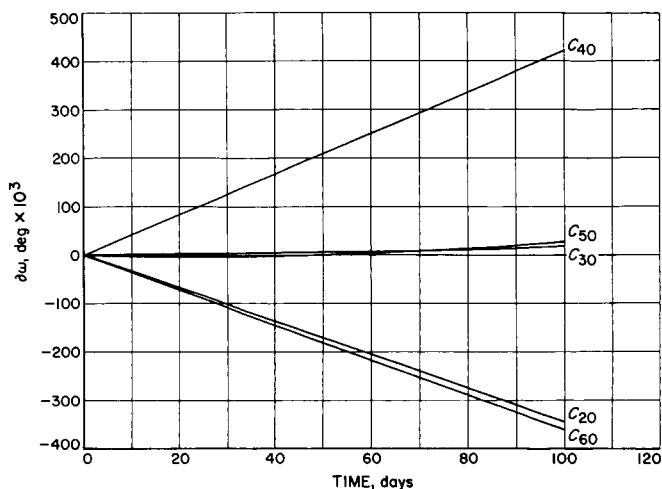


Fig. 10. Sensitivity of argument of perifocus with respect to zonal harmonics

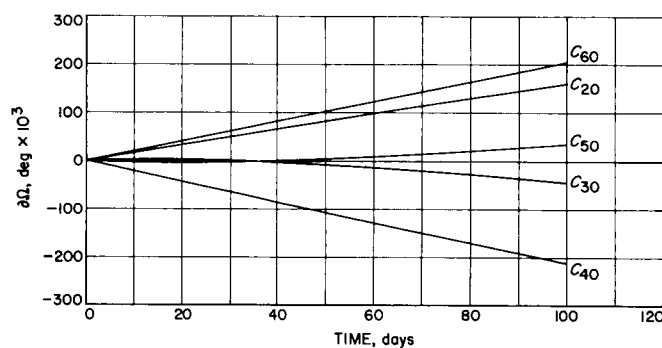


Fig. 11. Sensitivity of node with respect to zonal harmonics

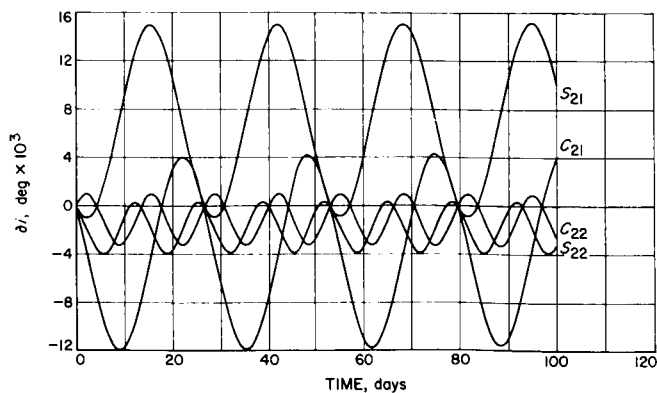


Fig. 12. Sensitivity of inclination with respect to second-order tesseral harmonics

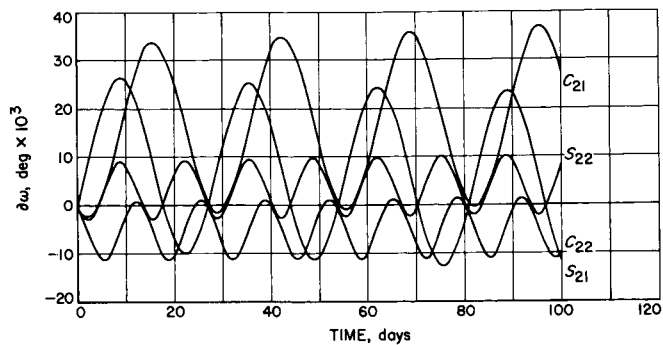


Fig. 13. Sensitivity of argument of perifocus with respect to second-order tesseral harmonics

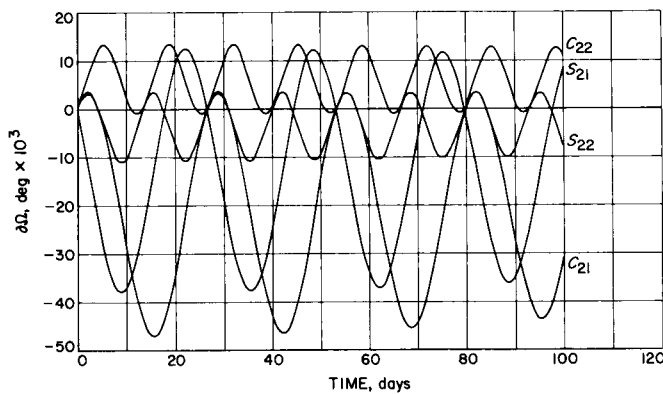


Fig. 14. Sensitivity of node with respect to second-order tesseral harmonics

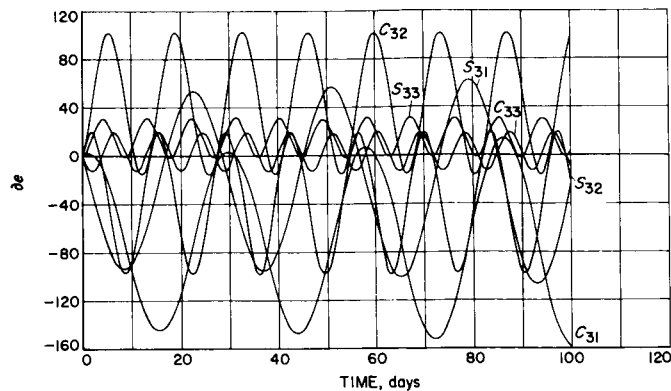


Fig. 15. Sensitivity of eccentricity with respect to third-order tesseral harmonics

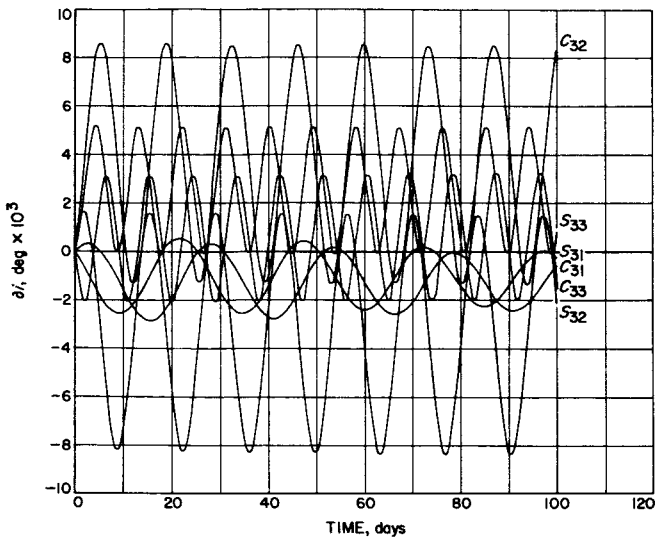


Fig. 16. Sensitivity of inclination with respect to third-order tesseral harmonics

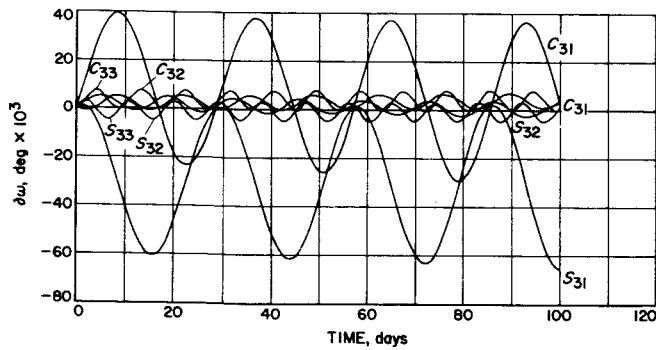


Fig. 17. Sensitivity of argument of perifocus with respect to third-order tesseral harmonics

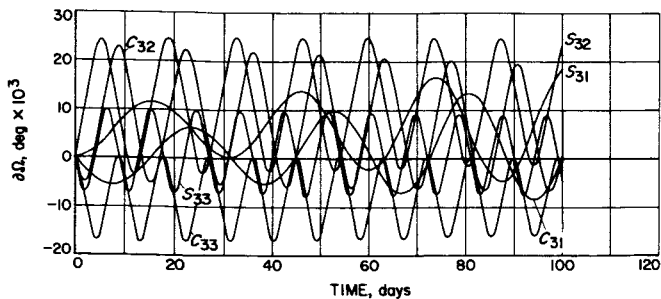


Fig. 18. Sensitivity of node with respect to third-order tesseral harmonics

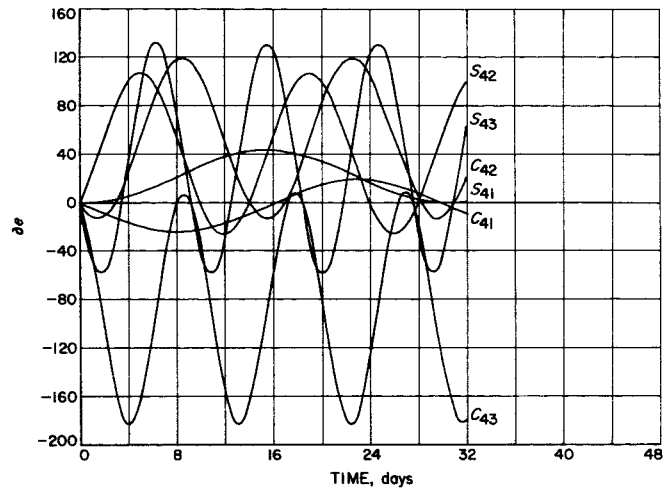


Fig. 19. Sensitivity of eccentricity with respect to fourth-order tesseral harmonics

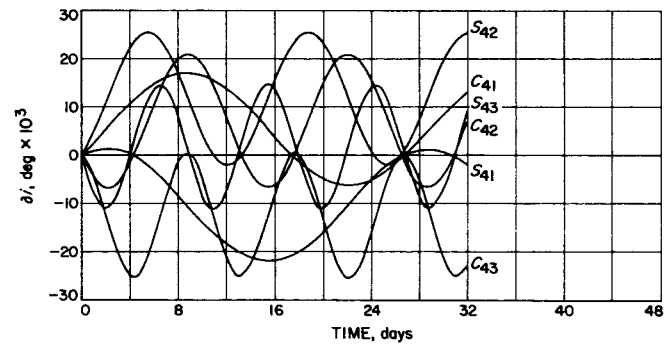


Fig. 20. Sensitivity of inclination with respect to fourth-order tesseral harmonics

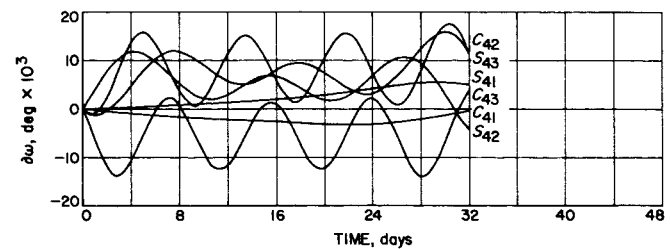


Fig. 21. Sensitivity of argument of perifocus with respect to fourth-order tesseral harmonics

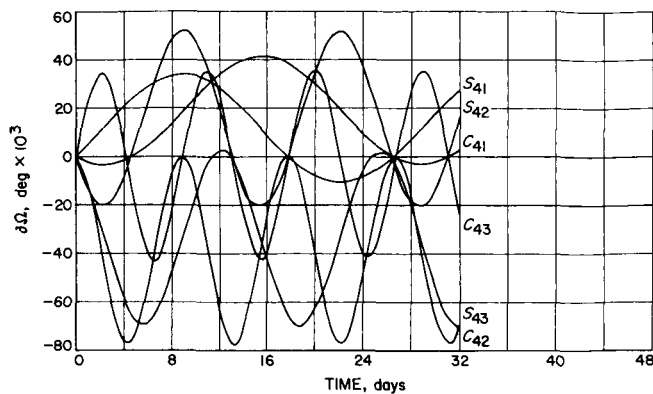


Fig. 22. Sensitivity of node with respect to fourth-order tesseral harmonics

F. Apollo Project Activities

D. W. Curkendall

The task reported here has these objectives: to provide the systems analysis effort to support the development of unified S-band to be used in the *Apollo* Program, to develop the capability to participate in the *Apollo* S-band qualification tests, and to assist the Manned Spacecraft Center (MSC) and Goddard Space Flight Center (GSFC) in planning and execution of the navigational aspects of the *Apollo* lunar landing mission. Specific items under this task will be selected each SPS report period for further discussion.

1. Tracking Data and Navigational Accuracy Analysis

With the data accuracy that may currently be achieved with the S-band tracking systems, the predominant error sources in the orbit determination process lie within the single precision orbit computation program. The *Apollo* navigational accuracy specifications are very stringent, requiring that double precision orbit determination programs be employed. The employment of these third-generation navigation programs will effectively remove what is now the largest single error source. The *Apollo* task includes items reported in Section III-D of this

SPS, entitled *Orbit Accuracy as a Function of Doppler Sample Rate for Several Data Taking and Processing Modes*, which is the first in a series of articles investigating the characteristic effect that different types of doppler noise sources have upon navigational accuracy. In this article, a one-dimensional tracking problem utilizing doppler data corrupted by white phase noise is analyzed and it is concluded that: (1) so-called "destructive" counting mechanisms (as opposed to continuously counting the doppler tone) should not be used in precision tracking systems and, (2) the possibility of using the total count in the doppler counter as a data type, rather than differencing adjacent counter readings, offers certain advantages and warrants further investigation.

2. Guidance Analysis

JPL's space guidance theory group has the task of extending the multiple maneuver guidance techniques developed in Refs. 3 and 4, in order to determine the optimal midcourse guidance policy for the *Apollo* mission profile during the translunar and Earth-return portions. The objectives are to develop appropriate extensions of existing guidance policy theory, analyze the *Apollo* profile, and to compare the results to those obtained assuming the use of simpler policies actually planned for *Apollo*.

3. Apollo Navigation Working Group

The systems analysis section at JPL participates in the *Apollo* Navigation Working Group, an unofficial multi-NASA center organization, chaired jointly by MSC and GSFC. The group's purpose is to coordinate, analyze, and study problems of the *Apollo* missions from a navigation point of view. Major efforts to date include the publication of two documents: the first (Ref. 5) describes broadly the *Apollo* mission profiles and documents the accuracy characteristics of the ground and onboard tracking systems, and the second (Ref. 6) is a collection of orbit accuracy studies based upon the system description in the first document.

JPL representation in this group ensures that current experience with the S-band tracking system, and existing orbit determination techniques, are made available to the *Apollo* Project. For example, approximately 60 passes of processed *Mariner IV* doppler data have been delivered to Bissett-Berman Corp., a subcontractor to MSC. The analysis of these data is the basis of the doppler error model used for *Apollo* navigation studies.

G. Goldstone Tracking and Testing Operations

J. Orbison

The Echo and Pioneer Stations continued to track the *Pioneer VI* spacecraft, as scheduled. Between tracking periods, Echo Station was involved with *Lunar Orbiter* tests, and the Pioneer Station with *Surveyor* tests.

1. Pioneer VI Project

a. Echo Station. Following the successful launch of *Pioneer VI* December 16, 1965, Echo Station tracked daily until January 14-15, 1966. Until February 15, a 3-day/wk tracking schedule was maintained, and a 5-day/wk schedule thereafter. With the exception of a cryogenic refrigerator failure during Pass 28, equipment operation was average.

January 12, 2 hr after acquisition during Pass 28, a sudden rapid warm-up of the maser occurred. A change-over to the parametric amplifier was made, and operation continued until investigation indicated that the trouble was in the Cassegrain cone, necessitating placing the antenna to zenith for repair. Pioneer Station assumed the tracking while Echo Station recorded the telemetry data via microwave from the Pioneer Station.

Investigation of the maser refrigerator revealed that all three mounting bolts holding the crosshead had separated, causing loss of vacuum and resulting in maser warm-up. A standby crosshead was installed and jacket vacuuming started, preparatory to maser cool-down. The Echo Station resumed scheduled tracking with Pass 29, January 13. Further investigation of the crosshead revealed that the displacer was "bottoming," straining the mounting bolts and resulting in their separation. Removal of 0.061 in. from the bottom of the displacer corrected the problem.

b. Pioneer Station. Subsequent to the move of the S-band system from the East Annex Building into the east wing of the Control Building, the *Pioneer VI* spacecraft was used as a signal source for full operational testing of the total system. Operating on a schedule of alternate days, Pioneer Station tracked during the days that Echo Station was not tracking. Pioneer Station received telemetry data have been recorded at Echo Station, via the microwave link. During the last 2 wk of February, Pio-

neer Station began full-time *Surveyor*/S-band system testing.

2. Surveyor Project

a. Pioneer Station. During the interval between the S-band system move and operational testing with *Pioneer VI*, Hughes Aircraft Co. personnel continued a series of subsystem tests with the *Surveyor* ground operations equipment. Currently, full compatibility tests and operator training are in progress.

3. Lunar Orbiter Project

a. Echo Station. The *Lunar Orbiter* spacecraft test model left Goldstone February 3, 1966. Between its arrival December 14, 1965 and its departure, a series of tests was performed, utilizing the flight components associated with the ground command and reconstruction equipment. Connected to a roof-mounted antenna, the spacecraft test model transmitted to, and received signals from, the Echo Station 85-ft antenna via a passive RF link.

Simulated flight operations were performed with commands originating in the Space Flight Operations Facility, transmitted to the Echo Station, and in turn to the spacecraft. The resultant telemetry was received at Echo and forwarded to SFOF in the same manner as during an actual mission. All three modes covering telemetry and video transmission from the spacecraft were tested at signal levels simulating lunar distances.

A pre-exposed film of a lunar landscape model, made from *Ranger IX* pictures, was used by the spacecraft for tests of the film-scanning operation and its associated electronics. The prepared test film was scanned in the spacecraft, signals transmitted to the Echo Station, recovered and processed by the ground reconstruction equipment (SPS 37-36, Vol. III, pp. 10-11). Tests of the spacecraft's camera and film-processing equipment were not performed at Goldstone.

System compatibility tests between the DSIF S-band system and *Lunar Orbiter* ground recovery equipment (GRE) were also performed. Except for an occasional interface problem, both systems were compatible.

Currently, test tapes prepared by Boeing Co. are being operationally tested at Echo Station prior to being sent to the overseas DSIF stations for systems tests.

Installed in January, two Scientific Data Systems 920 computers were operationally tested as part of the telemetry and command data handling subsystem (Fig. 23). Capable of three mission-dependent inputs and able to operate with any two simultaneously, the 920 computers provide command verification before transmission and recording of the received telemetry data. The subsystem is being used at Echo Station for *Pioneer VI* tracking and *Lunar Orbiter* testing.

4. Apollo Project

a. Goldstone Station. Located approximately 8 mi northwest of the Echo Station, the Apollo Station 85-ft X-Y antenna and Control Building are nearing completion (Fig. 24). A part of the Manned Space Flight Network, the Apollo Station will utilize certain support functions of the DSIF Goldstone Station and, ultimately, receive back-up support for its mission.



Fig. 23. Telemetry and command data-handling computers

References

1. Kaula, W. M., "Analysis of Gravitational and Geometric Aspects of Geodetic Utilization of Satellites," *Geophysical Journal*, Vol. 5 No. 2, pp. 104-133, 1961.
2. Moulton, F. R., *Introduction to Celestial Mechanics*, p. 399, McMillan Co., New York, 1914.

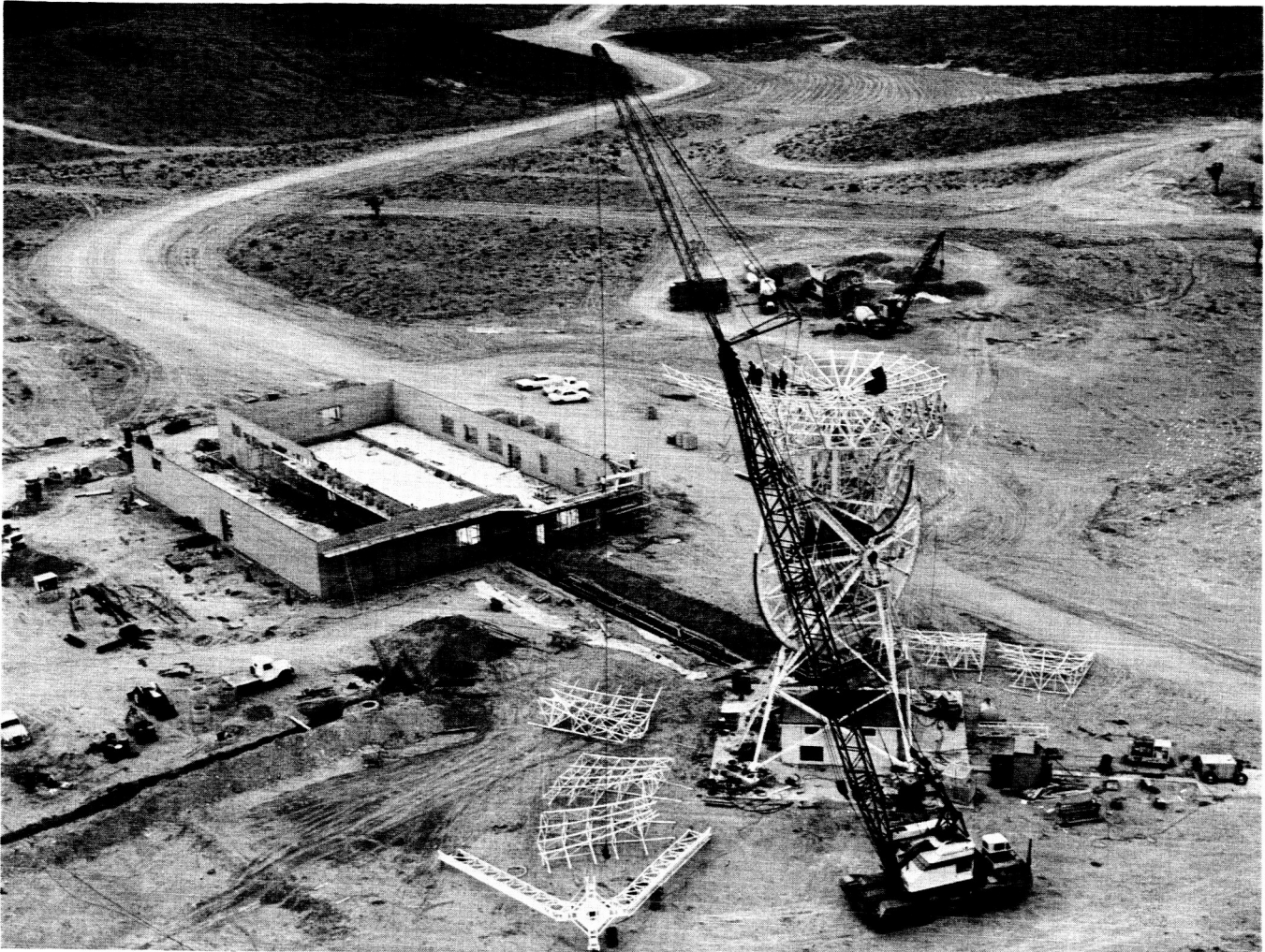


Fig. 24. MSFN Apollo Station under construction

References (Cont'd)

3. Pfeiffer, C. G., "A Dynamic Programming Analysis of Multiple Guidance Corrections of Trajectory," *AIAA Journal*, Vol. 3 No. 9, September 1965.
4. Curkendall, D. W., "Monte Carlo Simulation of an Adaptive Policy for Multiple Impulse Corrections of a Trajectory," *AAS Conference Proceedings, Advances in the Astronautical Sciences*, Vol. XIX, 1965.
5. Apollo Navigation Working Group Technical Report No. 65-AU-1.0, "Apollo Missions and Navigation Systems Characteristics," February 5, 1965.
6. Apollo Navigation Working Group Technical Report No. 69-AU-2.0, "Apollo Navigation Ground and Onboard Capabilities," October 8, 1965.